UNIVERSITY OF CAPE TOWN

PHYSICS DEPARTMENT

POLARIZATION IN NEUTRON-DEUTERON SCATTERING FROM 8 TO 22 MeV

by

Mary Steinbock

A thesis prepared under the supervision of
Professor F.D. Brooks in fulfillment of the
requirements for the degree of
Doctor of Philosophy in Physics.

December 1975

A B S T R A C T

The polarization in n-d scattering has been measured at incident energies 7.9, 16.4, and 21.6 MeV using neutrons from the $^{9}Be(\alpha,n)^{12}C$ and $^{3}H(d,n)^{4}He$ reactions. The polarization analyzer was a deuterated anthracene scintillation crystal. Recoil deuterons from n-d elastic scattering within the crystal were studied and pulse shape discrimination (PSD) was used to determine the left-right asymmetry of the recoils. The experimental method depends on the fact that the PSD response of the crystal is sensitive to the direction of the recoil deuteron relative to the crystal axes. The results obtained are compared with theoretical calculations from the literature and with other measurements. A comparison of the n-d and p-d polarization data reveals no evidence of breaking of the charge symmetry of nuclear forces.

ACKNOWLEDGEMENTS

I wish to express my appreciation to all those whose assistance has made this work possible. I am especially indebted to the following:

My supervisor, Prof. F.D. Brooks, whose guidance, encouragement and help were of prime importance for the completion of this work;

Prof. I.J. van Heerden of the Southern Universities Nuclear Institute, for his helpful discussions and co-operation throughout this work;

Dr. W.R. McMurray of the Southern Universities Nuclear Institute, for his advice and encouragement during the experiment;

Dr. J.J. Kritzinger and the staff of the Southern Universities Nuclear Institute for their friendly co-operation in keeping the accelerator running during the experiment;

The Physics Department of the University of Cape Town for the friendship, encouragement, and financial support I found during the work;

Mr. P.A. Back of the Physics Department of the University of Cape Town, for the construction of the necessary equipment;

Messrs. G.G. Laing, L.G. Fowle, E.J.N. Heald and D. Momsen of the Physics Department of the University of Cape Town for their friendship and many lessons in machining;

Mr. J.F. Rajdl of the Southern Universities Nuclear Institute for his electronic expertise and many helpful lessons;

Mrs. D.A. Simmonds of the Southern Universities Nuclear Institute for her valued friendship during the experiment, and her skillful job of typing the manuscript afterwards;

Mrs. M. Lewis who assisted with the typing of the manuscript;

The South African Council for Scientific and Industrial Research and the Atomic Energy Board of South Africa for the financial support of this experiment, also for the welcome extended to me during my stay in South Africa;

Finally, I wish to thank Dr. and Mrs. Elie A. Sayan and their family for the encouragement and friendship extended to me over the years. Without them, this thesis would have been impossible.

CONTENTS

LIST OF FIGURES

LIST OF TABLES

CHAPTER I

INTRODUCTION

Both theoretical and experimental work on the three-body system can be divided into two periods; pre- and post-Faddeev. Before 1961, which was pre-Faddeev, the theoretical work was directed along the lines which had proven highly successful in atomic physics. Quantum mechanics had been applied with great success to interpret a very wide range of phenomena in this field, including complex atomic and molecular structure. However, a key factor in this success was the fact that the basic law of force, the Coulomb law, was known. In contrast, nuclear physics was beset not only by the difficulties of applying quantum mechanics to complicated systems, but also by the additional difficulty that the basic nuclear force law was unknown (Ve57).

Thus, apart from the difficulty of handling the wave equation for a many-body system, it was not known which wave equation to solve. The problem in nuclear physics was therefore twofold: first, to find the laws of the nuclear forces, and second, to calculate the nuclear properties resulting from those forces (Bl52). Since there was no satisfactory fundamental theory of nuclear forces, the object was to find the law of force which, when applied to nuclei, would reproduce the observed properties. This attempt met with several difficulties. Knowledge of nuclear properties was not very accurate, so there have been several laws of force whose implications were in agreement with the then-present experimental data. Also, the methods of calculating nuclear properties for all but the simplest nuclear processes were based on approximations whose accuracy was doubtful at best. Hence, a reliable and unambiguous test for any given force law was seldom possible.

The starting point was the N-N interaction based on a study of two-body scattering experiments and bound states. However, scattering experiments for

the N-N interaction were not sufficient for a knowledge of forces off-the-energy shell. This kind of two-body information is available only from three-body experiments. The study of the three-body problem would, in principle, allow an estimate of the importance of three-body, and many-body, forces in nuclei. If the two-body force were known, and if no additional forces were present, the wave equation could be solved for the three-body system. Then, if the results agreed with the experimental data, there would be no need for invoking the three-body force. But the agreement with experiment was only approximate. The two-body force was not known well enough to delimit the three-body problem completely. The three-body system was sensitive to the finer details of the force law. Theories for three-particle scattering and reactions were not well developed at that time. Also, there was the possibility of relativistic corrections being more important in the three-body case than in the two-body case. In early times many of these difficulties were ignored by making simplifying assumptions regarding them.

The earliest theoretical attempts at solving the three-body problem were the variational methods (Mi69). These early variational methods were insensitive to the input potentials, which prevented a fair comparison of the results of the simplifying assumptions with experiments. The main advantage of the variational approach was in the great freedom in choosing trial functions which were not restricted to a 'no-polarization' approximation (Ve57), as were the approximations worked out by various authors (Fe35) (Bu52).

There were other varied and clever approximations worked out for the three-body problem. These included the resonating group structure method (Wh37), the Born approximation (Wu48), the high energy approximation (Gl59), impulse approximations (Ca59) (Fe59) and several other variational methods (Sa58). There were also phenomenological potentials by Gammel and Thaler (Ga57a) (Ga57b) to represent the perturbation reaction which used direct reaction

theory in which context the Born approximation was used (Ko64).

As far as experiment was concerned, already by 1935 attention was concentrated on simple scattering problems, which should have led to some knowledge of nuclear force. However, the experimental results were not very accurate, and several different forces could be postulated to give the same experimental results. It just wasn't possible to compare the assumptions and approximations of theory with the experimental results. These difficulties were further compounded by the fact that high speed computers weren't really available to investigators until around 1960. The state of the art in nuclear physics was in sharp contrast with the accurate variational methods of atomic physics.

The modern period, dating from the work of Faddeev (Fa61a) (Fa61b) (Fa63) (Fa65) and Amado (Am63) (Aa64) (Aa65) (Aa66) (Am66), began around 1961 (Du68) and was concerned with the exact treatment of the three-particle aspects of the three-nucleon problem, which were made manageable only by the sacrifice of some fidelity in the two-body interactions. This emergence of accurate three-body techniques (Mi69) following on the new theory of Faddeev seemed to have spurred the variational investigators into greater activity, with the result that the gap between the 'variational' and the so-called 'exact' treatments was narrowed down. There exists a vast amount of literature on the 'exact' theory of the three-nucleon problem, which has been the subject of extensive investigations for the last fifteen years, both from the point of view of the Schrodinger equation (Mi62) (Mi63) (Si63), as well as in terms of the Faddeev theory under the separable approximation. These methods, which have been extensively viewed in the literature, seem to give interesting results for n-d scattering (Aa65), and the breakup reactions (Ph66) (Aa66).

1.1 The nuclear force

At non-relativistic energies the nuclear force can be described by a potential which may be either theoretical in character, or purely phenomeno-logical, or

a mixture of both (Br67). Originally, phenomenological potentials were used because the information from two-nucleon data was not sufficient to determine potentials. These were usually simplified forms of two-body potentials, containing a number of parameters which were fitted to the nuclear data. A general form of such a potential could include central, tensor, and spin-orbit terms.

The classical explanation of the nuclear force has been given by Yukawa (yu35) in terms of the exchange of virtual pions. It has been found from experiment that the nuclear force is strong, repulsive at short range, attractive at long range, partly exchange in character, has saturation properties, is spin, isospin and momentum dependent, and approximately charge independent.

In that nuclear forces are now attributed to meson exchange, it is clear that the one-pion exchange potential (OPEP) is considered to play a fundamental role in any reasonable parameterization of nucleon-nucleon scattering theory (Ma70a). A proposal along these lines by Taketani, *et al.* (Ta51) went further in associating a region corresponding to close separations with a two-pion exchange potential (TPEP), and still closer separations with many-pion exchange (MPE), including the effects of heavy meson exchange (one-boson exchange, or OBE). The spin-orbit interaction has been attributed to the heavier bosons (No63).

There are some recognized difficulties with the two-body problem. The two-body data do not determine the potential uniquely, partly because even the extensive data available are still limited in accuracy and range, and partly because of inherent ambiguities. Scattering data will determine a potential uniquely only if the potential is local and only if there are no bound states, otherwise the scattering data do not suffice. Only limited information (McC68) about two-body forces is obtained from two-body scattering experiments. Many-body experiments depend on the potential, not on the two-body scattering information off-the-energy-shell is needed.

In order to completely specify the N-N interaction, the matrix elements between all possible pairs of initial and final 2N states, including those pairs that do not conserve energy and momentum, need to be known. The matrix involved is the transition, or t-matrix. Since energy and momentum are conserved in the elastic scattering case, such experiments yield information about the on-energy-shell elements of the t-matrix. Not only is it possible that the off-shell elements of the t-matrix may be important, it is possible that the t-matrix itself may be altered by the presence of other bodies (McC68). Many-body forces have not been found to be negligible. There is no *a priori* reason to expect all nuclear forces in nuclear matter (many-body forces) to be exactly the same as two-body forces for the two-body experiments. Information about the off-shell elements can be obtained from such processes as the photodisintegration of the deuteron and the emission of bremsstrahlung in nucleon-nucleon interactions. These processes, which in themselves do not conserve energy, are made to conserve energy overall, by the emission of a third particle (McK70).

There have been extensive studies performed on the three-particle system which have acquired particular prominance in the connection with the Faddeev equations (Fa61a) (Fa61b) (Fa65). These equations are formally based on earlier discussions of rearrangement collisions following the work of Ekstein (Ek56) and Gerjouy (Ge58) and complement the work of Amado mentioned above. If special assumptions are made regarding the two-particle interaction, the Faddeev equations reduce to those of Amado. They also have a direct bearing on three-particle correlations in nuclear matter (McK70).

The main advantage of the Faddeev formulation lies in the ability to include a wide range of two-body multichannel effects arising from polarizations, rearrangements, etc., within the three-body system, than would be possible with an appropriate two-body discription. Separable forms of the interaction allowing explicit realization of the various substructures of a three-body

system have been used (Lo64), and provide a quick insight into the theoretical structures expected of the three-body system. They can be made to conform closely with reality by suitably extending the rank of the input potential. Separable potentials can be used to realize the above effects explicitly and give good agreement with experiment for a large number of observables.

The three-nucleon bound state can give information concerning the off-shell behavior of the force, that is, about potential form. The traditional approach used the variational principle, but other methods including direct solution of the Faddeev equations are now at the level of the variational methods. By far the most important three-nucleon observable is the triton binding energy (De69). Various groups have reported calculations for the bound state using either the hard-core Hamada-Johnston (De71) (Hu71) or the soft-core Reid (Ma70b) (Tj70) (Ja71a) (He72) (Bh72) potentials, as stated by Amado (Am72). The most recent values reported for the binding energy are 7.75±0.5 MeV for the Reid potential (He72), and 6.5 - 6.7 MeV for the Hamada-Johnston potential (De71) (Hu71). The experimental value is 8.48 MeV (Am72). Sources for binding energy discrepancies are relativistic corrections, off-shell dependence, and the three-nucleon forces.

The Coulomb energy of the three-nucleon system is the difference in binding of ^{3}H and ^{3}He, the only other bound state; experimentally this value is 0.76 MeV. Delves and Hennel (De71) have done a very careful variational calculation with the Hamada-Johnston potentials and got 0.6 MeV after adjusting for the experimental triton binding energy (Am72). This discrepency has been around for some time and its importance stressed as a possible indication of charge symmetry (Ok71).

The three-body force is that force which depends on the simultaneous presence of three nucleons, and is without analogy in classical physics. To date, there

is no clear-cut evidence of the importance of the three-body force in nuclear physics. It is suggested (Br69) that 2 MeV of the binding energy of nuclear matter may be due to specifically many-body forces; however, knowledge of the interaction potential between nucleons is such as to make it impossible to identify one particular effect as evidence for three-body forces in the three-nucleon system (No68).

The problem of experimentally determining the three-nucleon scattering matrix for n-d scattering is quite complicated. Noyes (No67) states that there are 648 non-zero elastic scattering observables, and 2304 inelastic ones, and hence there are plenty of experiments from which to choose. Experiments must be picked judiciously so that they do not give the same combinations of amplitude already determined by earlier experiments, if progress is to be made. Of the large number of possible experiments, so far only a few types of observables have been measured: elastic and inelastic differential, and total cross sections; polarization of either protons or neutrons; vector and some of the tensor polarization coefficients of the deuteron; and one measurement of the Wolfenstein parameters D(depolarization) and R'(spin rotation) (Wo56). The development of a comprehensive theory as discussed by Noyes in his review article would help determine which amplitudes are the most dynamically significant, and therefore worthy of investigation. This particular work is concerned with the polarization in n-d scattering.

CHAPTER II

NUCLEON-DEUTERON SCATTERING

2.1 Charge symmetry and charge independence of nuclear forces

The hypothesis (Yu35) that the nuclear force is mediated by an exchange of charged and uncharged mesons between nucleons has provided much insight into nuclear physics. The hypothesis itself implies that some symmetry characteristics are to be expected in the nature of the nucleon-nucleon interaction. After allowance has been made for the Coulomb interaction in the case of the p-p system, the nuclear force is expected to be charge symmetric, with the n-n force identical to the p-p force. The nuclear force is also expected to be very nearly charge independent, the n-p force being essentially identical to the p-p and n-n forces (Ce64).

These expectations are in fact verified to a high degree by low energy nucleon scattering and from properties of mirror nuclei, together with other indications of the force symmetries. Wilkinson (Wi66) has drawn the conclusion that charge symmetry holds to greater than ninety-nine per cent, and charge independence to greater than ninety-eight per cent. Invoking the concept of isospin, charge independence can be equated to isospin invariance, which has also been the subject of extensive research.

The three-body scattering problem involving three nucleons, two bound and one free, can also be used to further test the charge independence of nuclear forces (McK70). The shape of the p-d polarization is well-known below 50 MeV, and more data on the n-d polarization is being accumulated. Charge symmetry implies that the results of p-d and n-d polarization should be nearly equal. It is reported by Haeberli (Ha70) that there may be some possible differences in the three-body data. Differences in polarization are also found for the charge symmetric scatterings of

n-T and p-^{3}He (Se70). Further investigations of these reactions should be profitable. Such investigations should, however, include a theoretical treatment which properly accounts for Coulomb effects.

2.2 Neutron-deuteron scattering

The importance of nucleon-deuteron scattering lies in the fact that it is experimentally the most easily studied three-particle continuum state (Ko63). In his review article McKee (McK70) reports on the development of new methods of handling three-body scattering reactions. These methods are both approximate ones incorporating variational or other wave functions into known potentials, and exact methods based on the expression of the three-body scattering in terms of coupled two-body amplitudes, after the manner of Faddeev. There are many references for these calculations appearing in the literature, especially by Sloan (Slo68) (Slo69a) (Slo69b)(Slo71) (Slo72a) (Slo72b); other contributors are (Am63) (Ko63) (Kl71) (Be72) (Br72) (Ca72) (Ja72) (Ko72) (Fi73) (Br74c) and (Sla72). Phase shift analyses by Arvieux (Ar67), Van Oers and Brockman (Va67a), Van Oers and Seagrave (Va67b), and Van Oers and Slaus (Va67c), have already done something to interpret elastic scattering data over a considerable energy range in terms of a consistent set of partial waves.

The deuteron has spin one and isospin zero, and so n-p scattering is in the $T = 1/2$ three-body channel only. There are two spin channels for the n-d scattering, the doublet ($S = 1/2$, $T = 1/2$) and the quartet ($S = 3/2$, $T = 1/2$). It is found that the doublet n-d scattering length gets progressively improved as the potential is extended from the effective S-wave form successively to include tensor and repulsive core effects (Mi69). In the presence of non-central two-body forces coupling spin and orbital angular momentum, transition amplitudes are not diagonal in the L-S representation. At essentially all energies, the dominant features of n-d scattering arise from the fact that the deuteron is loosely bound, which leads to the rapid onset of high partial waves in the scattering.

For n-d scattering at zero kinetic energy only S waves are important, and the spin channels are uncoupled, giving two n-d scattering lengths, a_2 (S = 1/2) and a_4 (S = 3/2). In the doublet channel the S-wave force is attractive, and the scattering length is sensitive to the details of the interaction. In the quartet channel the spins are parallel, and the particles are kept apart by the Pauli principle. In the quartet channel the S-wave force is repulsive, and the scattering length is insensitive to the interaction (Am69). According to Seagrave (Se70) the best values for the two scattering lengths are: $a_2 = 0.15 \pm 0.05$ fm, and $a_4 = 6.13 \pm 0.04$ fm.

Phillips (Ph68) points out that if the separable potential doublet scattering length results are plotted against the triton binding energy, a straight line results passing through 0.8 ± 0.2 fm at the experimental binding. The more modern doublet scattering length is currently taken as 0.15 fm (Se70). A recent calculation of scattering length and binding energy (De69) also seems to give values lying on Phillips' straight line. It appears that the relationship between the doublet scattering length and triton binding energy may be highly potential-dependent, and it may be premature to read any particular significance into these apparent discrepancies at this point in time.

In an early paper Christian and Gammel (Ch53) show that the first Born approximation in n-d scattering is due to nucleon exchange, which depends only on the deuteron binding energy. They perform a partial wave analysis leaving the S-wave free to be fitted, but all other waves are fit with the nucleon exchange Born term, this showing that nucleon exchange is the dominant mechanism for elastic scattering, and that this in turn depends only on the low energy n-p parameters (Am69). This idea is later developed by Amado (Am63) using the separable-potential approach. The n-d elastic differential cross sections as a function of center-of-mass angle show that the quartet term is the dominant one. There is also a strong forward and backward peaking in these cross sec-

tions. The backward peak can be represented by exchange scattering, and may be regarded as a reflection of the forward peak (Se70).

The experimental and theoretical angular distributions for n-d scattering have been reported by Seagrave and Cranberg (Se57) and by Aaron, Amado, and Yam (Aa65), and have later been reviewed by Amado (Am69). It is found that the theoretical angular distributions agree well with experiment, especially when the effects of the tensor force are approximately taken into account. It is further found that the ratio of the quartet to doublet spin state is large, the doublet state not contributing much to the elastic scattering cross section.

Deuteron breakup by protons or neutrons has been less thoroughly explored than elastic scattering since it is more difficult both experimentally and theoretically. The various sets of data (Ce64) (Il63) on the breakup reaction are, where comparable, in agreement with each other (De69). The general features of the breakup are given at all energies, but the detailed fit is not so good as for the elastic scattering data, which may reflect the importance of the more sensitive doublet channel for the breakup reaction. The major feature of the deuteron breakup reaction by neutrons is the strong final state interaction between the neutrons in the ^1S state (Am69).

The separable model calculations of Aaron and Amado (Aa66) and Phillips (Ph66) can produce the gross features of the low-energy, three-nucleon system. In doing so, they indicate that sophisticated three-body dynamics are essential and that the details of the interaction are relatively unimportant. The breakup reaction can also be regarded as a source of information on the neutron-neutron scattering length, the effects of which show up clearly as a strong final state enhancement in the reaction.

2.3 Polarization in neutron-deuteron scattering

Following Haeberli's review article (Ha70), the polarization which results in the scattered beam when unpolarized neutrons are scattered at angle θ_2^{cm} in the center-of-mass frame by unpolarized deuterons, is referred to as $P_2(\theta_2^{cm})$. In practice, rather than measuring the polarization of the scattered beam, a polarized incident beam is used and $P_2(\theta_2^{cm})$ is determined from the azimuthal variation of the cross section, that is to say, the analyzing power of the process is measured. The sign of the polarization is defined by the Basel convention (Ba61). When spin-flip is forbidden as it is in elastic scattering, the left-right asymmetry, or analyzing power, is equivalent to the polarization. A necessary condition to obtain polarization different from zero is that orbital angular momenta greater than zero must contribute to the scattering, otherwise there can be no spin-orbit term in the potential. It has been known for a long time that this condition is satisfied in neutron-deuteron scattering even at low energies since neutron-deuteron scattering is anisotropic (Ch53).

Under the influence of a spin-orbit force, an unpolarized neutron beam becomes at least partially polarized upon scattering. This is essentially a quantum mechanical effect and is due to interference. This partially polarized neutron beam, with spin 1/2, can be regarded as an incoherent mixture of two beams of opposite polarizations, and the beam is in a mixed spin state. The value of $P_2(\theta_2^{cm})$ can be taken as the expectation value of the component σ_d of the Pauli spin operator $\underset{\sim}{\sigma}$ in the distinguished direction $\hat{d}$ (Ma70a).

The specification of the most general mixed state of the spin 1/2 system requires three parameters; two angles which serve to define the axis of quantization, and the ratio N^+/N^- of the numbers of neutrons in the spin-up and spin-down orientations, respectively. Since the spin 1/2 system always possesses cylindrical symmetry around the direction of polarization, the polarized neutron beam can be thought of in terms of a mixture of two pure spin states. $P_2(\theta_2^{cm})$

is a vector quantity and is referred to as a vector polarization. In any scattering process involving a suitable force coupling spin and space co-ordinates, there is polarization, its sign and magnitude depending on the scattering angle. Polarization data generally are expected to give significant information about the shape and magnitude of the spin-orbit term in the potential; the magnitude of the polarization is proportional in first order to the strength of the spin-orbit term, and as accurate data have become available it has also been possible to learn something about the shape of the potential.

The recent advent of high-intensity polarized beams with a small energy spread has made possible a number of experiments which could not be performed previously. The usefulness of a polarized source clearly depends upon the intensity and polarization achieved, and in some reactions, polarization parameters can now be measured almost as easily as cross sections. Several reviews of such sources have been published (Ha67) (Da65). Polarized target-polarized beam techniques give high precision to scattering experiments provided by polarization techniques.

Polarization effects in nucleon-deuteron elastic scattering have been established since around 1966. Haeberli (Ha70) has constructed a contour map of some recent p-d polarization data below 50 MeV. An interesting feature of the polarization is that it becomes negative at backward angles in the vicinity of 19 MeV incident proton energy. This behaviour is now firmly established; the work of Garreta, *et al.* (Ga68) and of Faivre, *et al.* (Fa69) confirm Johnston's (Jo68) results at 22 MeV. The position of the observed minimum in the asymmetry distribution is near 110° in the centre-of-mass system, and a marked change in the shape of the distribution is seen to occur between 10.0 and 19.0 MeV incident proton energy. The Rutherford group have also published an interesting figure showing the variation with energy of the center-of-mass crossover angle from

positive to negative polarization. The data plotted all lie on a smooth curve except one Berkeley point (Me68).

It is clear that the polarization exhibits much interesting structure: the backward peak which develops at very low energy and gradually moves outward with angle as the energy increases, but which seems to saturate at about + 0.2, the very deep negative minimum which appears already below 20 MeV, and goes to large negative values at higher energy, and the small forward positive peak (No67). The impulse approximation gives no indication of this structure, even when off-shell scattering corrections are included (Ko63). Hüfner and de-Shalit (Hü65) have shown that this type of polarization structure can be correlated with the differential cross section in a diffraction model, and obtain a good fit to p-D polarization data at 40 MeV using a single parameter, but this hardly provides a dynamical explanation.

In comparison to the p-d results, there is no corresponding wealth of n-d experimental work. In fact, above 22.7 MeV only two measurements exist, 23.7 MeV (Wa63) and 35.0 MeV (Za73). The experiments themselves are of course more difficult, and few complete angular distributions of the polarizations have been obtained so far.

The existing data are discussed by Haeberli (Ha70) who gives a diagram incorporating the best of the neutron polarization obtained to date, excluding the very recent work of Morris, *et al.* (Mo74) and Zamudio-Cristi, *et al.* (Za73), and in comparison with the p-d work it is unremarkable. The point worth noting is that the negative dip at backward angles in the n-d case of elastic polarization at 22.7 MeV is apparently deeper for the neutron than it was for the proton case. In view of the difficulty of the experiments it appears possible that the difference arises from experimental errors. Accurate measurements of n-d elastic scattering and polarization at energies above 20 MeV would be valuable at this stage.

Differences in polarization have also been found between the charge symmetric scatterings n-T and p-^{3}He. In a recent article by Zamudio-Cristi, *et al.* (Za73) concerning a measurement of n-d polarization at the slightly higher energy of 35 MeV, it is further reported that for angles near the 120^o center-of-mass, corresponding to those near the minimum of the differential cross section, the n-d values of polarization are considerably more negative than those for p-d polarization. In addition, they are also more negative, as are the p-d values, than current theoretical values. So it seems quite worthwhile to investigate this problem further.

Until recently very little serious theoretical effort has been given to the polarization (Si69a) (Si69b). The exact solution of the three-body problem as given by Faddeev is beyond the means of present day computational facilities. Some recent authors (Kr70a) (Kr70b) (Aa70b) (Aa72a) (Aa72b) (Pi72a) (Pi72b) (Pi72c) have instead employed separable two-body interactions to approximate the exact solution. Polarizations in n-d scattering are predicted by these calculations (Pi72b). Other methods for predicting the polarizations have also been investigated by Seyler (Se69), Arvieux (Ar67) and Purrington and Gammel (Pu68). According to Haeberli (Ha70) the latter work gives a realistic prediction of polarization in nucleon-deuteron scattering at low energies. The authors use the Born approximation for n-d scattering in which the tensor interaction and the deuteron D state are included. A five parameter fit using the $^4S_{3/2}$ and $^2S_{1/2}$ eigenphases and the mixing parameters coupling S- and D-states were adjusted empirically as was the deuteron D-state admixture. Numerical calculations of the n-d cross section and polarization were made for 9.0 MeV neutron energy. The agreement with measured experimental data for both elastic scattering and polarization is quite satisfactory (Pu68).

Theoretical work is hindered, however, since accurate measurements for polarizations in neutron-deuteron scattering below 5 MeV are available over a large

angular range only at a few energies. Several early experiments for low neutron energies gave slightly positive polarization, but with errors sufficiently large to be consistent with zero polarization. Generally speaking, n-d polarization below 5 MeV can effectively be considered very small; only above 5 MeV does it attain values exceeding a few per cent. Data above 5 MeV are also relatively sparse, however, due to the considerable technical difficulties encountered in conventional neutron scattering experiments. No major experimental contribution to the n-d polarization problem has been made since the survey reported by Walter and Kelsey (Wa63) who presented polarization angular distributions at five energies, ranging from 1.9 to 23.7 MeV. Since that time, of course, work in this energy range has continued, as witnessed by the very recent efforts of Morris, *et al.* (Mo74) at 16.8 and 21.2 MeV, and the work of Zamudio-Cristi, *et al.* (Za73) at the higher energy of 35 MeV. The experimental situation will be treated in depth in Chap. III.

Noyes (No67) writes that the immediate theoretical needs for making efficient use of existing experiments and planning new experimental programs in the three-nucleon problem are: a low energy theory comparable to the effective range theory, an explicitly unitary parameterization of three-body reactions comparable to two-particle phase-shifts and inelasticity parameters, a complete transcription of the Faddeev two-particle subchannels into the three-particle invariant amplitudes and the unitary three-particle parameterization, and a model-independent high-J analysis for n-d scattering and breakup which exploits the loose structure of the deuteron to provide the analog to the OPE calculation in the two-nucleon system.

2.4 Motivation

As has been indicated above, there is a strong motivation for studying the polarization in n-d scattering. There are a number of applications for which measurements of the polarization of scattered neutrons give information not

readily available by other methods. The fact that the polarization depends on the interference of partial waves has the effect that the polarization is strongly affected by the presence of partial waves which undergo only small phase shifts. Measurements of the polarization, therefore, help in discovering the effect of phase shifts which are too small to be noticeable in the angular distribution. The polarization helps in restricting the possibilities to a small number, and in indicating qualitatively the absence or presence of phase shifts. The set of phase parameters which occur are determined by the experimental data.

Various potential models have been proposed to predict the n-d scattering data, along with determining some of the properties of nuclear forces. In general, the scattered neutrons will be polarized if spin-orbit interactions are present; the observation of polarization will, therefore, indicate the presence of such interactions. However, the interaction has a sufficiently complicated spin structure that it has not yet been possible to determine the scattering matrix from the experimental data. The eventual success of a potential model lies in reproducing the experimentally determined phase parameters.

Available n-d data are sparse. The only published measurements in the energy region of interest are Taylor, *et al.* (Ta70) at 7.8 MeV, Malanify, *et al.* (Ma66) at 22.7 MeV, Walter and Kelsey (Wa63) at 16.4 and 23.7 MeV, and most recently Morris, *et al.* (Mo74) at 16.8 and 21.1 MeV, Brüning, *et al.* (Br71a) at 7.9 MeV (in graphical form); there is also a recent measurement by Zamudio-Cristi, *et al.* (Za73) at the slightly higher energy of 35 MeV.

Although charge symmetry implies that the p-d and n-d polarization results should be nearly equal, a comparison of the 22.7 MeV results of Malanify, *et al.* (Ma66) with the p-d results of Faivre, *et al.* (Fa69) reveals possible differences at angles near the negative minimum. These differences have been noted in the review articles by Haeberli (Ha70) and by McKee (McK70). The more recent

results of Zamudio-Cristi, *et al.* (Za73) indicate a similar difference at 35 MeV. A comparison on n-T and p-^{3}He scattering at 22 MeV made by Seagrave, *et al.* (Se70) has revealed significant differences in the polarization.

Recent theoretical progress in describing N-d scattering has been reported by Pieper (Pi72a) (Pi72b) and by Doleschall (Do73). Using separable two-particle interactions both are able to reproduce the qualitative features of the polarization below 50 MeV. Pieper has even obtained a degree of quantitative agreement at energies less than 20 MeV.

The present work is motivated by the disagreement of p-d and n-d results at 22.7 MeV; by the lack of sufficient accurate data between 8 and 22 MeV; and by the recent success of theoretical calculations in this energy range.

CHAPTER III

PREVIOUS MEASUREMENTS AND THEORETICAL CALCULATIONS

3.1 Previous measurements

A number of measurements have been reported for the polarization of neutrons produced in scattering from deuterons. Compared to the case of p-d polarization, these measurements have been few in number due to the inherently greater technical difficulties encountered in neutron scattering experiments. The results for most of these experiments have been summarized by Haeberli (Ha70). Since that time only a few new measurements regarding n-d polarization at E_n < 40 MeV have been reported, namely, the work of Zamudio-Cristi, *et al.* (Za72) (Za73) at 35 MeV, and Morris, *et al.* (Mo74) at 16.8 and 21.1 MeV. The data for 35 MeV have been included here since they are relevant to this work. Table 3.1 is a summary of the available n-d polarization data near 8, 16 and 22 MeV, the region of interest for this work.

Perhaps the first attempt at comparing p-d polarization data with the charge symmetric n-d polarization was made by Barschall (Ba66) using the results of Conzett, *et al.* (Co64a) for p-d polarization, and those of Walter and Kelsey (Wa63) for the n-d polarization. However, since that time, more accurate data have become available due to improved experimental techniques. In his review article of 1970, McKee (McK70) has made the observation that the only point worth noting in the n-d polarization is the suggestion that the dip to negative values for backward angles at 22.7 MeV may be greater for n-d polarization than for p-d polarization. The recent n-d polarization data of Zamudio-Cristi, *et al.* (Za73) compared with the p-d data of Bunker, *et al.* (Bu68), both at 35 MeV, seems to confirm McKee's observation for the 22.7 MeV case.

The experimental results of Zamudio-Cristi, *et al.* (Za73) are shown in Fig. 3.1a. The asymmetry measurements were taken from 44.5° c.m. to 160° c.m. neutron angle.

TABLE 3.1

POLARIZATION IN n-d SCATTERING FROM 7.8 to 23.7 MeV

Ref.	Ta70	Br71a	Wa63	Mo74	Mo74	Ma66	Wa63
E_{inc}(MeV)	2.55	- - -	6.0	4.62	5.00	6.61	7.1
θ_1 (lab)	45	- - -	90	80	30	30	30
$P_1(\theta_1)$%	53.9±1.2	- - -	-50	50±6	35±2	46	60
E_n(MeV)	7.8	7.89	16.4	16.8	21.1	22.7	23.7
Reaction	^{9}Be(α,n)	^{9}Be(α,n)	T(d,n)	T(d,n)	T(d,n)	T(d,n)	T(d,n)
θ_2(CM)				$P_2(\theta_2)$%			
45		0.3±0.9		3.1±1.1		5.8±2.1	
59	3.7±1.2	3.8±0.9				2.7±2.5	
66				0.6±1.2			
73	5.0±1.4	5.0±1.2			-0.6±2.6		
86	7.2±1.4	3.3±1.8		0.9±1.1	-2.4±1.4	-8.4±1.9	
98	10.0±1.4	5.6±1.2		0.8±1.4	-5.7±1.5		
110	12.0±2.0	12.9±1.5		2.4±2.0	-6.6±2.1	-18.1±3.0	-12±5
120	12.5±1.7	15.3±1.5				-8.6±7.2	- 7±4
130	9.9±1.8	13.7±1.5	15±4	20.9±3.0		12.5±5.2	5±3
138	6.7±1.3	11.1±1.5	14±5		21.5±3.2	17.2±4.2	11±4
146	5.6±1.0	6.0±0.9	9±4	8.0±1.8	11.8±2.3	20.1±2.7	7±4
153	3.3±1.2	2.5±0.6				9.5±2.8	
159	2.5±1.1	1.2±1.2				7.6±2.7	
165	2.2±1.1						

The results display qualitatively the same structure as the p-d polarization data of Bunker, *et al.* (Bu68) at the same energy, but the n-d data are more negative for angles corresponding to those near the minimum of the differential cross section. Both sets of data are more negative than the theoretical value for 35 MeV (solid curve in Fig. 3.1a). The data are shown together with a theoretical curve interpolated from the calculations of Pieper (Pi72b), who gave theoretical curves at 2.0, 5.5, 10.0, 14.1, 22.7, 40.0 and 77.0 MeV. Using these values, it was possible to obtain interpolated theoretical curves at 35.0, 21.6, 16.4, and 7.9 MeV by using a computerized sline-interpolation procedure. The 35 MeV neutron beam had a polarization of $P_1(\theta_1) = 0.31 \pm 0.03$, with an uncertainty of approximately 10 per cent, and was produced by the $^2H(d,n)^3He$ reaction at 24.0° (lab.). A spin rotation magnet was used for rotating the neutron beam through an angle of 180° so that the asymmetries were measured by a stationary detector. The authors report that the backgrounds and errors have been suitably accounted for, and conclude that the difference between the p-d and n-d results appear to be real.

A direct comparison has also been made between the p-d and n-d polarizationa at 22.7 MeV laboratory energy. Garreta, *et al.* (Ga68) compared their p-d polarization measurements with the n-d polarization measurements of Malanify, *et al.* (Ma66). Here, too, the n-d data went to more negative values at the minimum near 115° c.m. for backward scattering. To this data can be added the p-d measurements taken by Faivre, *et al.* (Fa69). These results, all at 22.7 MeV, are displayed in Fig. 3.1b. The solid curve in the figure is the theoretical curve at 22.7 MeV in Pieper (Pi72b). Similarly, as in the 35 MeV case, the differences appear to be real.

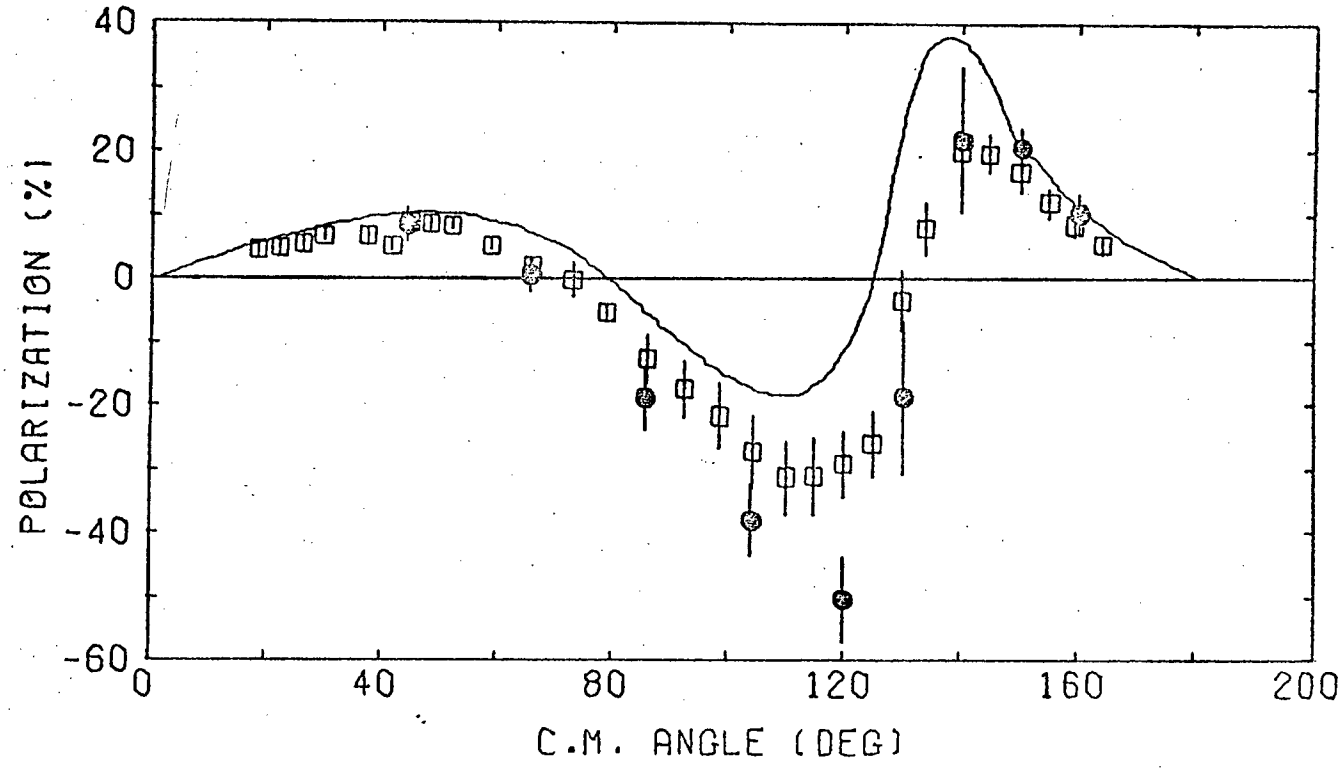

Fig. 3.1a The n-d and p-d polarization data for $P_2(\theta_2)$ plotted against c.m. angle θ for 35 MeV incident neutron energy.

● - neutrons, (Za73); □ - protons, (Bu68)

Solid curve for 35 MeV is interpolated from Pieper's calculations (Pi72b).

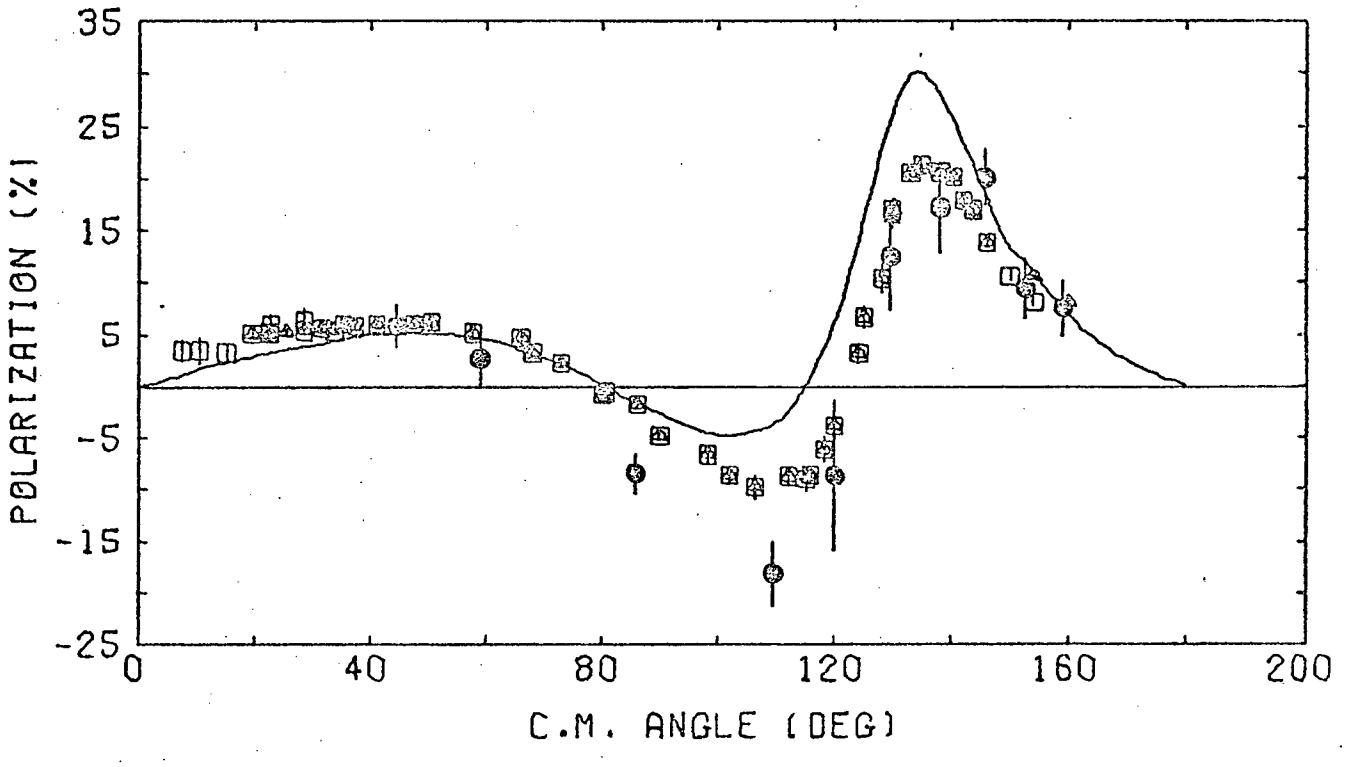

Fig. 3.1b The n-d and p-d polarization data for $P_2(\theta_2)$ plotted against c.m. angle θ for 22.7 MeV incident neutron energy.

● - neutrons, (Ma66); △ - protons, (Ga68); □ - protons, (Fa69).

Solid curve for 22.7 MeV is the calculation given by Pieper (Pi72b).

In addition to the 22.7 MeV neutron-deuteron data of Malanify, *et al.* (Ma66) mentioned above, the only other two measurements taken near this energy are the very early measurements of Walter and Kelsey (Wa63) at Wisconsin, and the more recent measurements at 21.1 MeV by Morris, *et al.* (Mo74) at Virginia. All three experiments used the T(d,n) reaction as the source of polarized neutrons, and all had a θ_1 (lab) of 30°. In addition, they all employed the method of rotating the neutron beam polarization $\pm 90^{\circ}$ so as to be either parallel or antiparallel to the normal to the n-d scattering plane, thereby cancelling 'false' instrumental uncertainties.

The Walter and Kelsey (Wa63) data at 23.7 MeV were obtained by using 7.1 MeV deuterons from a tandem electrostatic accelerator incident on a gaseous tritium target. The emitted neutrons were taken to be 60 per cent polarized (as from the mirror reaction $^{3}H(d,p)^{4}He$). The stationary deuteron scatterer was deuterium-enriched toluene (98% enrichment). The data were corrected for both multiple scattering and accidental coincidences, but no corrections were made for deuteron breakup background. It was estimated that such a correction would be of the order of 20 per cent.

For the Malanify, *et al.* (Ma66) measurements at 22.7 MeV, a 6.61 MeV deuteron beam impinging on a gaseous tritium target produced a neutron beam polarization of 46 per cent. A deuterium-enriched liquid scintillator, gross formula CD and atomic ratio H/D = 0.02, was used as a stationary scatterer. Because the experimental results were corrected for proton dilution, and because of the improved electronics, Malanify, *et al.* (Ma66) regard their data as the more reliable at this energy.

The most recent measurement of n-d polarization near 22 MeV was made by Morris, *et al.* (Mo74) at 21.1 MeV, using 5.0 MeV deuterons from a 5.5 MV Van de Graaff accelerator and a tritium-filled target. The resulting neutron beam had a polarization of 35 per cent. The scatterer was a liquid scintillator

consisting of deuterated NE213 with D:H ratio 108:1. Backgrounds measured by a two parameter background analysis ranged as large as 30 per cent of the total number of counts under the peak for scattering angles near the minimum in the cross section. Corrections to the asymmetries due to this background were assigned an uncertainty of 20 per cent. The resulting polarization measurements are similar to those of Malanify, *et al.* (Ma66) except that there is a noticable difference in the depth of the negative dip near the cross section minimum. In fact, Morris, *et al.* (Mo74) conclude that there is no evidence of violation of charge symmetry.

All available N-d polarization measurements near 22 MeV are summarized in Fig. 3.2. In order to make a comparison with the charge symmetric case, the p-d polarization data have been included. These data have been taken from the work of Faivre, *et al.* (Fa69), Megaw, *et al.* (Me68), Conzett, *et al.* (Co64a), and Garreta, *et al.* (Ga68). The general structure of the polarization exhibits a small forward positive peak, crosses over to negative values between 70° c.m. and 90° c.m., reaches a maximum negative value near 110° c.m., goes positive again between 115° c.m. and 125° c.m., and attains a saturation maximum near 0.20 for the backward peak.

It is of interest here to note the behaviour of the polarization as a function of energy. An early attempt to do so was that of Noyes (No67). In Fig. 3.3 the n-d polarization for energies near 8, 16, 22 and 35 MeV have been plotted as a function of center-of-mass angle, the curves having been fit with a draftsman's spline. Several observations can be made regarding the data: first, the negative minimum appears at approximately 18 MeV and then it moves backwards with a monotonically increasing magnitude; second, the minima for the energies greater than 20 MeV all appear to lie on a single straight line (labelled I-J in Fig. 3.3) at an angle of approximately 10° with respect to the polarization axis; third, it is seen that the angle at which

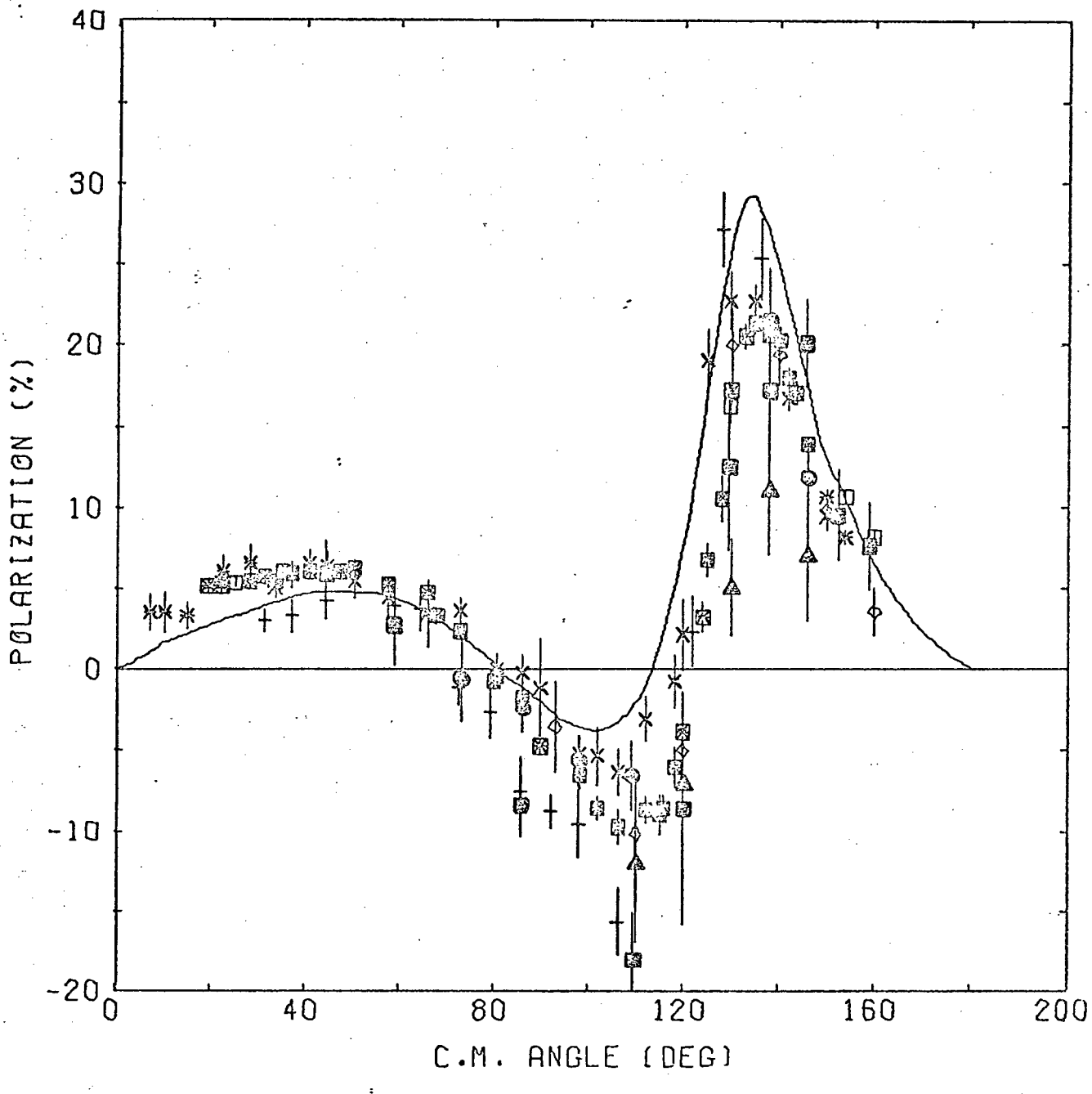

Fig. 3.2 N-d polarization data plotted against c.m. angle θ for incident nucleon energy near 22 MeV.

n-d; ▣ - 22.7 MeV (Ma66), ◍ - 21.1 MeV (Mo74), ▲ - 23.7 MeV (Wa63):

p-d; × - 20.1 MeV (Fa69), ◇ - 21.6 MeV (Me68), + - 22 MeV (Co64a),

* - 22.7 MeV (Fa69), □ - 22.7 MeV (Ga68).

Solid curve for 22.7 MeV is the calculation given by Pieper (Pi72b).

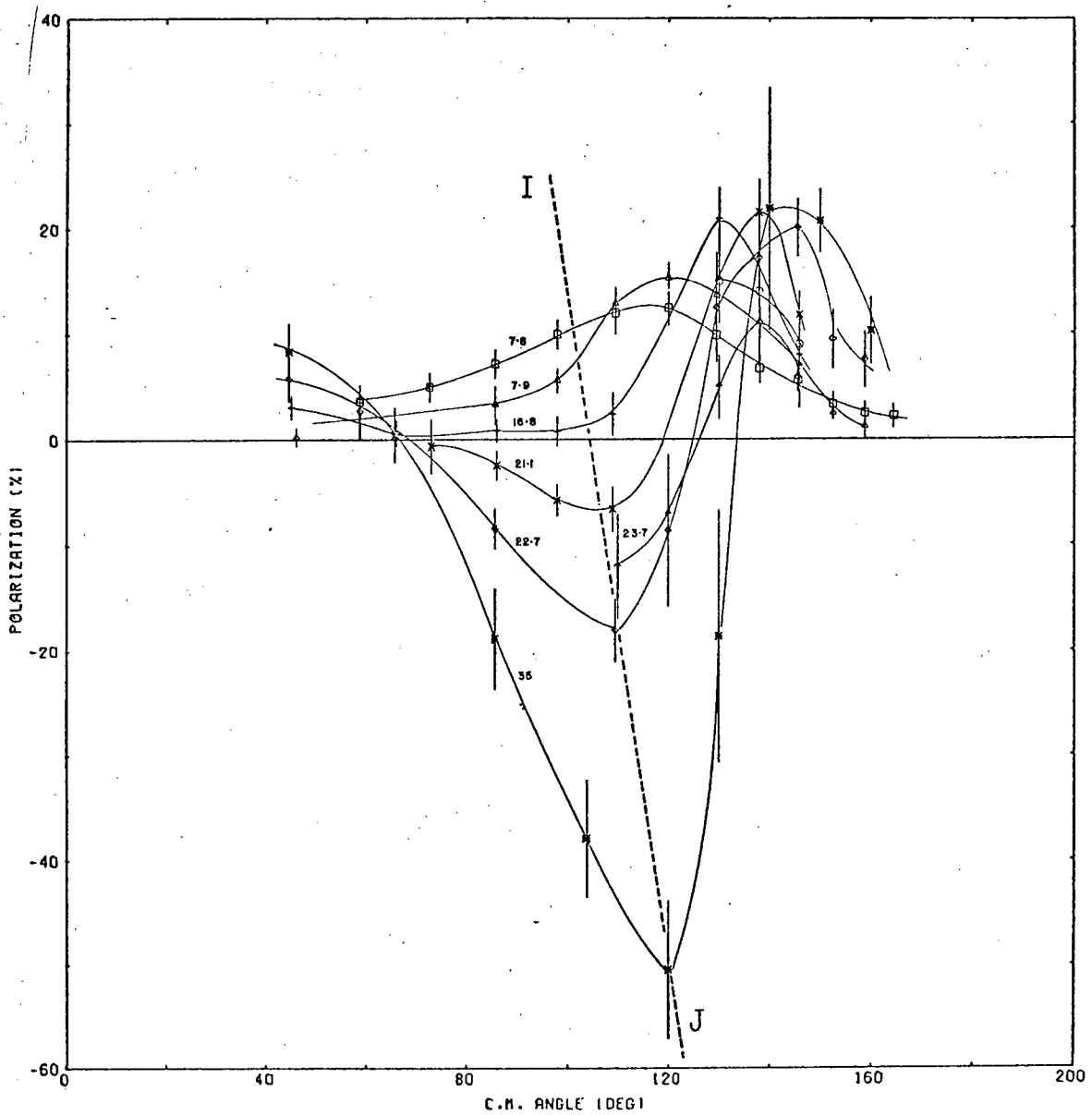

Fig. 3.3 Neutron-deuteron polarization for energies near 8, 16, 22, 35 MeV plotted against c.m. angle θ.

□ - 7.8 MeV (Ta70); Δ - 7.9 MeV (Br71a); ○ - 16.4 MeV (Wa63); + -16.8 MeV (Mo74); × - 21.1 MeV (Mo74); ◇ - 22.7 MeV (Ma66); Δ - 23.7 MeV (Wa63); * - 35 MeV (Za73).

The curves have been fitted with a draftsman's spline.

the polarization goes from negative to positive increases as the energy increases; and fourth, the backward maximum tends to move to larger angles as the energy increases, reaching a saturation value near 0.20. To this list of characteristics should be added the observation of Megaw, *et al.* (Me68) that the cross-over point from positive to negative polarization appears to be a monotonically decreasing function of energy apart from the result of Conzett, *et al.* (Co64a) at 22 MeV.

The p-d polarization measurements in the same energy range between 8 and 35 MeV are displayed in Fig. 3.4. The features of the curves agree qualitatively with those for the n-d polarization. The positive backward peak again tends to move towards larger angles with an increase in energy, as do the cross-over points for the polarization changing from negative to positive, and also from positive to negative. It is interesting to note that the negative maxima for the p-d plarization also appear to lie on the same straight line at 10° to the polarization axis (labelled I-J) in Fig. 3.4).

Megaw, *et al.* (Me68) have published a figure showing that the cross-over angle from positive to negative polarization appears to be a monotonically decreasing function of energy, with the exception of one point (Co64a). Their results are reproduced in Fig. 3.5a. All the data for this figure have been taken from p-d polarization results where there exist more measurements at forward angles (McK67), (Me68), (Co64a), (Jo66), (Bu68), (Co64b), (Gi66). From Figs. 3.3 and 3.4 it can be seen that a similar treatment of the n-d results is not possible in the absence of forward angle measurements. However, for both the n-d and p-d measurements, the polarization becomes a rapidly varying function with respect to c.m. angle in going from negative to positive polarization beyond 120° c.m. This rapid change enables the cross-over angle from negative to positive polarization to be determined more accurately than the forward positive to negative polarization cross-over angle, where the polarization function is a more slowly varying function of c.m. angle.

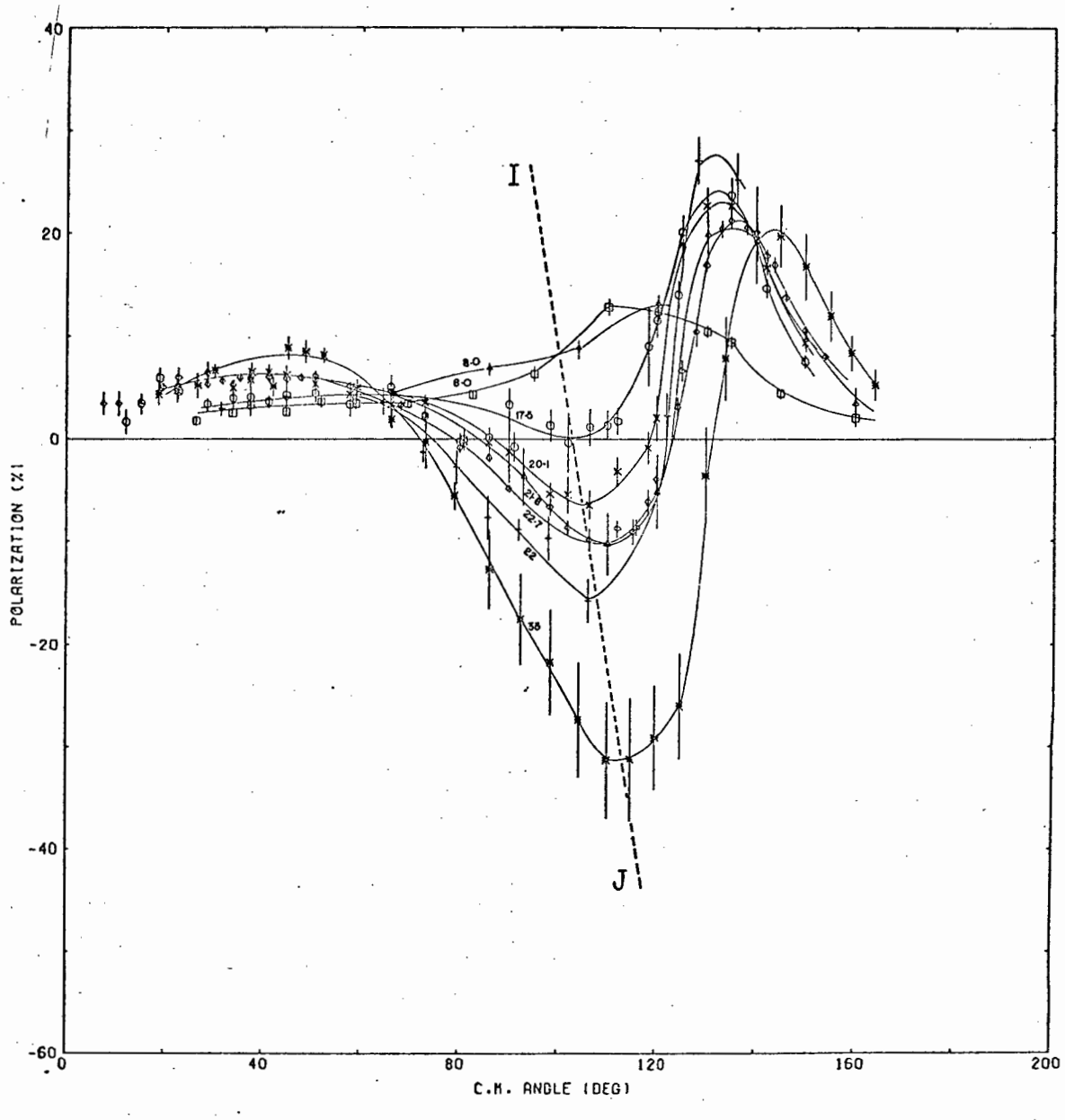

Fig. 3.4 Proton-deuteron polarization for energies near 8, 16, 22, 35 MeV plotted against c.m. angle θ.

△ - 8.0 MeV (Gr66); □ - 8.0 MeV (C67); ○ - 17.5 MeV (Fa69);
× - 20.1 MeV (Fa69); △ - 21.6 MeV (Me68); + - 22 MeV (Co64a);
◇ - 22.7 MeV (Fa69); * - 35.0 MeV (Bu68).

The curves have been fitted with a draftsman's spline.

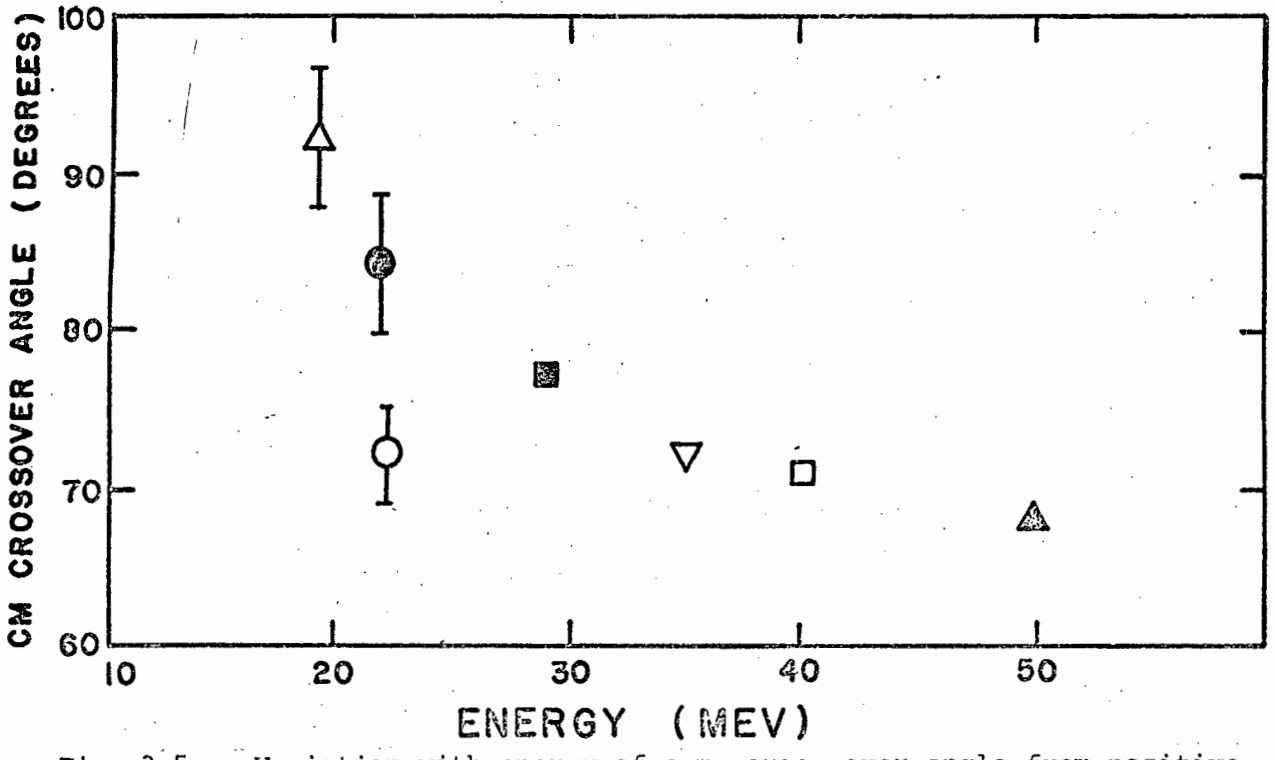

Fig. 3.5a Variation with energy of c.m. cross-over angle from positive to negative polarization in p-d scattering.

△ - 19.1 MeV (McK67); ◍ - 21.6 MeV (Me68); ○ - 22 MeV (Co64a);
▣ - 29 MeV (Jo65); ▽ - 35 MeV (Bu68); □ - 40 MeV (Co64b);
▲ - 50 MeV (Gi66) (from Me68).

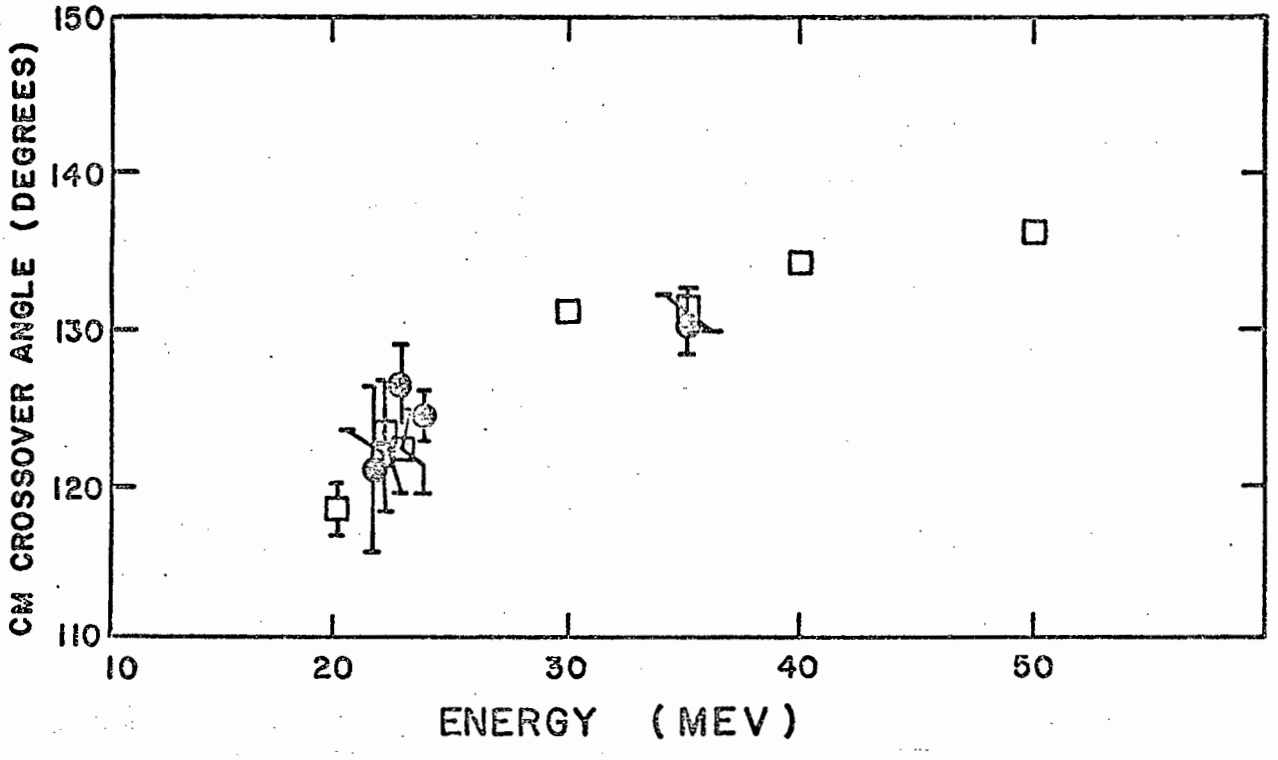

Fig. 3.5b Variation with energy of c.m. cross-over angle from negative to positive polarization in both p-d and n-d scattering.

◍ - neutrons; 21.1 MeV (Mo74), 22.7 MeV (Ma66), 23.7 MeV (Wa63), 35 MeV (Za73);

□ - protons; 20.15 MeV (Fa69), 21.6 MeV (Me68), 22 MeV (Co64a) 22.7 MeV (Fa69) (Ga68), 29 MeV (Jo65), 35 MeV (Bu68), 40 MeV (Co64b), 50 MeV (Jo66).

The results of the negative to positive cross-over angle determination are displayed in Fig. 3.5b. They show that this angle is a monotonically increasing function of energy within the energy range 20 to 50 MeV. The n-d results are indicated by the solid circles and the p-d results by the empty squares. Where error bars have been indicated they were meant to represent the error inherent in the angular resolution of the detecting device, and the estimated error in determining the exact cross-over point of the polarization. The data are from references (Mo74), (Ma66), (Wa63), (Za73), (Fa69), (Me68), (Co64a), (Ga68), (Jo65), (Bu68), (Co64b), and (Jo66).

All n-d data appear to fall on the same curve, within the indicated error bars. For practical purposes then, the cross-over angles *vs* energy reproduces for n-d polarization, the zero-polarization contour on Haeberli's p-d contour map (Ha70) from approximately 100° c.m. to 130° c.m. for E_n(MeV) from 30 to 50 MeV.

There have been only two measurements near 16 MeV for n-d polarization, that of Walter and Kelsey (Wa63) at 16.4 MeV, and that of Morris, *et al.* (Mo74) at 16.8 MeV. The 16.4 MeV measurements of Walter and Kelsey (Wa63) were obtained by using a 6.0 MeV deuteron beam and the T(d,n) reaction. The neutrons were (-)50 per cent polarized at a 90° lab angle. The quoted uncertainties in the $P_2(\theta_2)$ polarization values do not include those arising from the uncertainties in the neutron beam polarization. At the same time the measurements were made, information on the extent to which the assumption that nucleon polarizations produced in mirror reactions, as was used here, are nearly identical was not available, so the uncertainty in $P_1(\theta_1)$ was simply unknown. A change in the magnitude of $P_1(\theta_1)$ for both the 16.4 MeV and the 23.7 MeV measurements of these authors would affect the calculated polarizations by a constant multiplicative factor at all angles. The same detector system was used for

16.4 MeV as had been used for 23.7 MeV. Measurements at only three c.m. angles were taken, all being in the positive backward peak.

For the Morris, *et al.* (Mo74) measurements at 16.8 MeV, polarized neutrons at 80° (lab) were produced with the T(d,n) reaction using 4.62 MeV deuterons from a Van de Graaff accelerator. The neutron beam was (50±60) per cent polarized for the experiment. The sign of the source polarization was alternately changed by means of a superconducting magnet in order to cancel any 'false' asymmetries between the two side detectors. The scatterer was an NE213 scintillator and neutron-γ-ray discrimination was used to diminish γ-ray effects in this detector. The data were corrected for breakup reaction, multiple scattering, and accidental coincidences. Measurements were taken over the range 45° c.m. to 146° c.m.

In Fig. 3.6 a comparison is made between the 16 MeV n-d polarization data, and the closest charge-symmetric p-d data taken at 17.5 MeV by Faivre *et al.* (Fa69). The agreement is good between the n-d measurements at 16.8 MeV and the p-d measurements at 17.5 MeV; the n-d measurements at 16.4 MeV lie low compared to the p-d results for reasons mentioned above. The qualitative features of the polarization are similar to those for 22 MeV. There is a small positive forward peak, and a positive backward peak reaching a saturation value near 0.20. There is a tendency for the polarization to approach a minimum near 100° c.m.; this minimum goes negative for energies over 20 MeV. The theoretical curve is interpolated from Piepers results (Pi72b). It is clear that more n-d polarization measurements are needed at this energy.

The only two measurements which exist for n-d polarization near 7.9 MeV are those of Taylor, *et al.* (Ta70) and Brüning, *et al.* (Br71a). For the former experiment at 7.8 MeV the ^{9}Be(α,n) reaction was used as the neutron source,

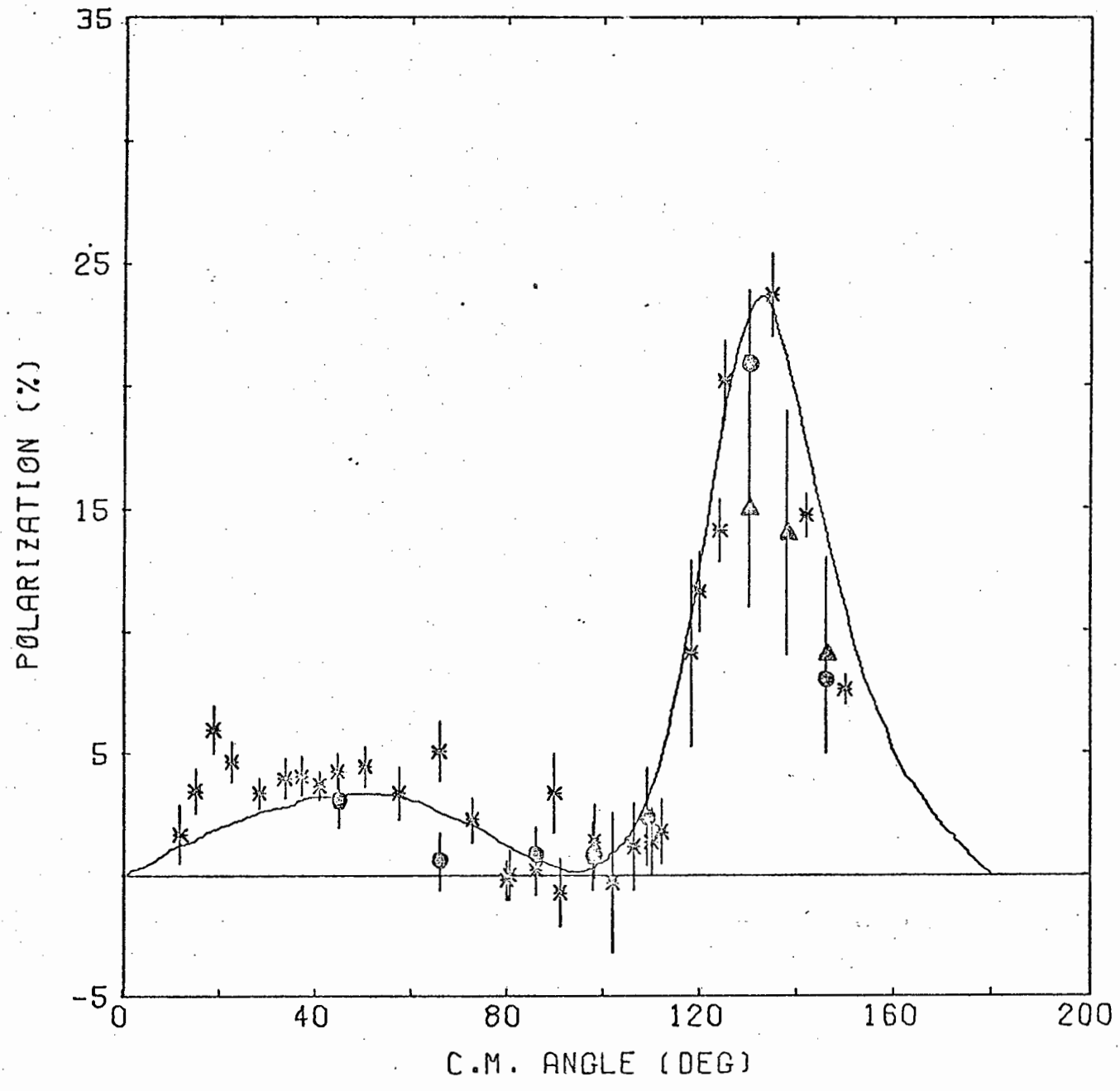

Fig. 3.6 Nucleon-deuteron polarization near 16 MeV plotted against c.m. angle θ.

n-d; ▲ -16.4 MeV (Wa63), ◉ - 16.8 MeV (Mo74);

p-d; * -17.5 MeV (Fa69).

The solid curve at 16.4 MeV is interpolated from Pieper's results (Pi72b).

having a polarization of 53.9 per cent at a reaction angle of 45° (lab) and a mean α-energy of 2.55 MeV. A deuterated liquid scintillator was used as analyzer and the asymmetries were measured over the angular range of 58° c.m. to 164° c.m. The neutron spins were precessed through 90° clockwise and counterclockwise with a solenoid allowing the roles of two side detectors to be interchanged. Deuteron breakup contributions were negligible at this energy, and the asymmetries were corrected for unpolarized backgrounds. A Monte Carlo scattering program was employed to correct for finite geometry effects and to show that the multiple scattering effects were negligible. The quoted uncertainties in $P_2(\theta_2)$ contain estimates for all known uncertainties including statistical error.

Brüning, *et al.* (Br71a) also employed the $^{9}Be(\alpha,n)$ reaction as neutron source at 7.89 MeV. This work post-dates that of Arvieux (Ar67). The detector was deuterated benzene. The polarization values obtained have not been tabulated as such, but have been presented in graphical form. In order to get the numerical results, the graph was enlarged and values were read from this enlargement. These values are presented in Table 3.1 above. It is possible that a small inaccuracy has been introduced into the data using this procedure.

In Fig. 3.7 the n-d results near 7.9 MeV are compared with the p-d measurements at 8.0 of Clegg and Haeberli (Cl67) and Grüebler, *et al.* (Gr66). The solid curve at 7.9 MeV is interpolated from Pieper's results (Pi72b). There is a simpler angular dependence in the results with the backward peak occurring at a smaller c.m. angle than is the case for higher energies. It does not reach the saturation estimate of 0.20 polarization for this energy, nor does it display a minimum value near 100° - 110° c.m. The measured polarization for n-d scattering agrees well with the charge-symmetric p-d results at 8 MeV and seems to indicate that for this energy the charge effects would probably be small. Here again, more n-d measurements are required.

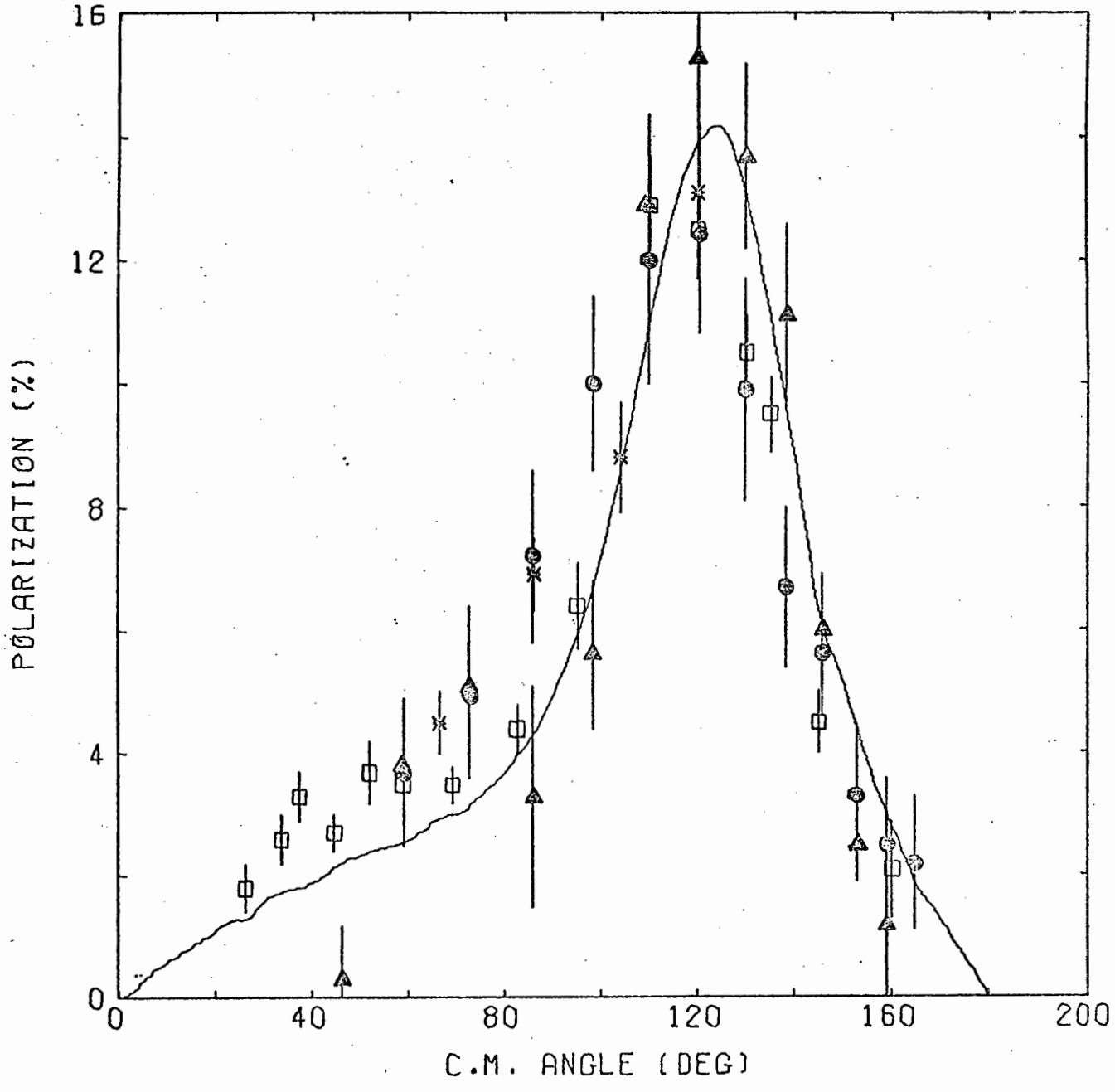

Fig. 3.7 Nucleon-deuteron polarization near 8 MeV plotted against c.m. angle θ.
n-d; ● - 7.8 MeV (Ta70), ▲ - 7.9 MeV (Br71a);
p-d; □ - 8.0 MeV (C167), * - 8.0 MeV (Gr66).
The solid curve at 7.9 MeV is interpolated from Pieper's results (Pi72b).

There have been n-d polarization measurements made below 8 MeV. A summary of the work is found in the following references: (El62) at 0.5, 1.0, 1.95 MeV; (Fe62) at 0.5, 1.0 MeV; (Be63a) at 1.0, 1.15 MeV; (Be63b) at 1.0 MeV; (Da60) at 1.0, 2.0 MeV; (Sm70) at 1.2 MeV; (Wa63) at 1.9, 6.0 MeV; (Cr59) at 2.1 MeV; (Wh58) at 2.26, 3.1 MeV; (Bu59) at 2.3, 3.1, 3.9 MeV; (Ja71b) at 2.6 MeV; and (Sc65) at 3.83, 4.57 MeV. The polarization data reported in these references support the qualitative descirption that the energy dependence of the polarization is consistent with zero below 5 MeV for all angles, although some early references indicated significant positive results. This energy range is outside the region of interest for this work.

3.2 Theoretical calculations.

The first theoretical calculations capable of reproducing the main qualitative features of polarization, with respect to both the angular and the energy dependence, were performed by Krauss and Kowalski (Kr70a), (Kr70b). The reasons for doing these calculations were that the polarizations were experimentally determined, and so the theoretical results could be directly compared and, theoretically, the behaviour of $P_2(\theta_2)$ was thought to place significant constraints on the structure of the scattering matrix itself. Both phenomenological considerations of $P_2(\theta_2)$ at energies up to 40 MeV have been reasonably successful and have indicated the possibility of relatively simple processes being responsible for the observed behavior of the polarization (Hu65), (Pu68). The primary reason for the lack of theoretical calculations prior to this work has been the prohibitive number of coupled integral equations which appear when introducing the necessary noncentral, tensor forces.

Three approximate methods have been proposed in order to exploit simplicities arising from the weak binding of the deuteron, the viabilities of which did not depend on special models of the two-particle interaction. All three of these procedures have the common feature of being unitarization techniques via the optical model, K-matrix, and N/D formalisms.

Krauss and Kowalski's investigation consisted of using Sloan's K-matrix method (Slo67) (Slo68) for calculating $P_2(\theta_2)$, and the elastic differential cross sections in the energy range of 11-40 MeV. As seen in Sec. 3.1 above, the experimental exploration of this region shows that $P_2(\theta_2)$ undergoes a pronounced variation between the extremes of this energy interval and therefore should provide an excellent test for computing $P_2(\theta_2)$. Also, the incident neutron energies are just large enough compared to the deuteron binding energy for approximations to three-particle dynamics to be justified, yet small enough to permit the incorporation of only the smallest amount of the two-particle interaction necessary for the introduction of tensor forces. The simplest, separable Yamaguchi forms (Ya54) for the S-wave singlet (^1S) and the S- and D-wave triplet ($^3S + ^3D$) nucleon-nucleon partial wave states were used for the calculations, the latter giving 7% D-state mixture for the deuteron bound state (McK70) (No68).

As a first effort this predicted polarization from 11-40 MeV was in reasonably fair qualitative agreement with the p-d experimental results of Faivre, *et al.* (Fa69) from 11-23 MeV, and with the results of Bunker, *et al.* (Bu68) and Conzett, *et al.* (Co64b) at 40 MeV. That is to say, the evolution of the negative dip with the increase in energy was predicted, although it remained too small in magnitude. The prediction for the small forward peak was fair, but for the positive backward peak was too low, presumably because it was correlated with the over-estimates of the large angle minimum in the cross sections of these authors. Their principal conclusion was that Sloan's K-matrix technique is a usable method for doing calculations on the N-d problem although they are complicated by the tensor forces.

Following this work, Aarons and Sloan (Aa72a) had calculated nucleon-deuteron polarizations in the range 11-23 MeV using the same unitary first order approximation, and exactly the same interactions and parameters of Krauss and Kowalski. The polarizations obtained at 11, 17.5 and 22.7 MeV were compared both to the

theoretical results of Krauss and Kowalski (Kr 70a) (Kr70b) and the experimental results of Faivre, *et al.* (Fa69).

These results of Aarons and Sloan (As72a), despite the fact that these authors used exactly the same techniques as the first authors, are entirely different, and disagree entirely with the measured experimental results. This disagreement also is reflected in the cross section calculations performed by Aarons and Sloan (Aa72a). The main objection to the Krauss and Kowalski computations was the cutting off of the partial wave expansion at too low a value in the total angular momentum J (Pi72a). This however, could not account for the nonreproducibility of results.

In another set of papers Aarons and Sloan (Aa72b) (Slo72c) have attempted to calculate polarizations over an energy range of 3-23 MeV. In the first paper exact calculations were performed using a non-central, spin-dependent, separable two-body interaction force having two separable terms. It was found that the model did not explain vector polarization since the results were very small compared to the measured results, plus of the wrong shape. In the second paper calculations were performed for the separable (^1S) and ($^3S + {}^3D$) potentials; first, using the Yamaguchi form factor as in the first paper, and second, taking into account the short range N-N interaction term. It was again found that changing the form factors and per cent D-state contribution had little effect on the polarizations. As before, the model did not predict the vector polarizations.

Pieper and Kowalski (Pi72a) recalculated the N-d polarizations and cross sections in the first order unitary model at 14.1, 22.7 and 40 MeV using a number of more realistic N-N input. Even then it was concluded that the Sloan approximation could not predict the N-d polarizations, since there occurred a strong dependence on the inclusion of P-wave N-N interaction potentials. The conclusions drawn by these authors were two:

first, the Sloan approximation isn't capable of predicting N-d polarizations at low energies, and second, any attempt to explain polarization in N-d scattering at low energies either by 'exact' or approximate three-body calculations, must include P-wave, two-nucleon amplitudes. In this regard, the P-wave component actually appears to be more significant than the tensor component of the $S = J = 1$ two-nucleon interaction.

A two potential formula based on the Alt, Grassberger and Sandhas equations (Al67) for three-body scattering was proposed by Pieper (Pi72b). In this technique the S-wave part of the N-N interaction was treated exactly and the P- and D-wave contributions were treated in first order. The energies for the calculations were from 2.0 to 77.0 MeV. The computed vector polarizations agreed well with the experimental results up to 14 MeV but above this value discrepancies appeared, becoming more severe with the higher energies. At 22.7 and 40 MeV the general features of the polarizations are still well-produced, except that the negative dip is too small in magnitude, while the positive backward peak is much larger than the saturation value of 0.2 expected from the experiment. At much higher energies the method becomes questionable since even the forward diffraction peak is not correctly predicted.

The breakdown in this method at the higher energies is attributable to several factors. At these energies first order perturbation theory may no longer be adequate, and it is precisely this perturbation that gives rise to the polarization. The potentials employed may not adequately represent the two-nucleon interaction at higher energies. There was no D-state in the deuteron.

Much work has been done on the polarization effects in N-d scattering by Doleschall (Do72a), (Do72b), (Do72c), (Do73), (Do74). From the work of others it became clear that both the P-wave term and tensor force had to be included for an adequate reproduction of the experimentally determined

polarizations. In his recent investigations Doleschall (Do74) constructed a different set of P-wave interactions and rank-2 tensor forces for performing calculations at 22.7 MeV neutron laboratory energy. The conclusions reached in the case of separable N-N T-matrices were that the three-nucleon scattering states do not depend significantly on the high energy on-shell N-N T-matrix, and that the polarizations were rather sensitive to the tensor force because of its low energy behavior.

To date no specific attempt has been made to calculate polarizations near 16 MeV. The closest theoretical values were the early ones of Krauss and Kowalski (Kr70b) and Aarons and Sloan (Aa72a) at 17.5 MeV which were compared to the experimental work of Faivre, *et al.* (Fa69).

Deductions regarding the polarization of nucleons below the breakup threshold were initially performed by Arvieux (Ar67) at 7.85 MeV and also at other energies. The scattering matrix for the N-d scattering was parameterized in terms of phase-shifts. The results were then applied to a phase-shift analysis of p-d scattering, including the polarizations. However, there occurred an error in the sign of the even-ordered observables so the results were invalid. The calculations were redone using the same formalism as Arvieux by Brüning, *et al.* (Br71a) for 7.89 MeV. The fitting procedure was such that the splitting of the quartet-P and D phases was obtained.

The only other calculation performed in this energy neighborhood is that of Purrington and Gammel (Pu68) at 9 MeV. The calculations involved a five parameter fit using the $(^4S_{3/2})$ and $(^2S_{1/2})$ eigenvalues. The mixing parameters coupling the S- and D-states were adjusted empirically as was the deuteron D-state admixture. The calculated polarizations of Purrington and Gammel (Pu68) at 9.0 MeV (solid curve) and of Brüning, *et al.* (Br71a) at 7.89 MeV (dashed curve) are shown in Fig. 3.8. The experimental data with

which they are compared are the same as in Fig. 3.7. It can be seen that both the curves are reasonably good fits although the Purrington and Gammel curve at 9.0 MeV lies lower than the Brüning, *et al.* (Br71a) curve at 7.89 MeV.

3.3 Other evidence of violation of charge symmetry

Differences in the polarizations between the charge symmetric scatterings n-T and p-^{3}He have also been found (Ha70), (Se70), (Wa69). In his review of the three- and four-nucleon system McKee (McK70) has indicated that the significant feature of these particular charge symmetric scatterings is that the neutron polarizations are greater in magnitude than the corresponding proton polarizations at all angles except for the cross-over point of 112° c.m. where both are zero.

Finally, it has recently been reported (Ze74) that for kinematically complete experiments on the reaction ^{2}H(n,2n)^{1}H neutron-neutron and neutron-proton final state interactions are observed. The experiments were analyzed with three-body calculations using different form factors for the nucleon-nucleon interactions. The analysis with a complete charge-dependent calculation using exponential form factors gave $a_{nn} = (-)16.3\pm1.0$ f.m. for the ($^1S_0$) neutron-neutron scattering length. The difference of this value to the neutron-proton length is reported to be about seven standard deviations.

3.4 Summary

It has been demonstrated that the n-d polarization measurements which already exist do not clarify the situation regarding breaking with charge independence. There is some evidence that there may be some breaking to a small degree; namely, the n-d polarization measurements of Zamudio-Cristi, *et al.* (Za73) at 35 MeV as indicated in Fig. 3.1a, and the n-d polarization

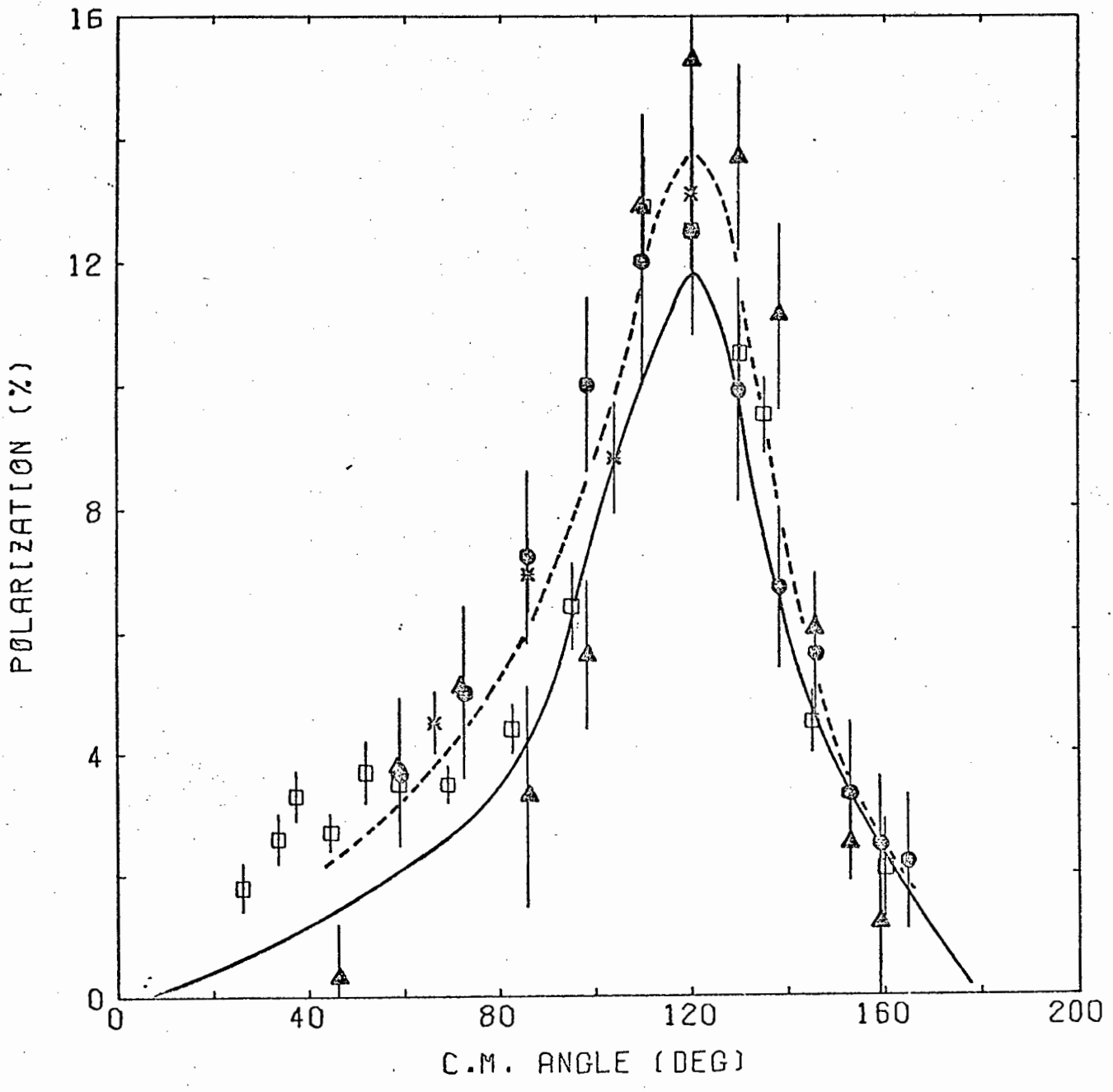

Fig. 3.8 Nucleon-deuteron polarization near 8 MeV plotted against c.m. angle θ.
n-d; ◍ - 7.8 MeV (Ta70), ▲ - 7.9 MeV (Br71a);
p-d; □ - 8.0 MeV (Cl67), * - 8.0 MeV (Gr66).
The solid curve is the calculation due to Purrington and Gammel at 9.0 MeV (Pu68) and the dashed curve is the calculation due to Brüning, *et al.* (Br71a) at 7.9 MeV.

measurements of Malanify, *et al.* (Ma66) as shown in Fig. 3.1b. In addition, there are the results of the charge symmetric scatterings n-T and p-^{3}He as reported in references (Ha70), (Se70), (Wa69), and the measurement of the neutron-neutron scattering length reported by Zeitnitz, *et al.* (Ze74).

On the other hand, there is no indication of breaking with symmetry either in the 7.9 MeV n-d polarization data of Taylor, *et al.* (Ta70) and Brüning, *et al.* (Br71a), or in the 16 MeV n-d polarization results of Walter and Kelsey (Wa63) and Morris, *et al.* (Mo74). Also, in the more recent measurement of n-d polarization at 21.1 MeV by Morris, *et al.* (Mo74), there is no indication of breaking with symmetry. Clearly, then, there is a need for more measurements of n-d polarization.

CHAPTER IV

THE EXPERIMENT

4.1 Introduction.

The polarization experiments discussed in Chapter III relied on the interchangeability of two detectors for the asymmetry measurements. In this work the left-right asymmetry was observed using the anisotropic scintillation properties of a deuterated anthracene crystal. Before making asymmetry measurements the anisotropy properties of the crystal were investigated.

It has been established that certain scintillation crystals, especially anthracene, stilbene, and quaterphenyl (Bi67), (He59), (He61a), (He61b), (Ki61), (Ki62), (Ki67), have a relatively longer scintillation decay time for heavily ionizing particles like protons and α-particles than for electrons. In particular, crystalline anthracene has slow scintillation decay, high scintillation response, and a directional anisotropy of these properties (Ts62). This directional anisotropy of the scintillation decay has been the basis for using anthracene crystals as a neutron polarimeter (Br74b). The technique of pulse shape discrimination (PSD) (Br58) has been used to sense the direction of proton recoils from n-p scattering within the crystal, thereby providing a means for determining the asymmetries in n-p scattering. This method has been used previously for studying the polarizations in n-p scattering at neutron energies of 16.4 and 21.6 MeV.(Br71b) (Br74b) (Jo74).

This work is an extension of that reported in references (Br71b) (Br74a) (Br74b) and (Jo74) where natural anthracene was used as the neutron polarimeter. Here, it was determined whether a similar method could be used to study polarization in n-d scattering; that is, the asymmetry of deuteron recoils from n-d scattering within the deuterated crystal was determined.

4.2 The deuterated anthracene crystal

The crystal used in this investigation was especially made by Nuclear Enterprises (G.B.), Edinburgh, Scotland. Deuterated anthracene enriched to an isotopic purity of 98 per cent was supplied by Prochem Ltd., Croydon, Surrey, England. The material was repurified to scintillation grade at Nuclear Enterprises and a crystal was grown in the form of a right cylinder of dimensions 10 mm (diam.) x 21 mm (height) and mass 2.4077 g.

Comparisons were made between different geometries and methods of optical coupling between the crystal and photomultiplier cathode. It was found that direct coupling of crystal to cathode via either of the end faces of the former gave very non-uniform light collection. The most effective coupling was obtained using a small polished lucite light-pipe (Fig. 4.1a). in which the crystal was mounted with its cylindrical axis parallel to the photocathode. The interfaces between crystal and light-pipe and between light-pipe and cathode were optically coupled by means of silicone fluid (DOW Corning 200 Fluid, viscosity grade at 25^{o} C 10^{6} c.s.). Diffuse reflector (NE562) painted on aluminium foil was placed over (but not optically coupled to) the light-pipe.

The quality of the pulse height resolution obtained from the deuterated anthracene crystal in this mounting is illustrated by pulse height spectra taken using ^{137}Cs and ^{60}Co γ-ray sources (Fig. 4.1b). The single Compton edge of the ^{137}Cs curve corresponds to the 0.66 MeV γ-ray energy, whereas the spectrum taken with ^{60}Co shows two distinct Compton edges corresponding to the two γ-ray energies of 1.17 and 1.33 MeV, from this source.

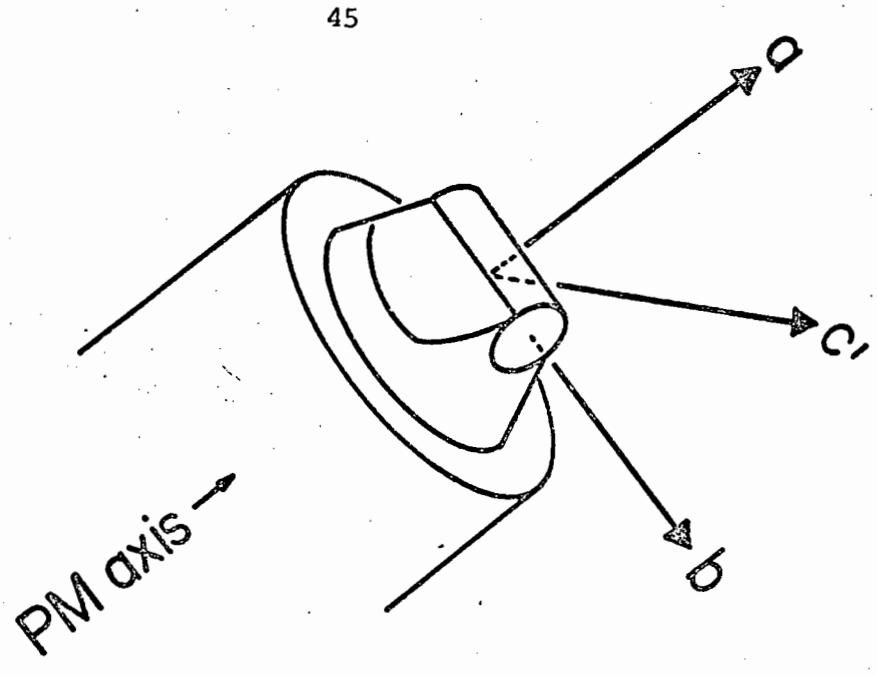

Fig. 4.1a Deuterated anthracene crystal mounted in light-pipe.
This figure shows the deuterated crystal axes a, b and c' as defined in the text.

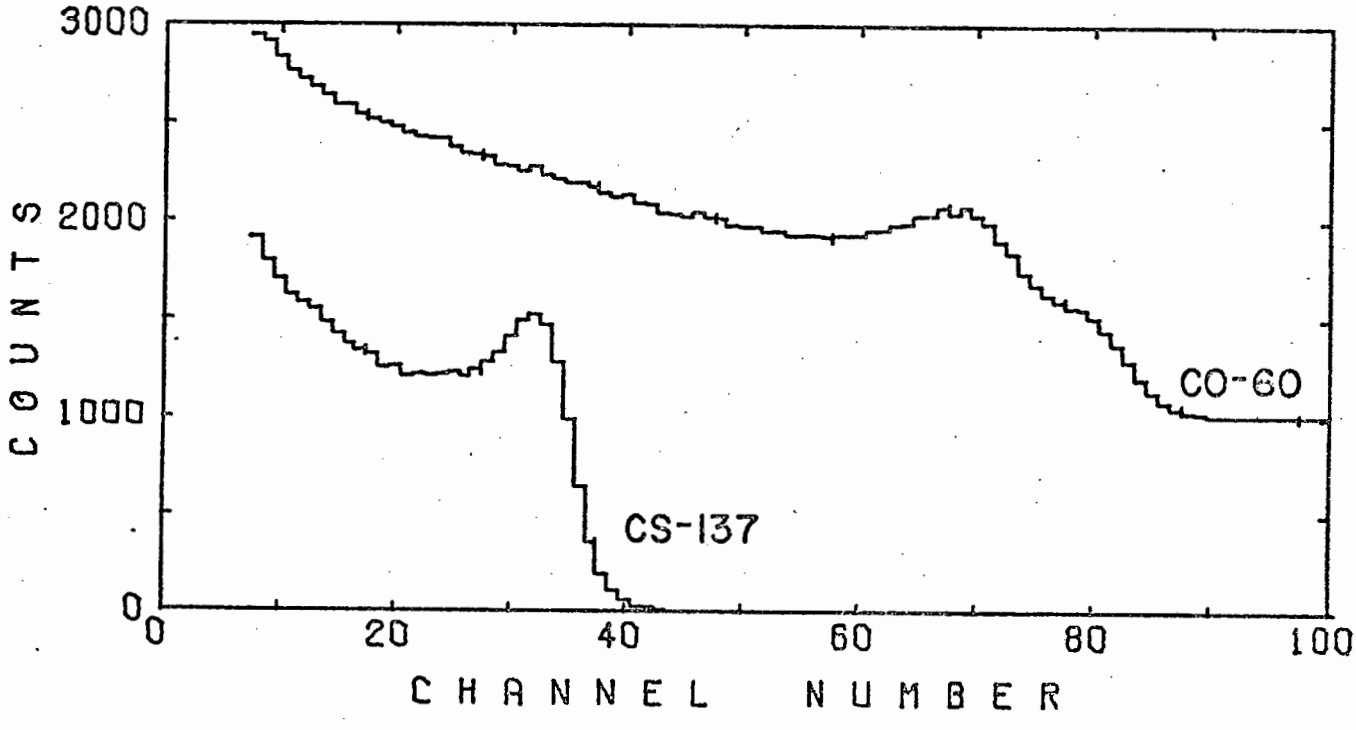

Fig. 4.1b Pulse height spectra for deuterated anthracene crystal.
The quality of pulse height resolution for the deuterated anthracene crystal is illustrated by pulse height spectra taken with ^{60}Co and ^{137}Cs γ-ray sources. The ^{60}Co spectrum shows two distinct Compton edges corresponding to the two γ-ray energies of 1.17 and 1.33 MeV from this source, and the ^{137}Cs spectrum shows the single Compton edge of the 0.66 MeV γ-ray of ^{137}Cs. The count rates for both curves are arbitrary.

The reference directions for the anisotropy properties of anthracene are the crystal axes, specifically the mutually perpendicular '*a*' and '*b*' axes (Ts62) (Ts65) (Br74a) and the so-called artificial *c'*-axis, defined as perpendicular to the *ab*-plane. Therefore, the *a*-, *b*- and *c'*-axes give a cartesian reference frame for describing the directional dependence of scintillation properties. The directions of these axes were not determined explicitly either for the present deuterated crystal or for the natural anthracene crystals used in the above-mentioned work with anthracene (Br74a). However, the work of others (He59) (He61a) (He61b) (Ts65) and (Ol68) on anthracene had previously indicated that the minimum and maximum pulse height responses L were obtained for ions travelling in the directions of the *b*- and *c'*-axes. Therefore, the reference directions used in the present work were established in terms of initial measurements of beam directions which gave minimum and maximum L-responses. These initial measurements showed that the direction of minimum-L (*b*-axis) lay parallel to the cylindrical axis of the deuterated crysal and that the direction of maximum-L (*c'*-axis) lay approximately perpendicular to the cylindrical axis, as would be expected. Thus, when mounted in the light-pipe as shown in Fig. 4.1a, the *b*-axis lay perpendicular to the photomultiplier axis. A standard mounting in the light-pipe was adopted, whereby the crystal was rotated about its cylindrical axis until the direction of maximum-L (*c'*-axis) was perpendicular to the plane defined by the photomultiplier axis and the cylindrical axis of the crystal. In this mounting, therefore, the *a*-axis of the crystal was aligned parallel to the photomultiplier axis.

For convenience, a polar co-ordinate frame, called the 'crystal frame', was further defined. In this crystal frame the photomultiplier axis is the polar axis ($\theta = 0^{\circ}$) and the cylindrical axis of the crystal is taken as the polar azimuthal axis ($\phi = 0^{\circ}$). This crystal frame forms the reference frame for the anisotropy measurements of the scintillation properties. The crystal

frame defined in this work for the deuterated anthracene crystal does not coincide with that used previously for anthracene. For the deuterated crystal the polar and aximuthal axes of the crystal frame coincide with the a-axis and b-axis, respectively. For the anthracene crystal (Br74a) (Br74b) the polar axis coincided with the artificial c'-axis of the crystal and the azimuthal axis made a 40°-angle with the b-axis.

4.3 Neutron production

The neutron beams used for this work were obtained from the three reactions T(d,n), D(d,n) and ^{9}Be(α,n). The incident particles were produced by the 5.5 MV CN Van de Graaff pulsed accelerator of the Southern Universities Nuclear Institute (S.U.N.I.), Faure, Cape. The accelerator is equipped with a Klystron bunching system (F157) which delivers a pulsed beam of approximately 2 ns duration at a frequency of 2 MHz for a deuteron beam. The accelerator is capable of beams currents of 5 μA; for this work a beam current of 2 μA was used throughout. The beam energy was monitored by a nuclear magnetic resonance (NMR) probe inserted into the field of the 90° analyzing magnet of the accelerator. The calibration of the NMR probe was periodically checked by observing the threshold (1.881 MeV) of the ^{7}Li(p,n)^{7}Be reaction (Gi60) (Go63) (Ma63).

Both the tritium and deuterium targets were gaseous, and were operated at an average pressure of 0.8 atmosphere. The tantalum-backed cells were 10 mm in length and were separated from the accelerator vacuum by Havar foil windows of thickness 3.52 mg-cm^{-2}. These targets were kept cooled by a pressurized jet of air directed at the cell. The ^{9}Be target was a 279 μg-cm^{-2} thick layer of natural beryllium deposited on a tantalum backing, and was made locally. The subject of targets and their windows used for the production of neutrons has been treated extensively by Coon (Co60). Methods of obtaining polarized fast neutrons and the currently best sources are discussed by Walter (Wa71).

The pulsed-beam time-of-flight method was used for selecting the primary component in the neutron spectrum from whichever reaction was being used. For the D(d,n) reaction which was used for calibrating the deuterated crystal, the flight path was 2.00 m, while for the polarization measurements using the T(d,n) and ^{9}Be(α,n) reactions, the flight path was 0.5 m and the timing resolution obtained was 4-9 ns FWHM. Separate high resolution time-of-flight measurements had been made previously (Jo72) (Pa73) in order to examine the neutron spectra from the T(d,n) and D(d,n) reactions under various experimental conditions; namely, bad beam optics, the effects of shielding, and good beam optics with no shielding. From these earlier measurements it was determined that open geometry should be used for this experiment.

The deuteron beam used in this experiment was readily available. However, it was necessary to develop a technique at this time for producing the α-particle beam used for the ^{9}Be(α,n) reaction. This was very ably accomplished by the S.U.N.I. accelerator group (Kr72) (Kr73). With the availability of the cross-field analyzer for particle selection and because the use of hydrogen resulted in a long life for the filament coating, a beam of singly charged ^{4}He was extracted from the duoplasmatron by using a mixture of gases to the proportion of 25 per cent helium (monatomic) and 75 per cent hydrogen (diatomic). This gas mixture was sufficient for producing a pulsed α-particle beam with currents similar to those obtained with the deuteron beam.

The energy loss from the incident beam for each target has been determined (Ma60) (Ma68) and is shown graphically in Fig. 4.2 for an incident particle energy range from 1 to 6 MeV. The thickness of the beryllium deposit corresponded to an energy loss of approximately 50 keV (Aj60) for an α-particle beam of 2.55 MeV incident energy. Thus the average α-energy (E_{α}) in

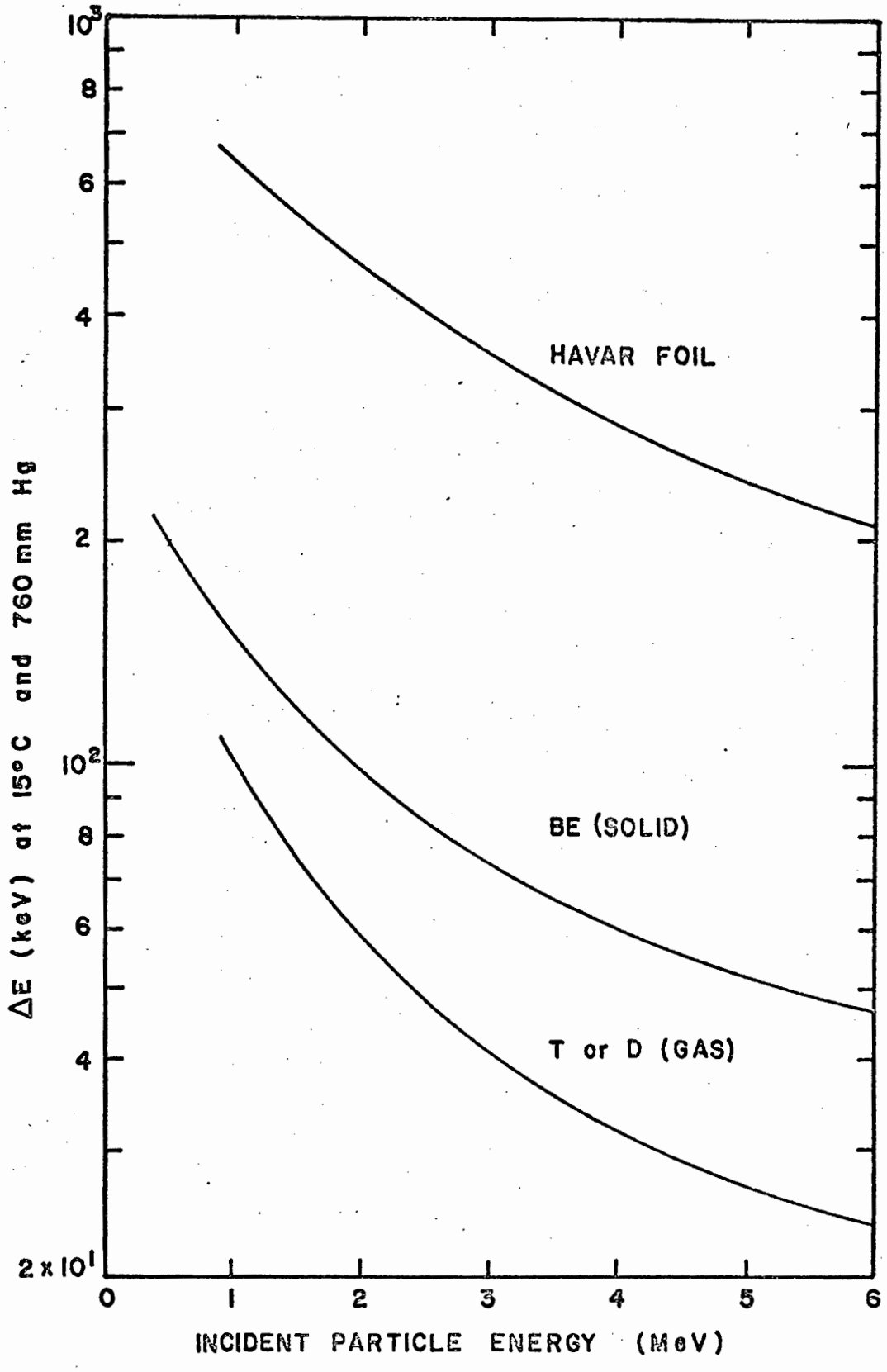

Fig. 4.2 Total energy loss for incident beam particles in target materials. The values of ΔE in (keV) are shown for different target materials as a function of incident particle energy. The upper curve represents the energy loss of deuterons in the 3.52 mg-cm^{-2} thick Havar foil used for the gaseous targets while the lowest curve represents the energy loss in the target gas. The middle curve represents the energy loss of α-particles in the solid Be target 279 μg-cm^{-2} thick.

the target was 2.50 MeV. Therefore for a laboratory angle of 40° with respect to the α-beam, the neutrons were emitted with a mean energy (E_{n_o}) of 7.85±0.02 MeV, as extrapolated from the data of reference (St70).

For the gas targets employing a thin Havar foil window (Cr71) (Mo71) the energy loss for the Havar alloy was calculated (Ma60) (Ma68) (Wh58b) using the four main constituents of the alloy, Cr, Fe, Co, and Ni, and assuming the additivity of stopping effects. According to Porter, *et al.* (Po70) results calculated in this manner would be approximately 15 per cent higher than any experimentally determined values. The energy loss for deuterons in gases of the hydrogen isotopes (tritium and deuterium) has been determined from reference (Ma60).

The incident particle energy for the D(d,n) reaction was 4.50 MeV, the energy loss in the target 250 keV, giving a mean energy of 8.0 MeV for the emitted neutrons. The T(d,n) reaction used 5.20 MeV deuterons and had an energy loss of 270 keV. Here the mean neutron energy at 20° (lab) was 21.6 MeV, and at 80° (lab) was 16.4 MeV. Both the D(d,n) and T(d,n) reactions have been thoroughly discussed by such authors as Brolley and Fowler (Br60) and Goldberg (Go63).

Time-of-flight spectra have been obtained for all three reactions used in this experiment. The spectrum for the D(d,n) reaction used in calibrating the deuterated crystal is shown in Fig. 4.3 for a flight path of 2.00 m and was taken at 0° neutron angle of emission. A strong γ-ray peak is seen but there is also a strong neutron peak of 8 MeV mean energy. While obtaining the time-of-flight spectrum the PSD portion of the electronic circuitry was not operative, but during the actual running, a time-of-flight window was set on the neutron peak; this window included some of the prompt γ-rays which were then separated from the neutron group by the PSD circuitry.

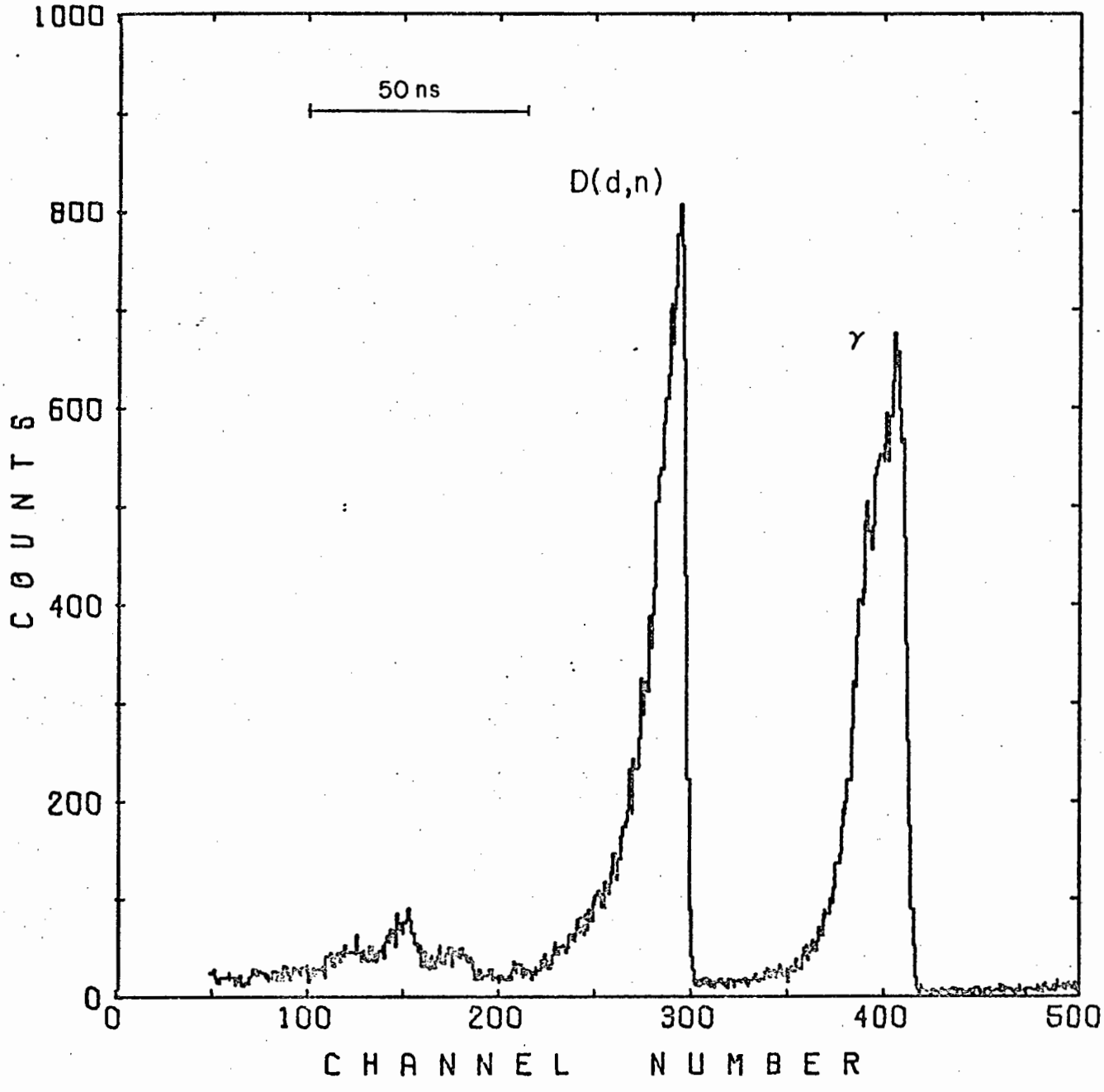

Fig. 4.3 Time-of-flight spectrum for 8 MeV neutrons from the D(d,n)^{3}He reaction for the deuterated crystal calibration.
The spectrum was recorded without PSD gating at a flight path of 2.0 m during the anisotropy calibration runs.

4.4 Electronics

The crystal assembly was optically coupled to a magnetically shielded RCA 6810 A photomultiplier tube, selected because of its favourable dark noise spectrum and high quantum efficiency. The base of the tube was equipped with a voltage divider chain similar to that of Hyman, *et al.* (Hy64) so chosen as to preserve linearity over a wide dynamic range. The dynode potential divider circuit is shown in Fig. 4.4. Circuit components were chosen to preserve voltage stability to better than one per cent for peak currents of 10 ma at dynode thirteen. Detailed accounts of the design of photomultipliers are given in the following references (Hy64) (Be63c) (Be64) (RCA70) (PHI70).

The pulse shape discrimination (PSD) circuit (Br59) was coupled to the base of the detector as indicated in Fig. 4.4. Three pulse outputs, designated 'fast', L, and S, were taken from the photomultiplier circuitry. The 'fast' output operated the time-of-flight system, the amplitude of the 'linear' output L indicated the total light in the scintillation and the amplitude of the PSD output S indicated the 'shape' of the scintillation which is a function of the decay times of light emission, and therefore of the nature of the particle.

Optimum timing resolution ($\sim$ 2 ns) was obtained with constant fraction timing discriminators (ORTEC 463). This permitted 22 MeV neutrons to be resolved from the γ-rays at the flight path of order 0.5 m. Because of a high γ-ray count a pile-up rejector (Canberra 1464) was introduced into the circuitry to prevent distortion of accumulated spectra.

The electronic circuit used for processing the photomultiplier output signals is shown in Fig. 4.5. The arrangement is similar to that used in previous work (Br74a) (Br74b) (Jo72) (Pa73). The 'fast' electronics on the left of

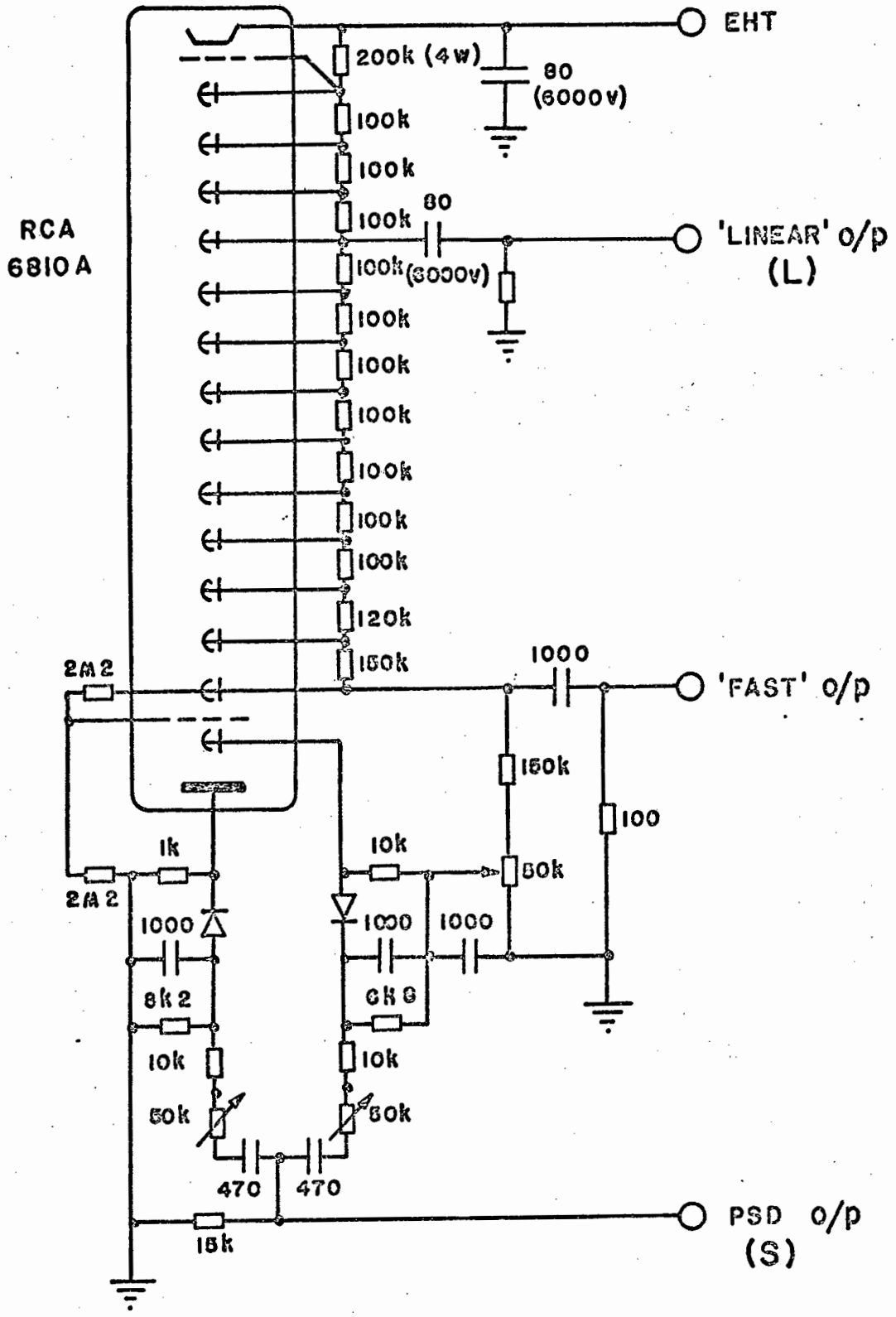

Fig. 4.4 Pulse shape discrimination circuit.

The dynode chain potential divider and pulse shape discrimination circuit was used with a magnetically-shielded RCA 6810 A photo-multiplier tube, the electronics being encased in the detector housing.

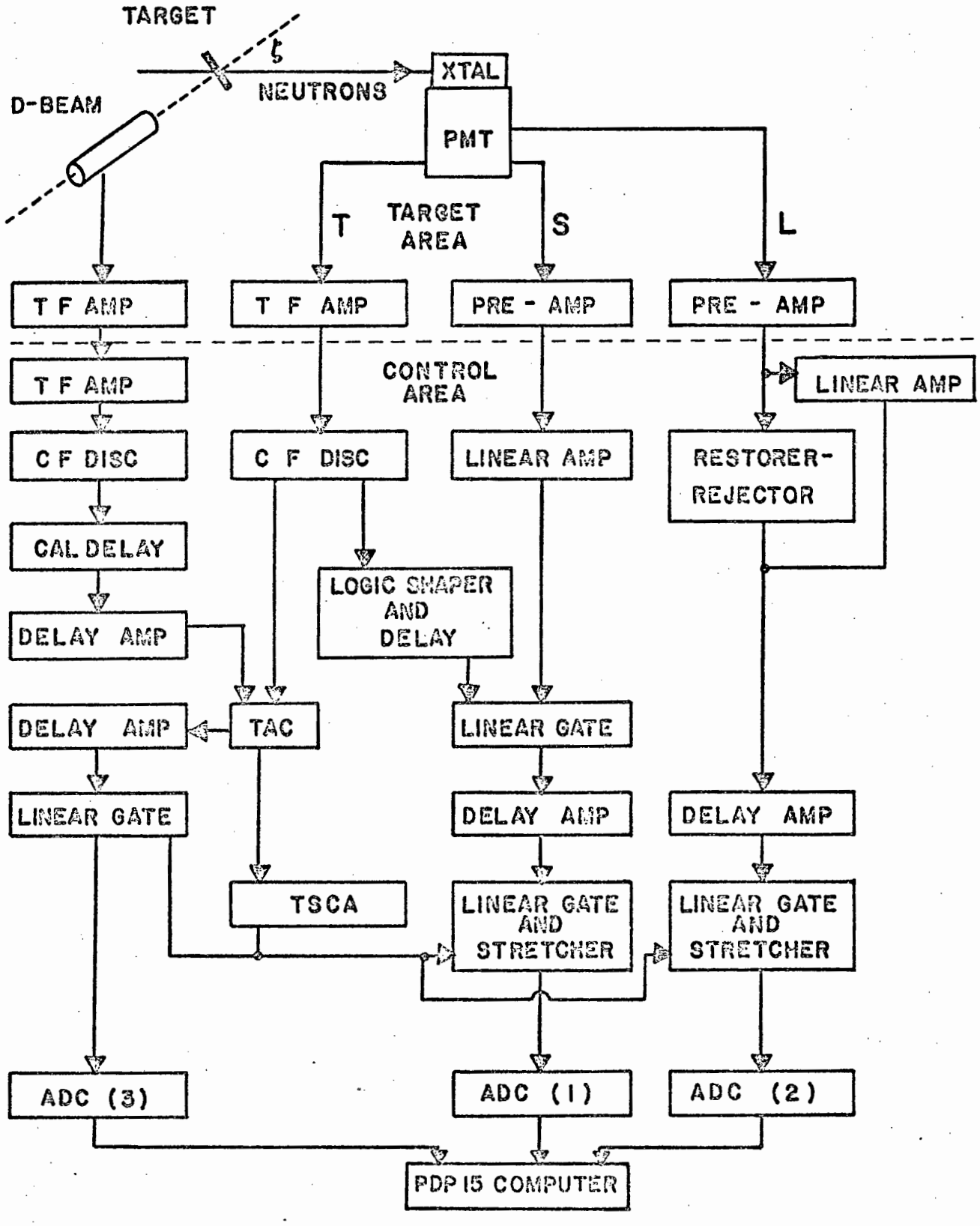

Fig. 4.5 The block diagram of the electronic system.

The 'fast' electronics on the left of the diagram were used for operating the time-of-flight system, and the 'slow' electronics on the right produced the L and S pulses which were analyzed in the computer to obtain LS-spectra.

the diagram were used for operating the time-of-flight system, and the 'slow' electronics on the right produced the L and S pulses. The events falling within a window set on the primary neutron peak in the time-of-flight spectrum were accumulated in a two-parameter LS-spectrum of counts versus L versus S. The LS-spectra, accumulated in a PDP 15 data acquisition system, were transferred to magnetic tape for processing on the UNIVAC 1106 at the University of Cape Town.

Throughout the running of the experiment the beam current was monitored by a current integrator (B165) and the neutron flux by a long counter (Ha47). These monitors provided consistency checks and reduced possible systematic uncertainties. The total number of trigger pulses arriving at the linear gate was counted for each run, the time for each run was monitored, and the total number of events occurring within the time window was also monitored.

4.5 Anisotropy of scintillation properties

The direction dependences of L and S for deuterated anthracene are illustrated by the LS-spectra shown in Figs. 4.6 and 4.7, which were obtained using incident neutrons of energy 21.6 MeV. Fig. 4.6 shows isometric plots obtained at two mutually perpendicular orientations of the crystal to the neutron beam. The orientations are those which gave maximum (Fig. 4.6a) and minimum (Fig. 4.6b) pulse height responses L respectively. The two orientations correspond to mutually perpendicular directions to the neutron beam. The orientation giving the minimum L (Fig. 4.6b) is that in which the cylindrical axis of the crystal is aligned parallel to the neutron beam. It is from this observation, together with the assumption that the anisotropy properties of deuterated anthracene are similar to those of anthracene (Ts62) (Br74b), that it was deduced that the *b*-axis of the deuterated crystal lies parallel to its cylindrical axis. It was similarly assumed that the orientation at which maximum L is observed (Fig. 4.6a) is that in which

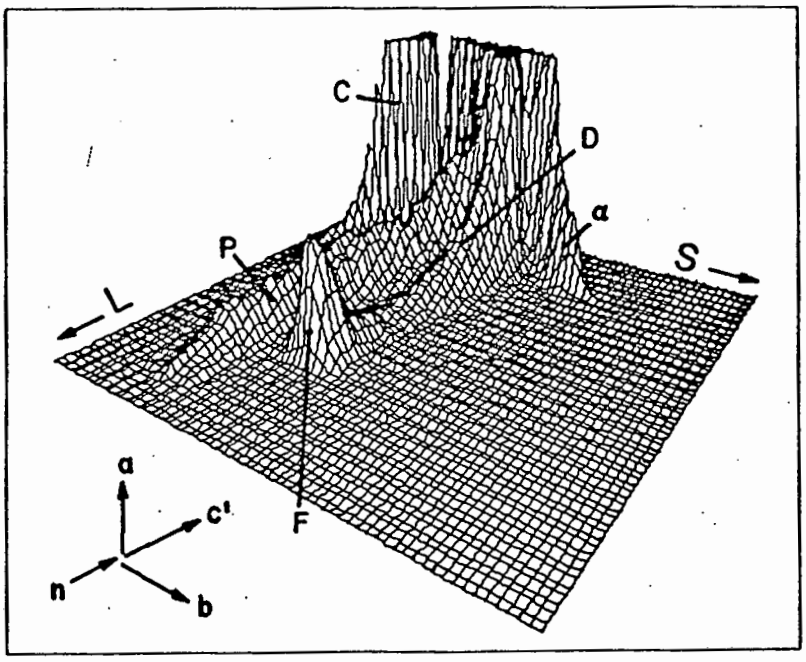

Fig. 4.6a LS-spectrum for 21.6 MeV neutrons directed parallel to the *c'*-axis of the deuterated anthracene crystal (maximum-L orientation). The ridges are due to: Compton electrons (C); breakup protons (P); recoil deuterons (D); and α-particles (α) from reactions on carbon. The peak F corresponds to forward recoiling deuterons.

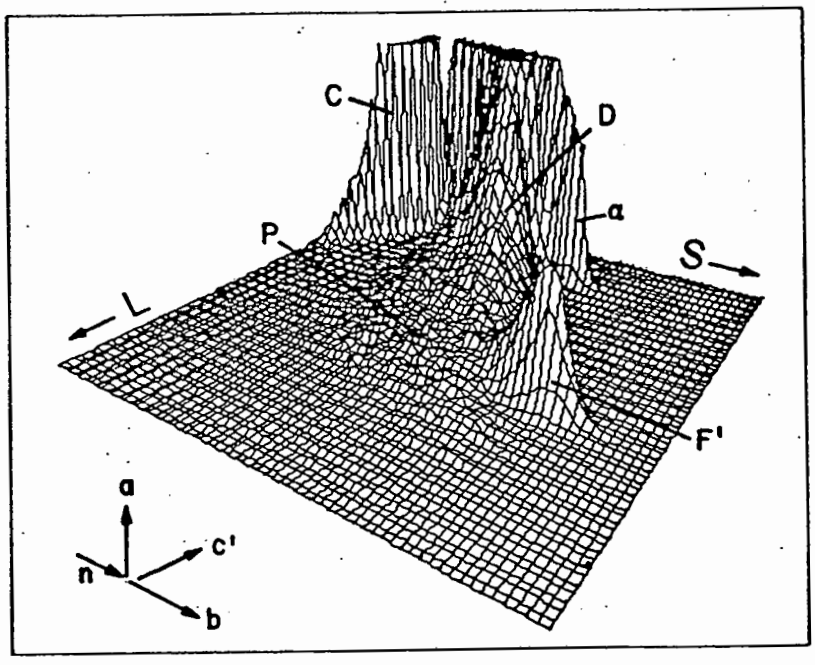

Fig. 4.6b LS-spectrum for 21.6 MeV neutrons directed parallel to the *b*-axis of the deuterated anthracene crystal (minimum-L orientation). The ridges are due to: Compton electrons (C); breakup protons (dispersed) (P); recoil deuterons (D); and α-particles (α) from reactions on carbon. The peak F' corresponds to forward recoil deuterons.

the artificial c'-axis of the crystal is aligned parallel to the neutron beam. The standard mounting of the crystal (Fig. 4.1a) can therefore be defined as that in which a rotation of 90° about the photomultiplier axis will transform from the orientation of maximum L to that of minimum L, or vice versa. The a-axis of the crystal is therefore expected to coincide with the photomultiplier axis in the standard mounting. For convenience the orientations giving the minimum L and maximum L are referred to as the b- and c'-orientations respectively, the reference therefore indicating that the neutron beam is assumed to be aligned parallel to the corresponding crystal axis in each case.

Figs. 4.7a and 4.7b show contour plots of the LS-spectra displayed in Figs. 4.6a and 4.6b respectively. Much of the structure in the spectrum at the c'-orientation (Figs. 4.6b and 4.7b) is similar to that observed for anthracene (Br74b), at the corresponding orientation. The observed ridges can be attributed (Br74b) to the following: Compton scattering (C); alpha particles (α) from the reactions on the carbon component of the crystal; and the elastic scattering ridge, consisting in this case of recoil deuterons (D). In addition there is a proton ridge (P) attributed to the deuteron breakup reaction D(n,p)2n, and a proton-escape ridge (E). The different components C, α, D, P and E in Fig. 4.6a are clearly distinguishable over much of the pulse height range L, illustrating the good PSD characteristics of the deuterated crystal at the c'-orientation.

The proton, deuteron, and alpha components are not clearly resolved in the spectrum (Figs. 4.6b and 4.7b) taken at the b-orientation. These results are also consistent with those obtained for anthracene where the relatively good PSD resolution obtained at the c'-orientation could be understood (Br74b) in terms of the detailed directional dependence of the scintillation properties

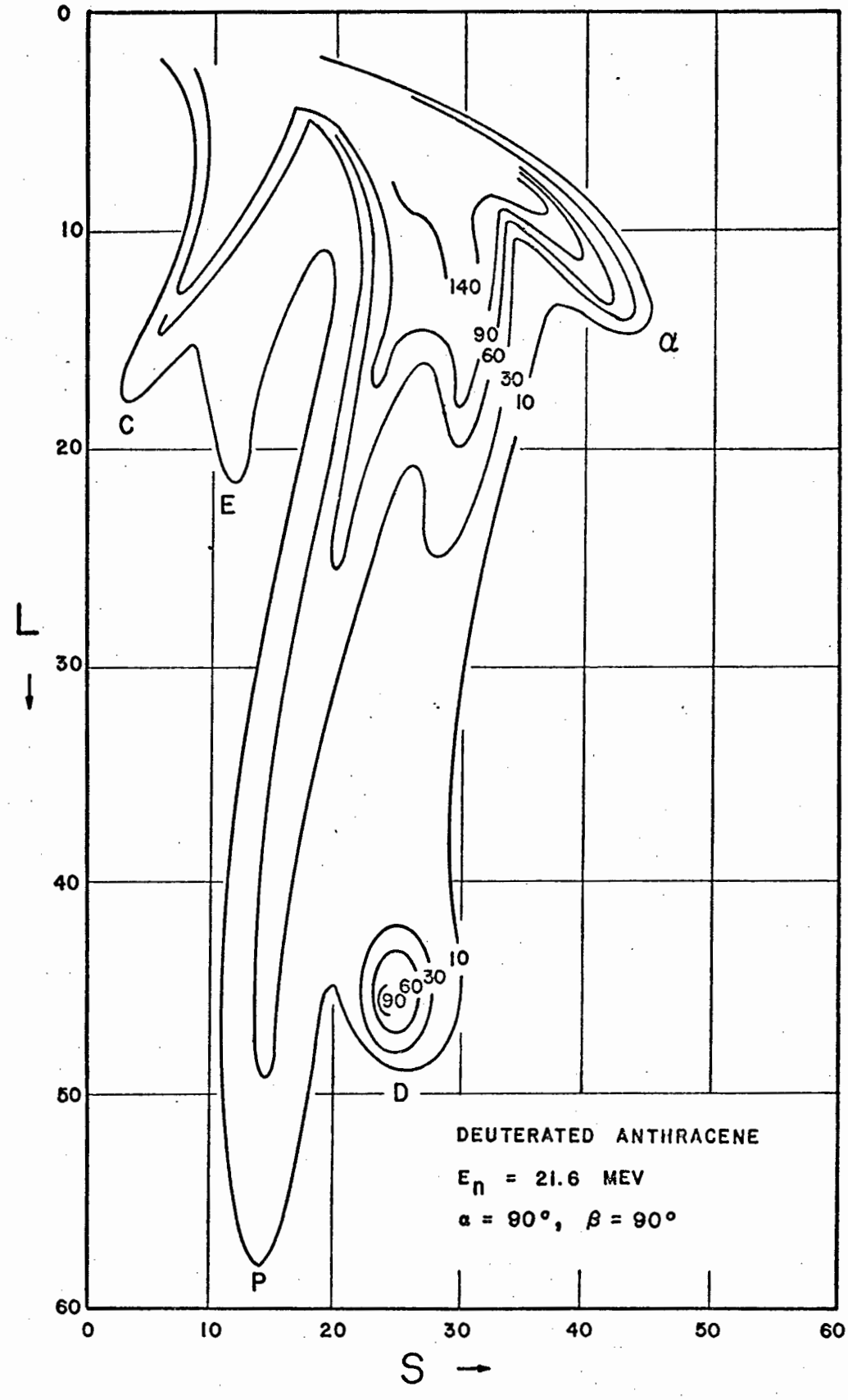

Fig. 4.7a Contour plot of an LS-spectrum for 21.6 MeV neutrons on the deuterated anthracene crystal at maximum-L orientation.

The above is a contour plot of the isometric display in Fig. 4.6a. The symbols C, P, D, α, and E indicate that the corresponding ridges are due to Compton electrons, breakup protons, recoil deuterons, α-particles from reactions on carbon, and proton escapes. The relative count rate is given for each contour level.

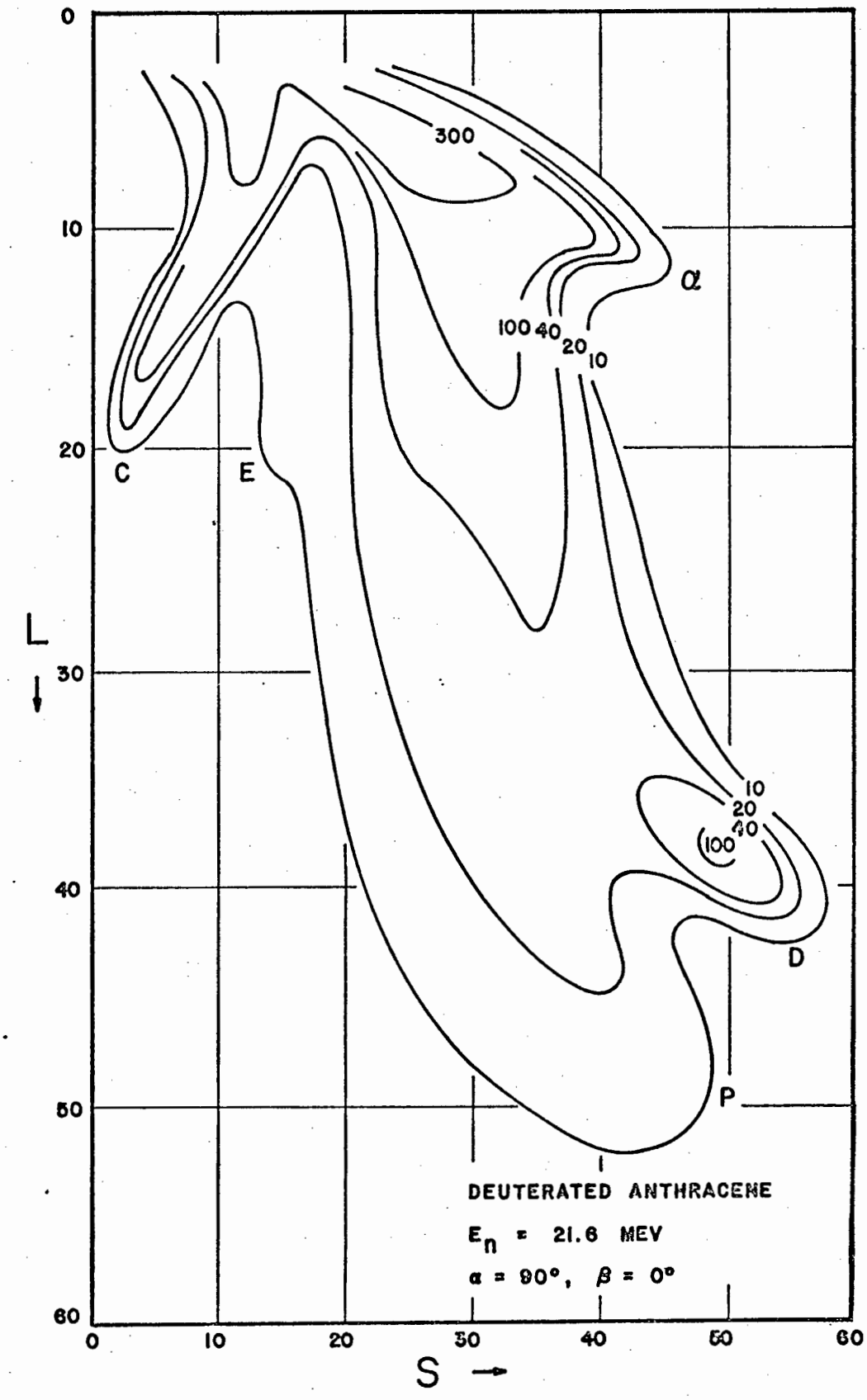

Fig. 4.7b Contour plot of an LS-spectrum for 21.6 MeV neutrons on the deuterated anthracene crystal at minimum-L orientation.

The above is a contour plot of the isometric display in Fig. 4.6b. The symbols C, P, D, α, and E indicate that the corresponding ridges are due to Compton electrons, (dispersed) breakup protons, recoil deuterons, α-particles from reactions on carbon, and proton escapes. The relative count rate is given for each contour.

of that crystal. The c'-axis of the crystal approximates more closely than any other direction to an axis of symmetry for the directional dependence of the PSD output 3. The kinematics of nuclear reactions and scattering restrict the directions of product or recoil nuclei of a particular energy to the surface of a cone with the neutron beam as axis. Thus at the c'-orientation deuterons or protons of a particular energy are dispersed in directions which tend to uniform S responses, and the loci of the corresponding particles are consequently relatively well-defined in the LS-plane. The opposite is true for the b-orientation since the b-axis of the crystal approximates very poorly to an axis of symmetry for the direction dependence of the PSD output.

The characteristic forward and backward peaking in the angular distribution for n-d elastic scattering are also manifested (Figs. 4.6 and 4.7) in the peaking of the deuteron ridge (D) at its low-L and high-L extremities, respectively. The high-L limit of the deuteron ridge corresponds to forward recoiling deuterons and the characteristic deuteron peak in this region corresponds to the backward peak in the n-d differential elastic cross section. The sharp cutoff on the high-L side of the deuteron peak is of particular interest. Firstly, it illustrates the good pulse height resolution of the crystal and, secondly, the coordinates of the ridge give a measure of L and S for a well-defined deuteron direction and energy, i.e., forward recoils. The recoil deuteron energy at the edge is given by

$$E_d = 4M_dM_n/(M_d + M_n)\,E_n = \frac{8}{9}\,E_n \qquad \ldots (4.1)$$

where E_n is the neutron energy.

The directional dependence of L and S at different deuteron energies E_d may therefore be studied by using monoenergetic neutrons of the appropriate energy E_n given by Eq. 4.1, observing the LS-spectrum at different orientations to the neutron beam and recording the coordinates of the edge of the deuteron peak in each spectrum. As previously (Br74b), but with slightly modified

notation, the pulse height anisotropy A_L and the directional resolving power R are defined as follows:

$$A_L = (L_{c'} - L_b)/\langle L \rangle_{bc'} \quad \ldots (4.2)$$

and

$$R = |S_{c'} - S_b|/\langle \Delta S \rangle_{bc'} \quad \ldots (4.3)$$

where L is the L-coordinate of the edge of the deuteron peak, the subscripts c' and b denote the orientation of the crystal, and brackets $\langle\rangle_{bc'}$, denote averages of measurements at the b and c' -orientations. The PSD outputs $S_{c'}$ and S_b in Eq. 4.3 represent the centroid S values of the deuteron ridge at the constant pulse height $L = L_b$. The term ΔS in the denominator of the same equation denotes the full-width at half-maximum of the deuteron ridge at $L = L_b$.

Measurements of A_L and R at four energies in the E_d range 3-20 MeV are listed in Table 4.1 and plotted in Fig. 4.8.

TABLE 4.1

ANISOTROPIES VERSUS DEUTERON ENERGIES FOR DEUTERATED ANTHRACENE CRYSTAL

E_d (MeV)	3.02	6.93	14.58	19.20
A_L	0.257	0.241	0.198	0.143
R	0.52	2.3	3.6	6.0

The results of the detailed study of the directional dependences of L and S at E_d = 7 MeV are presented in the section below.

4.6 Direction dependences of L and S for 7 MeV deuterons

The direction dependences of L and S at E_d = 7 MeV were studied using the forward recoils from an 8 MeV neutron beam produced by the $D(d,n)^3He$ reaction.

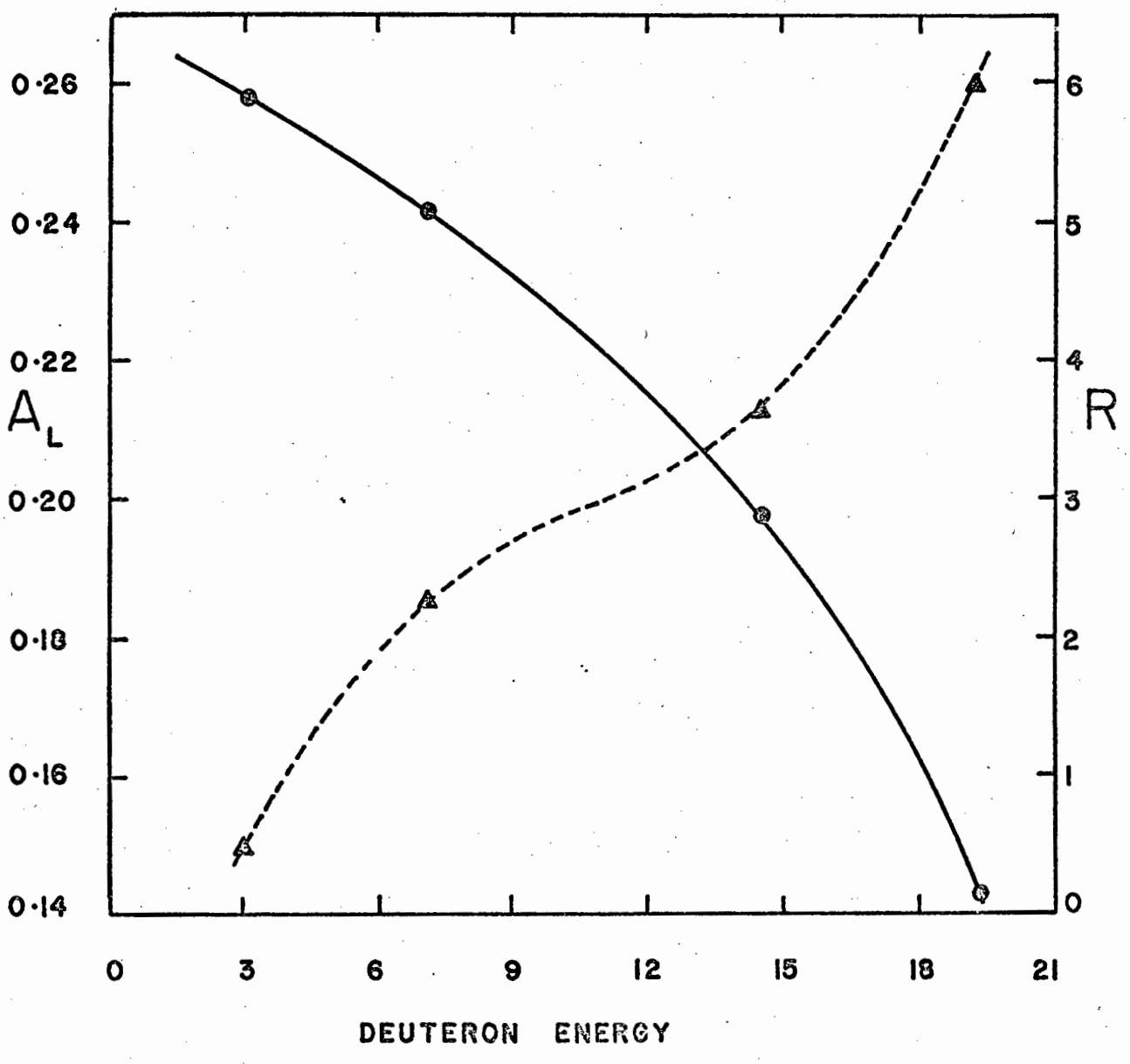

Fig. 4.8 Pulse height anisotropy A_L and resolving power R for deuterated anthracene as a function of recoil deuteron energy.

Circles (solid curve) represent the pulse height anisotropy and triangles (dashed curve) represent the resolving power R.

LS-spectra were obtained over a range of 200° in steps of 20° for θ and over a range of 240° in steps of 30° for φ, thus giving coverage over a solid angle in excess of 2π. These measurements included several complementary pairs which confirmed that the pulse height was backward-forward invariant for the opposing directions (θ,φ) and (π - θ, π + φ). This identity was then assumed for the rest of the data and used to extend the contour plots over the full 4π solid angle range.

The data used for the calibration were corrected for the long-term electronic drifts that were periodically monitored. The true zero for the L-parameter which is linear, was ascertained by running two LS-spectra with the crystal oriented for the maximum response. The second spectrum was obtained at an L-amplifier (as in Fig. 4.5) gain set to one-half that of the first spectrum. All data were appropriately adjusted for this zero-correction. The results obtained at θ = 0° were checked for consistency for all values of φ.

The directional dependence of the pulse height L(θ,φ) was studied by observing the high-L value at which the forward-recoil deuteron peak dropped to half-amplitude for different orientations (θ,φ) of the crystal. The directional dependence of the PSD amplitude S(θ,φ) was studied by comparing PSD amplitudes S at a constant pulse height, L_{min}, the latter pulse height being the minimum observed limit of the high-L at half-amplitude, for the different crystal orientations (θ,φ). All L values obtained in this manner were plotted as a function of θ for the different values of φ, and conversely, as a function of φ for the different values of θ as a consistency check. All S values were treated in a similar fashion. L and S were found to vary smoothly (approximately sinusoidally) with either θ or φ. This was also the case for anthracene (Br74a). Data obtained for deuterated anthracene at E_d = 7 MeV (corresponding to E_n = 8 MeV) are presented in contour plots of L(θ,φ) and S(θ,φ) in Figs. 4.9 and 4.10.

4.7 Discussion

These data in Figs. 4.9 and 4.10 together with those in Table 4.1, show that the pulse height anisotropy and PSD anisotropy properties of deuterated anthracene are indeed similar to those of anthracene but do exhibit small differences. The directions corresponding to the maxima or minima of L or S were found to be independent of the deuteron energy in the crystal, and so the directional properties of the crystal were defined in terms of these maxima and minima. The pulse height anisotropy, A_L, has been defined by Eq. 4.2, and the directional resolving power R by Eq. 4.3. A_L is a measure of directional variation of the pulse height relative to the average pulse height. Using the Rayleigh criterion, a value of R exceeding unity means that the PSD anisotropy is suficient to distinguish deuterons recoiling in the mutually perpendicular directions corresponding to the maximum or minimum PSD outputs. It is seen from Table 4.1 and also Fig. 4.8, which gives both A_L and R as a function of recoil deuteron energy, that the deuterated crystal satisfies this criterion for deuteron energies exceeding about 4 MeV. Interpretations of the anisotropies have been given by various authors (Bi67) (Br74a) (Br74b) (Jo72) (Bo61).

A point of particular interest, revealed by results of this experiment, is the different symmetry properties of the L and S anisotropies of deuterated anthracene. As can be seen from Fig. 4.10 the S-anisotropy is symmetric about the $\phi = 0^\circ - 180^\circ$ line whereas the L-anisotropy, as can be seen from Fig. 4.9, does not show such a symmetry. This is in contrast to the results for natural anthracene where the L and S anisotropies showed similar symmetry properties. An L-anisotropy plot which is symmetric about $\phi = 0^\circ - 180^\circ$ may be obtained for the deuterated crystal by transforming the data of Fig. 4.9 to a different coordinate frame, other than the crystal frame, namely, a frame whose polar axis is oriented at direction $\alpha = \theta = 25^\circ$, $\beta = \phi = 270^\circ$ in the crystal frame. Such a plot is shown in Fig. 4.11.

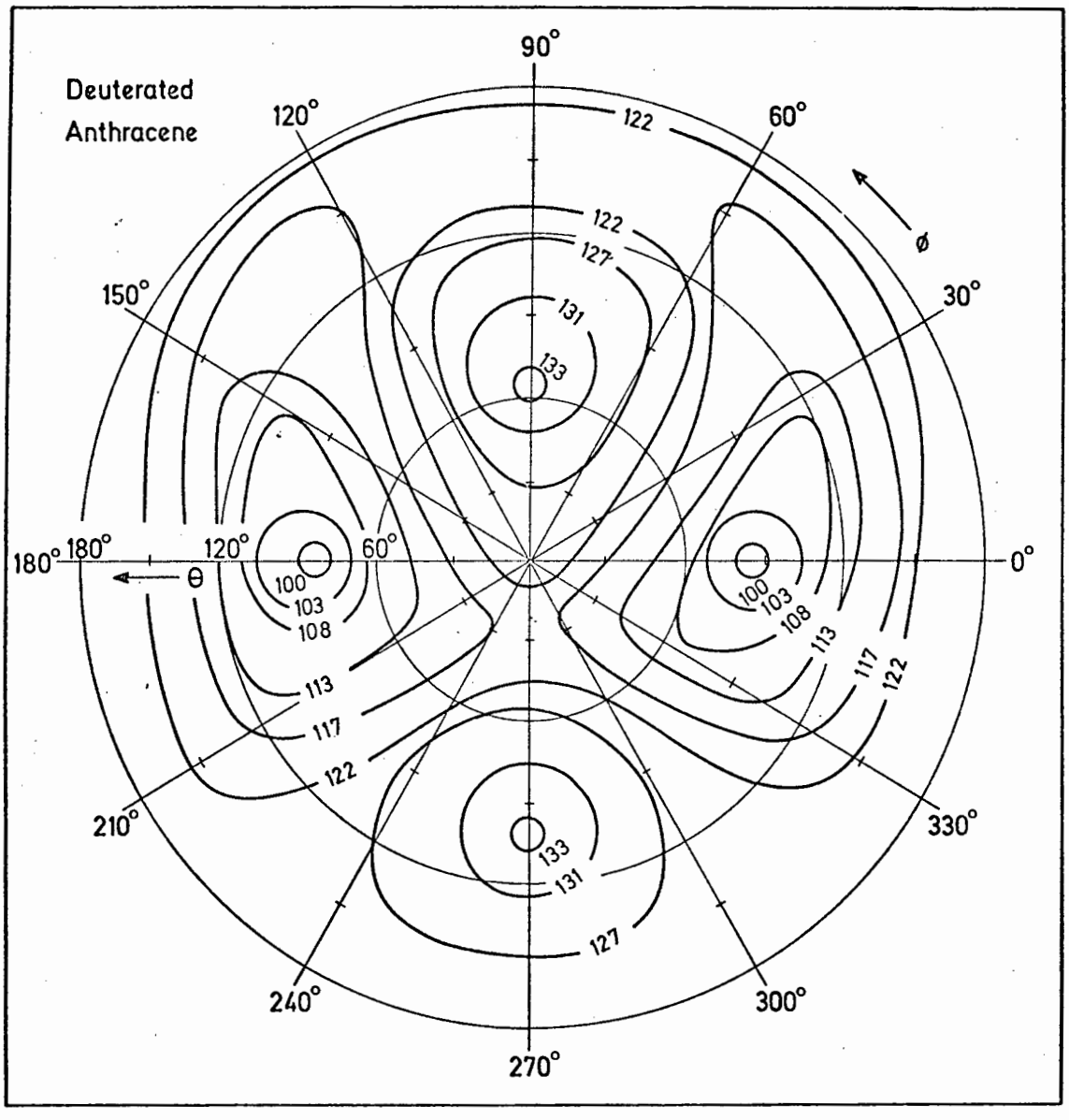

Fig. 4.9 Contour map of the pulse height response of deuterated anthracene crystal to 7 MeV deuterons.

The map shows contours of equal pulse height $L(\theta,\phi)$ as a function of deuteron direction (θ,ϕ) in the crystal frame. The figure written on each contour line indicates the L value of the contour relative to the L value of the lowest contour level.

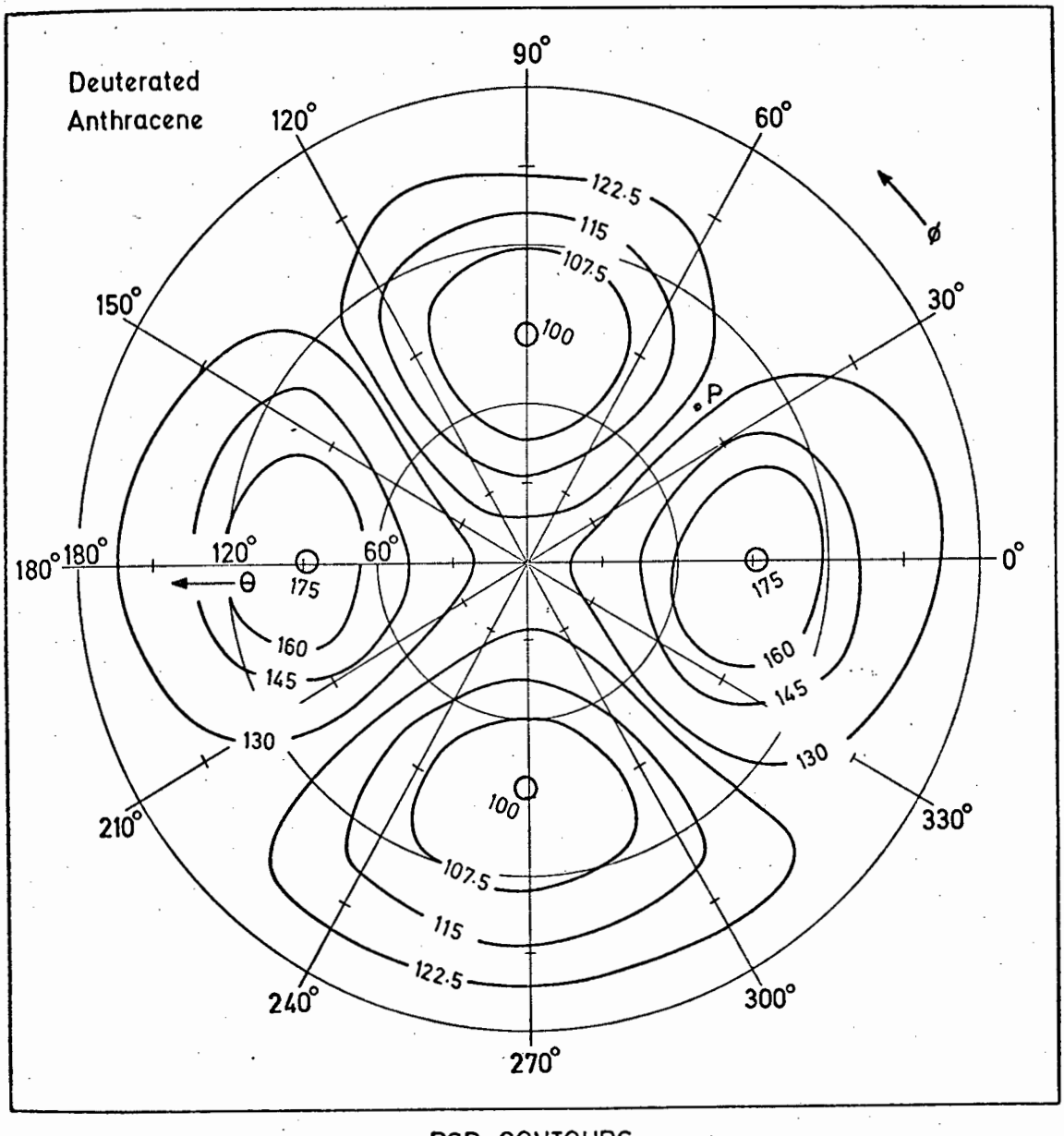

PSD CONTOURS

Fig. 4.10 Contour map of the PSD response of the deuterated anthracene crystal to 7 MeV deuterons.

The map shows contours of equal centroid PSD output $S(\theta,\phi)$ at $L = L_b$ (see text) as a function of deuteron direction (θ,ϕ) in the crystal frame. The figure written on each contour line indicates the S value of the contour relative to the S value of the lowest contour level. The point 'P' is referred to in Chapter 5.

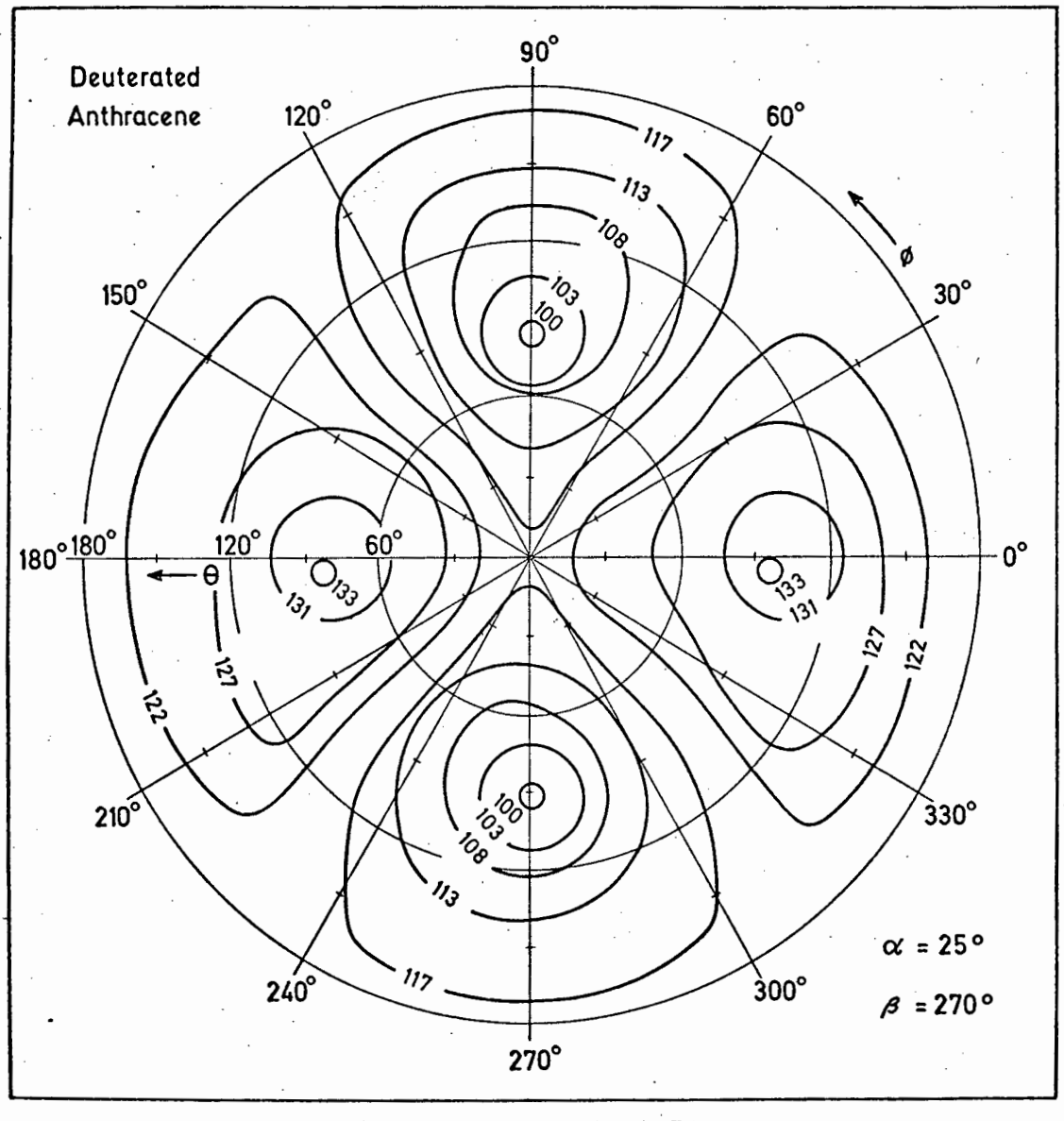

Fig. 4.11 Transformed contour map of the pulse height response of deuterated anthracene crystal to 7 MeV deuterons.

The contours of Fig. 4.9 are transformed to a new reference frame in which the polar axis is oriented at $\alpha = \theta = 25^{\circ}$, $\beta = \phi = 270^{\circ}$ in the crystal frame.

The reason for this difference between anthracene and deuterated anthracene is not obvious. However, further investigations might perhaps shed some light on the physics of PSD phenomena. Such phenomena are considered (Bi67) (Br74a) (Br74b) (Jo72) (Bo61) to involve molecular excitation and energy transfer processes which might be affected by substituting deuterons for protons in the anthracene molecule.

CHAPTER V

THE DEUTERATED ANTHRACENE POLARIMETER

5.1 The deuteron polarimeter

The deuterated anthracene polarimeter is basically a development or extension of the natural anthracene polarimeter (Br74b) (Jo74), hence the methods of operation and data reduction are based on those devised for natural anthracene. For polarization analysis the deuterated crystal must be oriented to give maximum variation of PSD response output S for recoils to left and right of the neutron beam direction. Assume that the incident particle and outgoing neutron (i.e., neutron beam) of the source reaction define a horizontal plane. Then, as for anthracene (Br74a) the optimum orientation is that in which the a-axis of the crystal is vertical and the neutron beam is directed between the b- and c'-axes as illustrated in Fig. 5.1. At such an orientation the direction of the neutron beam in the crystal frame is that corresponding to the point 'P' in Fig. 4.10, whose co-ordinates are $(\alpha,\beta) = (\theta,\phi)_{crystal} = (90^{o},40^{o})$. Henceforth the co-ordinates (α,β) will denote the neutron direction in the crystal frame or, equivalently, the crystal orientation relative to the neutron beam. The unsubscripted variables θ and ϕ will denote the direction of the recoil deuteron (from n-d scattering in the crystal) in the laboratory frame. In this (lab) frame, the polar axis ($\theta = 0^{o}$) is the neutron beam and the azimuthal axis ($\phi = 0^{o}$) is defined by projecting the bombarding particle in the source reaction (e.g., d in T(d,n) or α in $^{9}Be(\alpha,n)$) onto the azimuthal plane, that is, the plane normal to the polar axis. For calibrations the crystal may be oriented at $(\alpha,\beta) = (90^{o},90^{o})$, the maximum-L orientation, or at $(\alpha,\beta) = (90^{o},0^{o})$, the minimum-L orientation.

In addition, two other axes of rotation are introduced (see Figs. 5.2a and 5.2b): (i) a rotation of the crystal about the horizontal neutron beam designated by the angle δ ; and (ii) a rotation designated by the angle ζ ,

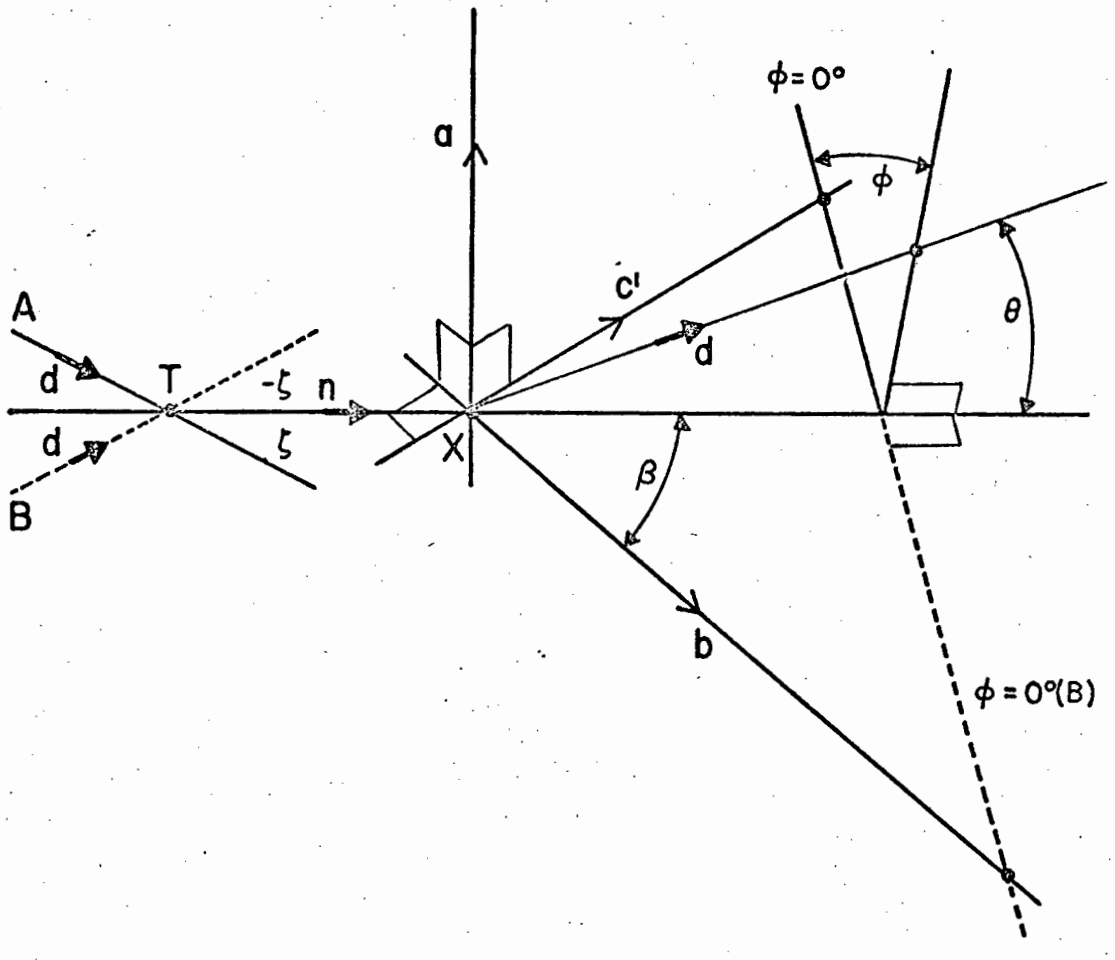

Fig. 5.1 Diagram showing orientation of a-, b-, and c'-axes of deuterated crystal (center X) to neutron beam n.

The azimuthal axis $\phi = 0^{\circ}$ is defined by projecting the incident deuteron beam onto a plane normal to the deuteron beam. The dashed lines illustrate changes implied by a switch from position A to position B.

of the whole detector assembly about a vertical axis through the source. The magnitude of $|\zeta|$ determines the energy and polarization of the neutron beam incident upon the crystal. The sign of ζ and the rotation δ are convenient parameters for asymmetry measurements as outlined below.

The photomultiplier assembly was mounted in a goniometer frame (Figs.5.2a and 5.2b) which permitted the crystal to be rotated independently about α, β, δ, and ζ. The framework was a rigid structure, constructed from steel and aluminium alloy and designed to achieve accurate rotational symmetry about the δ, ζ, α and β axes while at the same time restricting the quantity of scattering material in the vicinity of the crystal to a minimum. Fig. 5.2a shows the angles of rotation for the deuterated crystal in greater detail.

The choice of $(\alpha,\beta) = (90^{\circ},40^{\circ})$ as polarization orientation is illustrated by transforming the PSD contours of Fig. 4.10 to a reference frame in which the neutron beam is in the direction $(\alpha,\beta) = (\theta,\phi)_{crystal} = (90^{\circ}, 40^{\circ})$ in the crystal frame (Fig. 5.3). The contours in Fig. 5.3 thus represent the S response of the crystal to 7 MeV recoil deuterons as a function of direction (θ,ϕ) in the laboratory frame. This holds true for the rotation $= 0^{\circ}$ about the neutron beam. For the rotation $\delta = 90^{\circ}$, Fig. 5.3 would be rotated 90° in the ϕ direction since the δ-axis is the neutron beam. In this case, then, it will be seen that for $\theta<90^{\circ}$, recoils to the left (corresponding to the upper half of Fig. 5.3) give high-S (S>115) while recoils to the right (lower half of Fig. 5.3) give low-S (S<115). For the rotation $\delta = 270^{\circ}$ the opposite conditions obtain. These positions are defined as A and B, respectively, in accordance with the practice followed with the natural anthracene polarimeter (Br74b), since a deuteron recoil from the neutron beam to the c'-axis is in the same sense (A) or opposite sense (B) as the direction of neutron emission relative to the incident beam of the source reaction. As before, there are three convenient ways of changing between positions A and B: (i) by changing

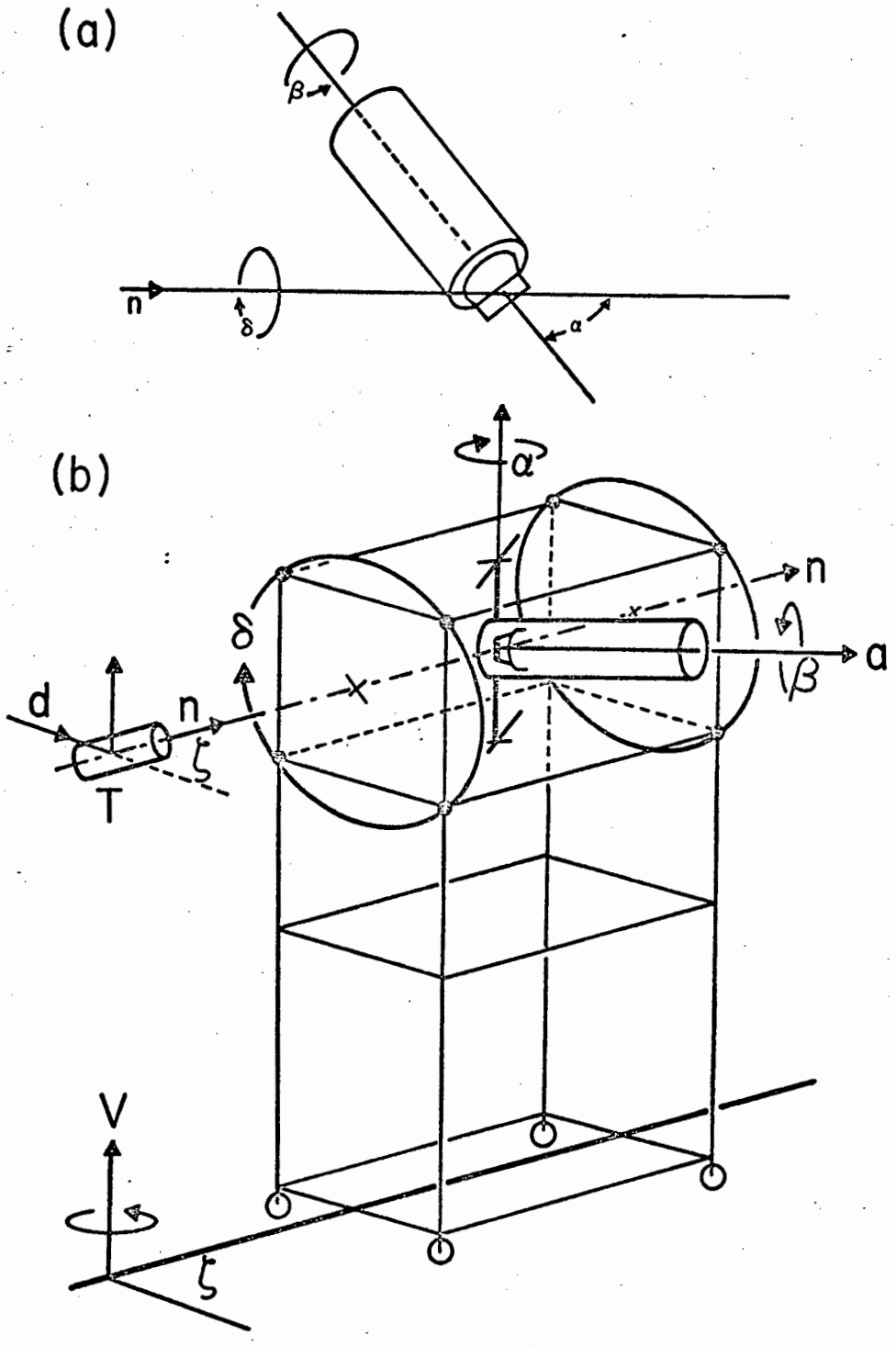

Fig. 5.2a Orientation of the crystal.

The orientation (α,β) of the crystal is defined by the angle σ between the neutron beam and photomultiplier axis, and the angle of rotation β of the photomultiplier-crystal assembly about the photomultiplier axis. The complete assembly can also rotate about the neutron beam (δ = angle of rotation) without changing α or β.

Fig. 5.2b Diagram showing goniometer.

The photomultiplier assembly is mounted in a goniometer frame for rotation (δ) about the neutron beam. The frame, complete with its stand, can also be rotated (angle of rotation ζ) about a vertical axis V.

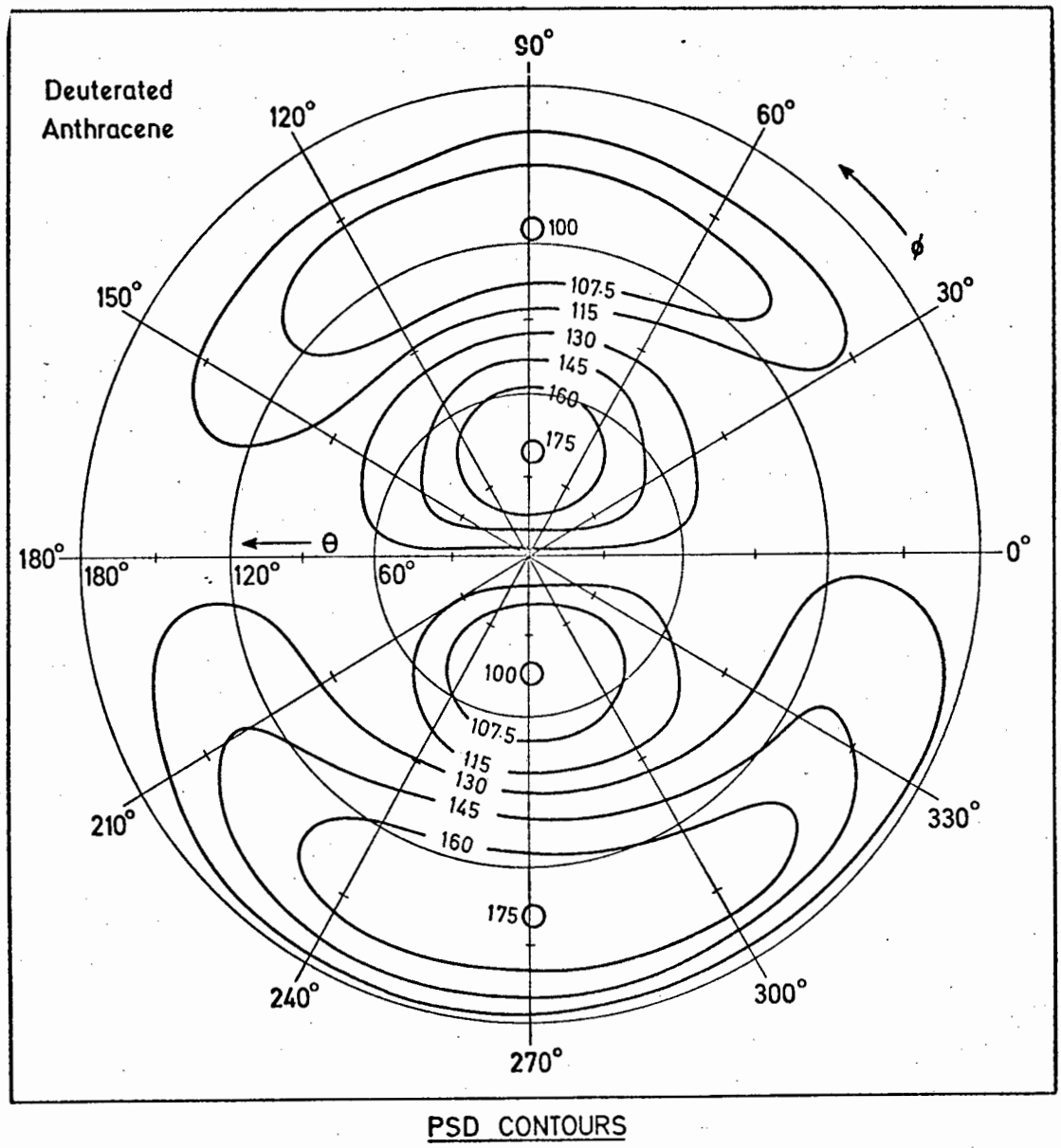

Fig. 5.3 Contour map of the PSD response of the deuterated anthracene crystal at polarization orientation to 7 MeV deuterons.

The map shows contours of equal centroid PSD output $S(\theta,\phi)$ after the crystal has been rotated from $(\alpha,\beta) = (\theta,\phi)_{crystal} = (0^{o},0^{o})$ (see Fig. 4.10) to the polarization orientation $(\alpha,\beta) = (\theta,\phi)_{crystal} = (90^{o}, 40^{o})$. The figure written on each contour line indicates the S value of the contour relative to the S value of the lowest contour level.

ζ to $-\zeta$: or (ii) by changing δ to $(\delta + \pi)$; or (iii) by rotating the crystal about it's a-axis, in this case by changing β to $(2\pi - \beta)$.

5.2 Operation for monoenergetic recoil deuterons

5.2.1 Measurement of the recoil deuteron asymmetry

The operation of the polarimeter may be described in terms of an idealized simplified situation as follows. Assume a monoenergetic, positively polarized incident neutron beam and consider only those events in which neutrons are scattered at a specific c.m. angle θ_2^{cm}. Assume that the analyzing power in n-d scattering, $P_2(\theta_2^{cm})$, is positive for the angle θ_2^{cm}. The associated deuteron recoils will be at the lab angle

$$\theta = 1/2\ (\pi - \theta_2^{cm}) \qquad \text{...Eq. 5.1}$$

and the recoil deuteron energy will be

$$E_d(\theta) = 1/2\ (\ 1 - \cos\theta_2^{cm})\ E_d(0^o) \qquad \text{...Eq. 5.2}$$

where $E_d(0^o)$ is the forward deuteron recoil energy given by Eq. 4.1.

Assume that E_n and θ_2^{cm} have been so chosen as to make $E_d(\theta) = 7$ MeV. Also assume for the moment that competing reactions, multiple neutron scattering and recoil deuteron escapes from the crystal are negligible. Now suppose the crystal is in the A position. Only the S-spectrum of the recoil deuterons is considered. Since θ will necessarily be less than 90^o, there will be, as outlined above in Sec. 5.1 and from Fig. 5.3: (i) low-S (S<115) if the deuteron recoil azimuthal angle ϕ is in the range $\phi = 180^o \pm 90^o$; and (ii) high-S (S>115) if the deuteron recoil azimuthal angle ϕ is in the range $0^o \pm 90^o$. When the crystal is in the B position the reverse conditions obtain.

For the above assumptions more neutrons will scatter towards the $\phi = 0^o$ side of the incident neutron beam than the $\phi = 180^o$ side. Consequently more recoils will be directed towards the $\phi = 180^o$ side than the $\phi = 0^o$ side, that is, there will be more events of low-S than high-S recorded.

The S-spectrum for such a situation is illustrated schematically in Fig. 5.4a. Neglecting for the moment any effects associated with the finite resolution of the S-measurement, the S-spectrum can be divided (Fig. 5.4b) at $S = S_m (=115)$ into two components, a component $N_<$ representing the integrated counts of events having $S<S_m$ and $N_<$, the integral of events having $S>S_m$. Then the deuteron recoil asymmetry $\varepsilon(\theta)$ is given by (Br74b)

$$\varepsilon(\theta) = \tfrac{1}{2}\pi\,(\Delta N_A/N_A) \qquad \text{...Eq. 5.3}$$

where $\Delta N = N_< - N_>$, $N = N_< + N_>$ and the subscript A indicates data taken in the A position. By combining runs taken in the A and B positions and normalizing so that $N_A = N_B = N$, an expression for $\varepsilon(\theta)$ is obtained:

$$\varepsilon(\theta) = (\pi/4N)\,(\Delta N_A - \Delta N_B) \qquad \text{...Eq. 5.4}$$

which is insensitive to small errors in the choice of S_m. In practice, it is convenient to define S_m as the median of summed A and B spectra. Finally, the polarization in the n-D elastic scattering at the associated neutron c.m. scattering angle θ_2^{cm} is given by

$$P_2(\theta_2^{cm}) = -\varepsilon(\theta)/P_1(\zeta)\ . \qquad \text{...Eq. 5.5}$$

5.2.2 Correction for proton background from deuteron breakup

The deuterated anthracene polarimeter is similar to its natural anthracene counterpart in many ways. However, one major difference between the two arises from the deuteron breakup reaction D(n,2n)p which occurs in the deuterated crystal. This can produce an appreciable background of proton events, necessitating a modification of the procedures for determining $\varepsilon(\theta)$ as described in Sec. 5.2.1.

The breakup reaction adds a proton component to the S-spectrum for monoenergetic deuterons (Fig. 5.4b). The components (Fig. 5.4c) of the resulting spectrum (Fig. 5.4d) are therefore a deuteron component similar to Fig. 5.4b and a pro-

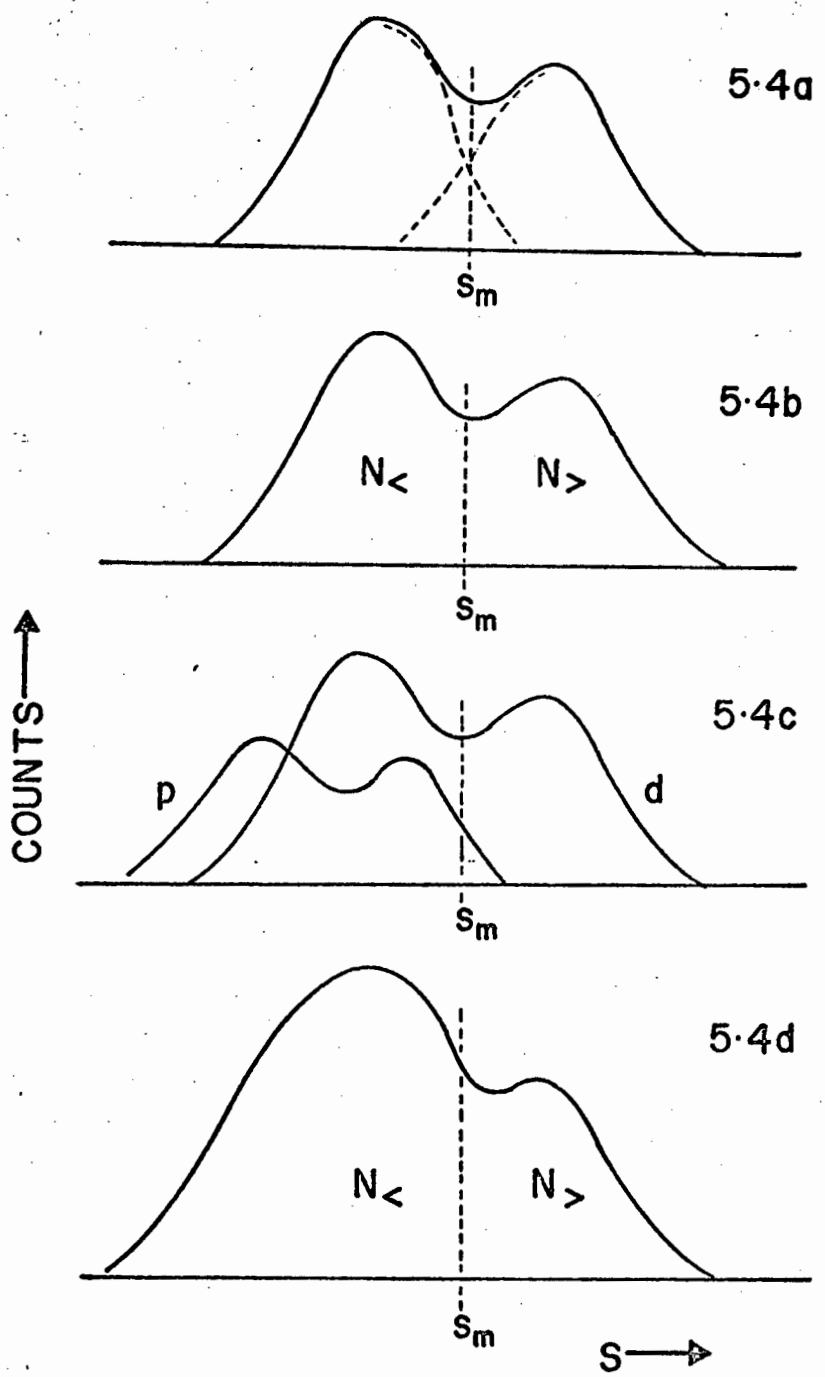

Fig. 5.4 Schematic illustration of method for determining asymmetry of deuteron recoils.

Fig. 5.4a Projected S-spectrum for monoenergetic deuterons showing the asymmetry in left and right deuteron recoils. The dashed lines show the high and low components associated with left and right deuteron recoils. The deuteron-median S_m for a pair of A and B runs is indicated.

Fig. 5.4b The projected S-spectrum can be divided at $S_m = 115$ into two components, a component $N_<$ below S_m, and a component $N_>$ above S_m.

Fig. 5.4c A proton component due to the breakup reaction is added to the deuteron component.

Fig. 5.4d The net spectrum obtained by adding the two components of Fig. 5.4c. The proton component contributes mostly to $N_<$ while $N_>$ remains relatively unaffected.

ton component also similar to Fig. 5.4b, overlapping the deuteron component but displaced towards lower S-values by the PSD shift between protons and deuterons. From observations of this shift (Fig. 4.6a or 4.7a) it can be assumed that the proton component will not extend significantly beyond the S-value S_m as indicated in Fig. 5.4c. Therefore the proton events are added to the $N_<$ component of the S-spectrum (Fig. 5.4d) and consequently to the difference ΔN, and will cancel in the difference $(\Delta N_A - \Delta N_B)$ for normalized A and B spectra. The effect of the protons is therefore to dilute the observed asymmetry $\varepsilon(\theta)$ by increasing the total number of events N in the denominator of Eq. 5.4 without affecting the numerator. This dilution may be corrected by multiplying N by a factor $(1 - f_p)$ in which f_p represents the fraction of events in the S-spectrum (Fig. 5.4d) which are due to protons. Thus the equation for $\varepsilon(\theta)$ becomes

$$\varepsilon(\theta) = \pi(\Delta N_A - \Delta N_B)/4(1 - f_p)N. \qquad \text{...Eq. 5.6}$$

The fraction f_p can be estimated from measurements made at a crystal orientation different to that used for the asymmetry measurements, namely, the c'- or L_{max}-orientation mentioned in Sec. 4.5 above. Protons and deuterons are clearly resolved in spectra taken at this orientation (see e.g., Fig. 4.6a or 4.7a) and the fraction f_p can be determined. More details of the methods used will be given in the sections below.

The presence of the proton component also implies that the 'deuteron-median' S_m no longer coincides with the median of the summed (A + B) projected spectrum. However, since the proton component lies almost entirely below S_m (Fig. 5.4c), S_m can be obtained by removing a fraction f_p of the summed spectrum, from it's low side, and determining the median of the remaining high-S component as illustrated in Fig. 5.5.

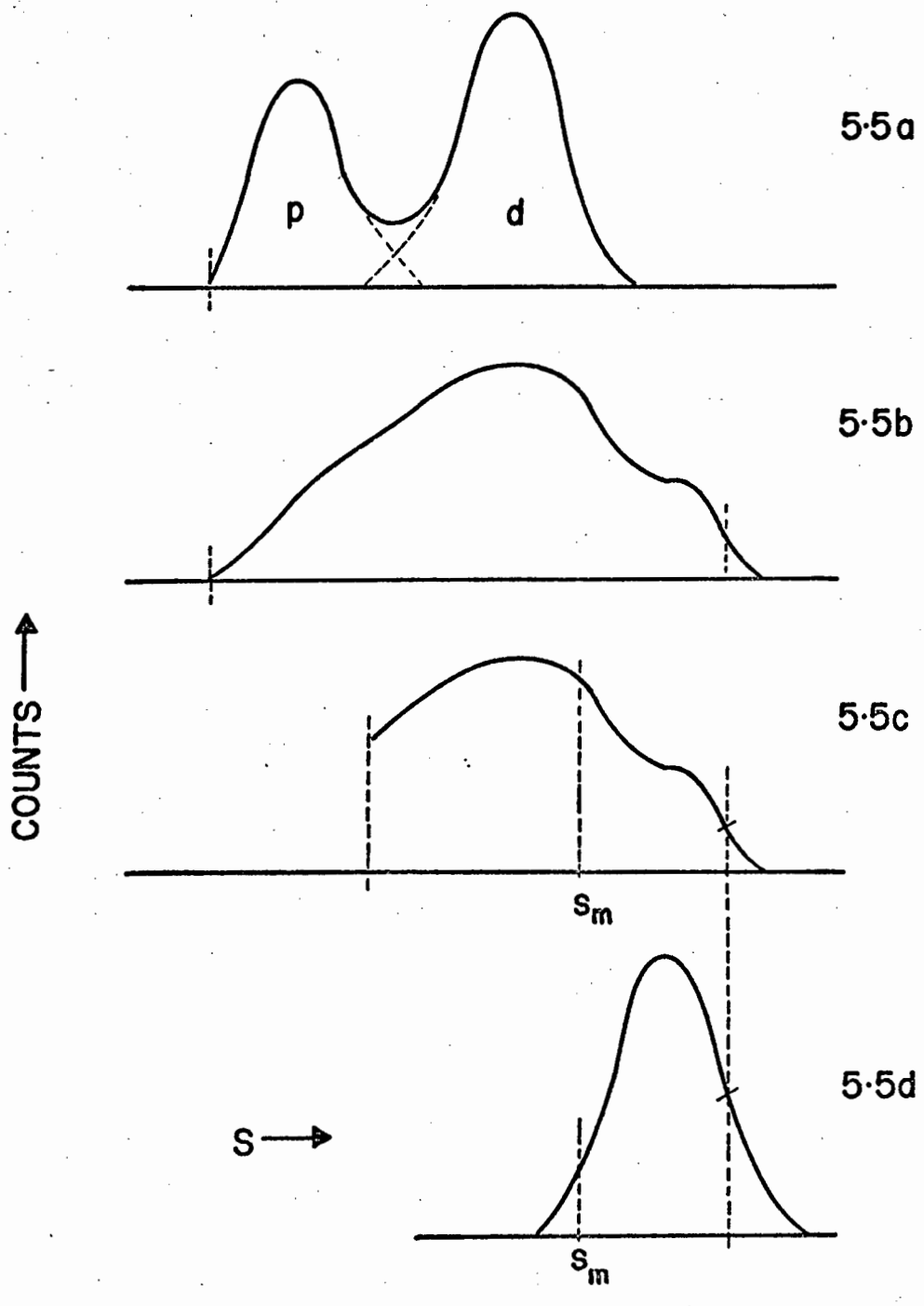

Fig. 5.5. Determination of proton fraction f_p, the deuteron median S_m, and the asymmetry factor f_A.

Fig. 5.5a Projected S-spectrum of a section (angle bin) of L_{max} run (see Fig. 4.6a or Fig. 4.7a). The proton fraction f_p is the fraction of counts in the proton group p.

Fig. 5.5b Projected S-spectrum of a section of a polarization run.

Fig. 5.5c The fraction f_p has been removed from 5.5b. This is done for an A run and a B run, and the two projected spectra are then normalized to the same total area (counts) and summed. The median S_m of the resultant distribution is determined.

Fig. 5.5d The point of inflection on the high-S side of projected spectrum is matched to that of a 'standard' Gaussian. The fraction f of the 'standard' Gaussian in the region $S > S_m$ is determined, then f_A is calculated from Eq. 5.14.

5.3 Determination of asymmetry as a function of recoil angle

5.3.1 Outline of the method

In an actual experiment using a monoenergetic neutron beam falling on the deuterated anthracene crystal, the LS-spectrum includes components from recoil deuterons, from breakup protons, and from other types of events; and the deuteron component includes recoils at angles θ ranging from 0° - 90°. An LS-spectrum, obtained during the same series of runs as those shown in Figs. 4.6 and 4.7, using 21.6 MeV incident neutrons is shown isometrically in Fig. 5.6, and as a contour plot in Fig. 5.7. At this 'polarization orientation' the characteristic forward recoil edge ($\theta = 0^{\circ}$) lies at an (L,S) position which is intermediate between the limiting positions F and F' of the corresponding edge in Figs. 4.6 and 4.7. For recoils at $\theta > 0^{\circ}$, that is, for deuteron energies less than $E_d(0^{\circ})$ and consequently for pulse heights L less than that of the edge, the deuteron ridge broadens relative to those of Figs. 4.6 and 4.7. A similar broadening occurs for the proton ridge with the result that the proton and deuteron ridges overlap and merge over most of the L-range, in the manner illustrated in Fig. 5.4.

The method adopted for determining $\varepsilon(\theta)$ is to divide the proton-deuteron region of the LS-spectrum into a series of angle bins, each corresponding to a particular range of recoil angle θ_{min} to θ_{max} and mean recoil angle $\theta = 1/2\ (\theta_{min} + \theta_{max})$. Assume for the moment that both the L and S parameters are measured with perfect resolution. From the L and S anisotropy data of Sec. 4.5 it can be shown that the locus, in the LS-plane, of deuteron recoils at constant θ and different ϕ is, to a good approximation, a straight line. The loci of θ_{min} and θ_{max} therefore define the boundaries of the angle bin θ in the LS-plane. Two such lines indicating the boundaries for the bin corresponding to neutron centre-of-mass scattering angle $\theta_2^{cm} = 130^{\circ} \pm 5^{\circ}$ are shown in Fig. 5.7. After defining these boundaries the counts data between them is projected onto the S-axis and $\varepsilon(\theta)$ may be determined from the resulting

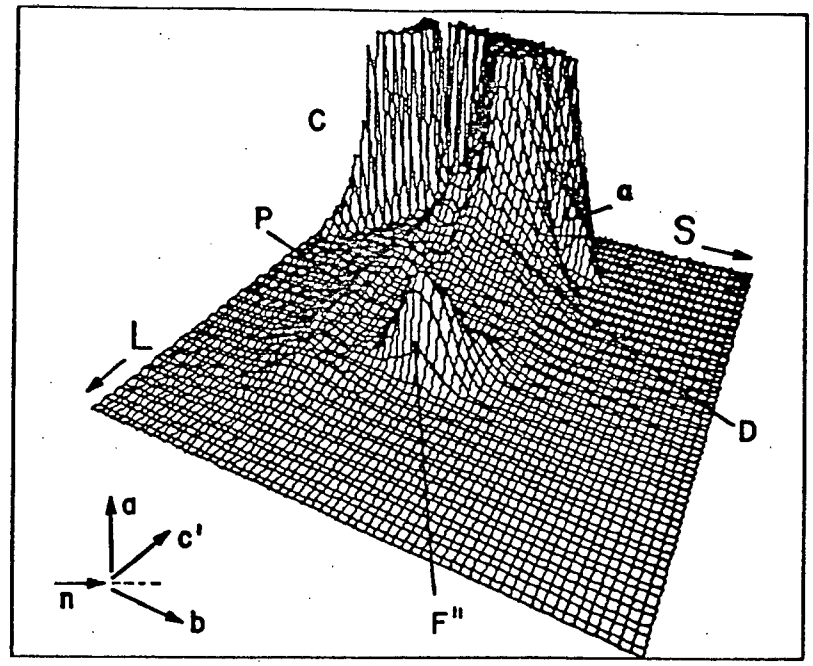

Fig. 5.6 LS-spectrum for 21.6 MeV neutrons in the direction $(\theta,\phi) = (90^{\circ},40^{\circ})$ in the *bc'*-plane (polarization orientation).

The ridges are due to: Compton electrons (C); breakup protons (P); recoil deuterons (D); and α-particles (α) from reactions on carbon. The deuteron ridge is seen to be broadened relative to that in Fig. 4.6a. The peak F'' corresponds to forward recoil deuterons at polarization orientation and lies between that for L_{max}-orientation, F (Fig. 4.6a) and that for L_{min}-orientation, F' (Figure 4.6b). The counts (vertical) scale in this plot is arbitrarily truncated at 500 counts.

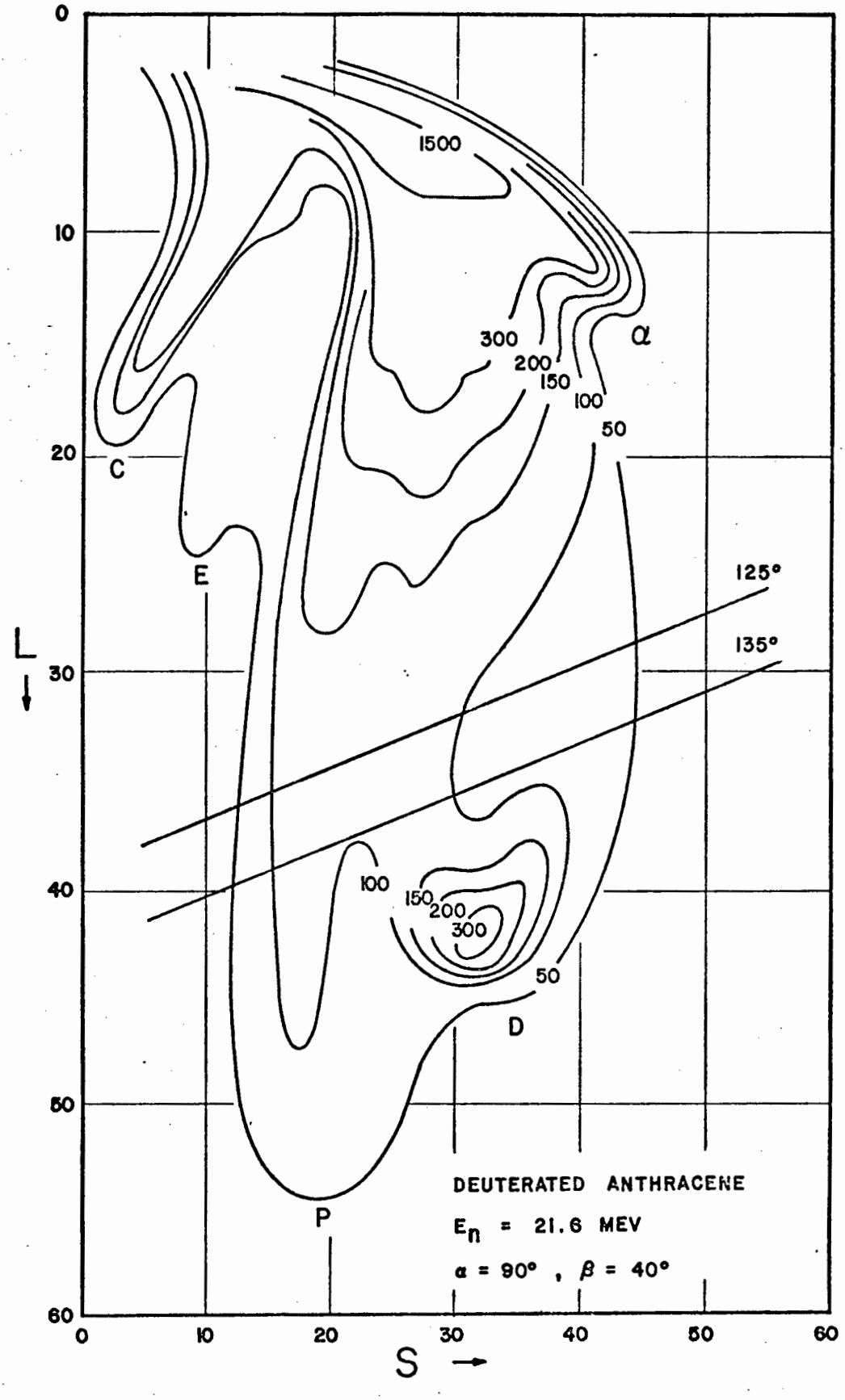

Fig. 5.7 Contour plot of an LS-spectrum for 21.6 MeV neutrons on the deuterated anthracene crystal at the polarization orientation.

The above is a contour plot of the isometric display of Fig. 5.6. The symbols C, P, D, α, and E indicate that the corresponding ridges are due to Compton electrons, breakup protons, recoil deuterons, α-particles from reactions on carbon, and proton escapes. The relative count rate is given on each contour level. Two lines indicating the boundaries for the bin corresponding to neutron center-of-mass scattering angle $\theta_2^{cm} = 130^\circ \pm 5^\circ$ are indicated.

S-spectrum using the procedures described in Sec. 5.2

5.3.2 Determination of angle bin boundaries

The bin boundaries are defined by referring to the pulse height versus energy (L vs E_d) data and anisotropy data (A_1 vs E_d) for the deuterated crystal (Chap. IV). From the calibration experiments described in Sec. 4.5, loci in the LS-plane, of the edges F (Fig. 4.6a) and F' (Fig. 4.7a), are defined for different deuteron energies. These are the loci of the (L,S) points for deuterons moving parallel to the c'-axis and b-axis of the crystal, respectively. The calibrations of L vs E_d and A_L vs E_d, together with L vs E_d data from the literature, enable the deuteron energy scales along each of these loci to be defined. This is illustrated schematically in Fig. 5.8 where the loci F and F' are presented, superimposed upon a few of the contours reproduced from Fig. 5.7. Now the boundary corresponding to neutron centre-of-mass scattering angle θ_2^{cm} is also the locus of a constant deuteron energy E_d given by Eq. 5.2 and will therefore intersect the F and F' loci at this energy on each of their respective scales. Thus each bin boundary may be defined as the straight line intersecting these loci at the appropriate energy E_d.

The method of projection is illustrated schematically in Fig. 5.9, in which the square grid represents a section of the LS data matrix; the bin boundaries are represented by the lines aa and bb and sections of the loci F and F' are indicated. The lines aa and bb are each divided into twenty equal parts and corresponding subdivisions are joined as shown in the figure. This is continued with the same dividing intervals on either side of the loci F and F'. The elements of the projected spectrum are now defined by the resulting subdivision of the angle bin. For the example shown in Fig. 5.9, for instance, the events in element (i,j) of the LS data matrix will be distributed between elements n and (n + 1) of the projected spectrum in the ratio of the shaded and unshaded areas of square (i,j). The events within the aabb region of the angle bin are thus redistributed among a set of 20 elements or sectors of

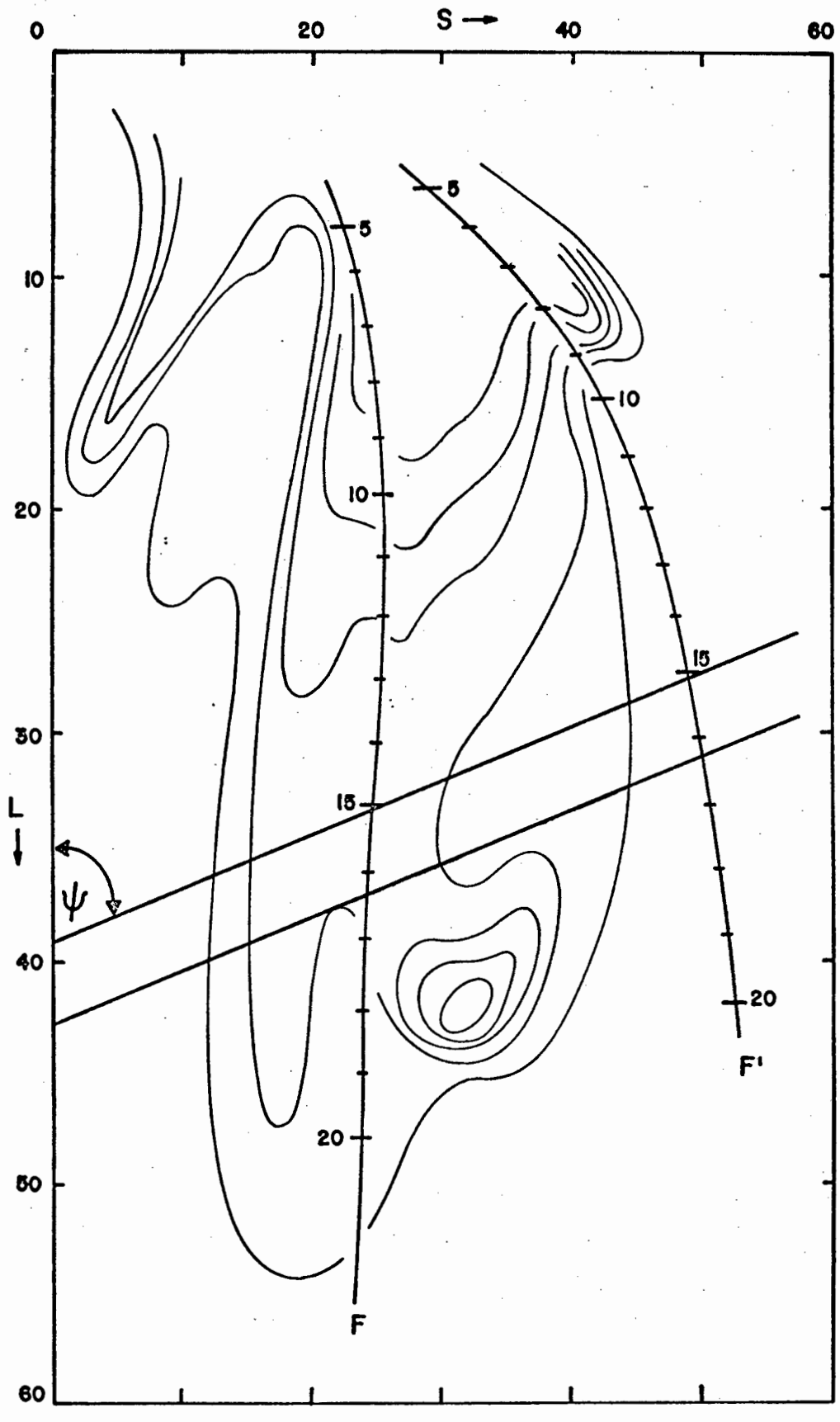

Fig. 5.8 Method for determining angle bin boundaries.

The loci F and F' are superimposed upon some of the contours reproduced from Fig. 5.7. The deuteron energy scale along each locus is given. The boundary corresponding to θ_2^{cm} intersects both the F and F' locus at the same deuteron energy, and makes an angle ψ relative to the L-axis (see text).

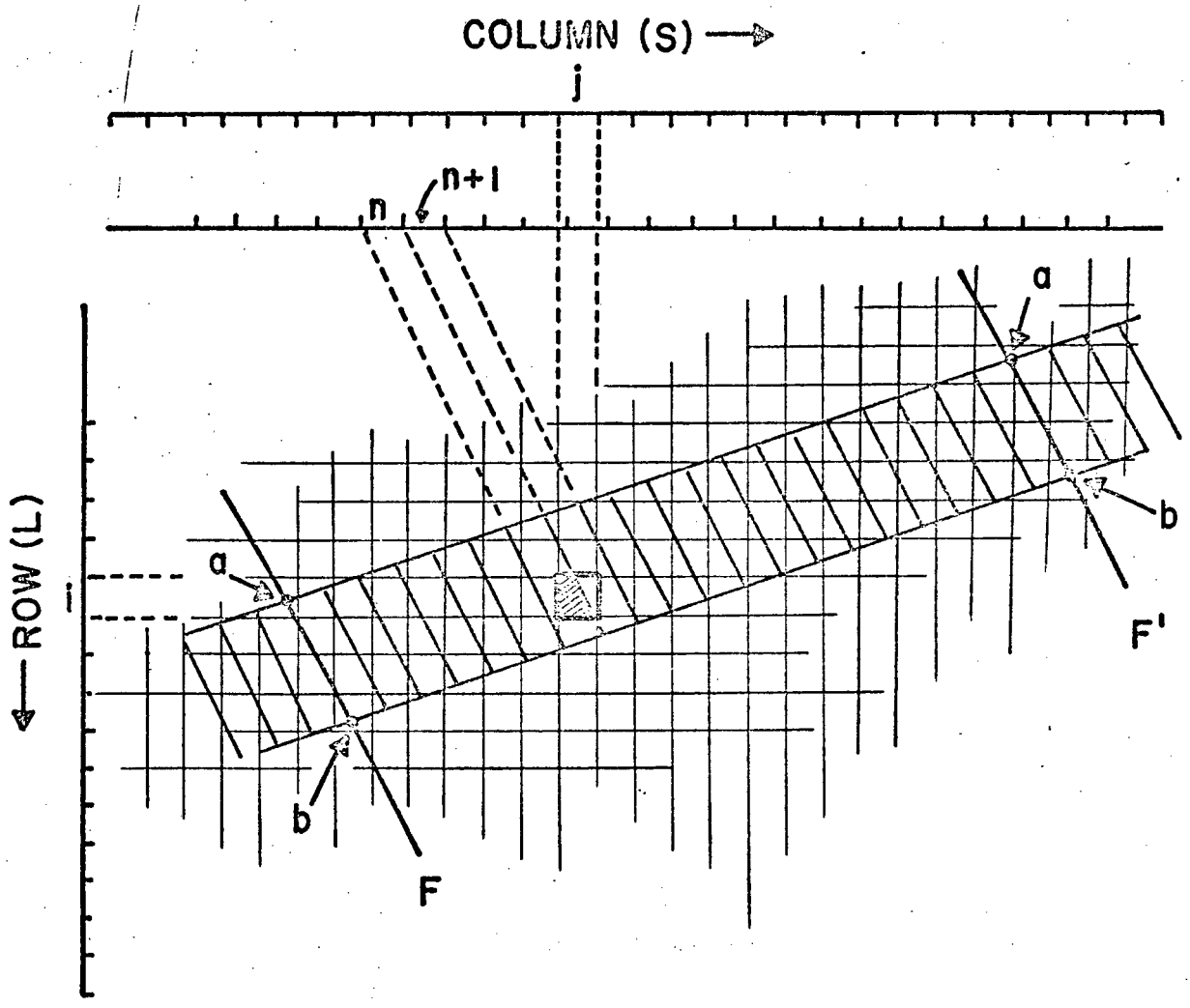

Fig. 5.9 Schematic illustration of method used for redistribution of events within an angle bin.

A typical angle bin defined by the lines aa and bb is sub-divided into 20 equal sectors between the loci F and F'. The square grid represents the elements of the LS data matrix. The events in element (i,j) of this matrix are distributed between elements n and (n + 1) of the projected spectrum (see Sec. 5.3.2).

the projected spectrum. The remaining events within the bin are similarly redistributed among further channels on either side of this set of 20 sectors.

5.3.3 *Determination of the proton fraction f_p*

The proton fraction f_p is determined from the LS-spectrum (Figs. 4.6a and 4.7a) recorded at the L_{max} or c'-orientation of the crystal, at which the proton and deuteron ridges are well resolved. It is assumed that the anisotropy properties of deuterated anthracene for protons will be similar to those for deuterons, that is, if any pair of bin boundaries are taken which extend across the LS-plane and if a proton of energy E_p lying between these boundaries is considered, then the locus for protons of this energy will also be a line lying between these boundaries. The relative number of protons and deuterons in this angle bin will therefore be independent of crystal orientation. For a given angle bin, therefore, the proton fraction f_p can be estimated by projecting the corresponding segment of the LS-spectrum obtained at the c'-orientation (see Fig. 5.5a) onto the S-axis and determining the fraction of events in the (well resolved) proton group of the projected spectrum.

5.4 Limitations and corrections

In practice the determination of the asymmetry must obviously differ in some respects from the procedures outlined in Secs. 5.2 and 5.3, since the practical situation differs from the ideal situation described in those sections. The practical situation may be complicated by effects such as: stability of electronics; mechanical misalignment or asymmetries in the apparatus; multiple scattering of neutrons in the crystal; escape of protons or deuterons from the crystal; proton, deuteron, or alpha events from neutron-induced reactions on carbon in the crystal; and the finite resolution of the L and S measurements. The limitations imposed by each of these effects must be assessed, and the errors arising from the effects must be considered, and whenever possible, be corrected or at least minimized.

5.4.1 *Electronic stability and mechanical symmetry*

The stability of the L and S electronics is obviously of crucial importance to the operation of the deuterated anthracene polarimeter since both the angle and the asymmetry measurements depend on the LS-spectrum. However, the 'edge' of the deuteron ridge (F in Fig. 4.6a) provides a convenient monitor of the stability of both the L- and S-channels. Since this edge corresponds to forward recoil deuterons, the associated (L,S) co-ordinate may be assumed to be independent of rotations about the neutron beam or δ-axis (see Fig. 5.2). In other words, for runs at the polarization orientation, the position of the edge should be stable from run to run, even when changing from the A position to the B position. Therefore, any movement of the edge (for 'polarization' runs) may be taken as evidence of electronic instability or of mechanical misalignment of the apparatus.

The stability of the L-channel is monitored by projecting the deuteron ridge onto the L-axis. The slope of the edge in the projected L-spectrum is a measure of the short-term L-stability and the position of the edge is a measure of the long-term L-stability. The stability of the S-channel is monitored by projecting the edge row (that is, the row corresponding to the edge in the projected L-spectrum) onto the S-axis. The width and position of the deuteron group in this projected spectrum are then sensitive to short-term and long-term instability respectively, in the S-channel, and also to the mechanical symmetry of the apparatus; for example, the symmetry of rotation about the δ-axis. After monitoring the L- and S-stability in this way, electronic drifts and mechanical asymmetries may, if small (less than about 3%), be neutralized by redispersing the LS-spectrum with respect to the appropriate unstable parameter L or S. One LS-spectrum of a set is taken as standard and the counts in the remaining spectra are redistributed in order to match the deuteron edge and the position of the deuteron group in the projected edge row with those of the standard. The procedures used are similar to those described in reference

(Br74b).

5.4.2 *Multiple scattering of neutrons*

The mean free paths of 7.9, 16.4 and 21.6 MeV neutrons in deuterated anthracene are 5.1, 7.4, and 7.9 cm, respectively. Since the linear dimensions of the crystal used are much smaller than these figures, the multiple neutron scattering in this crystal can be safely neglected.

The lucite light-pipe used in conjunction with the crystal (see Fig. 4.1) is also a possible source of secondary scattered neutrons. However, the linear dimensions of the pipe are also small compared to the neutron mean free paths, and moreover, the pipe is so positioned that only a small fraction of neutrons scattered within it will be directed towards the crystal.

5.4.3 *Escape of deuterons from the crystal*

Since the ranges of deuterons in deuterated anthracene vary from 0.4 to 2.1 mm for deuteron energies of 8 to 22 MeV, deuteron escape from the present crystal is a significant effect, especially when using high energy incident neutrons. As in the case of the natural anthracene polarimeter (Jo74), the pulse height and PSD responses are affected in such a way that the escaping deuterons are displaced towards lower L- and lower S-values in the LS-spectrum. Escape is more probable for deuterons moving parallel to the c'-axis than for those moving parallel to the b-axis, because the dimensions of the crystal in these directions are 10 mm and 20 mm, respectively. Therefore, the effect is larger for the $N_<$ component (corresponding to the c'-direction) than for the $N_>$ component. The lower bound for the calculation of $N_<$ can be chosen to exclude the escape component, thereby reducing ΔN as well. However, the effects on ΔN_A and ΔN_B should neutralize one another when these two quantities are subtracted in Eq. 5.4. Deuteron escape does not affect the numerator of Eq. 5.6,

therefore, and does not lead to false asymmetries, although it may enhance the observed asymmetry slightly by reducing the denominator of this equation. The extent of this enhancement can be estimated from the LS-spectrum observed at the L_{max} orientation (e.g., Fig. 4.7a). Escaping proton events may be distinguished in this spectrum, hence the extent of deuteron escape can be estimated and a correction applied if necessary.

5.4.4 *Reactions on the carbon component of the crystal*

The alpha ridge corresponding to the $^{12}C(n,\alpha)^{9}Be$ and $^{12}C(n,n')3\alpha$ reactions is a prominent feature of the LS-spectra (e.g., Figs. 4.7 and 5.7) obtained using the deuterated crystal. In addition to this, the carbon component of the crystal contributes events to the deuteron and proton ridges, via the $^{12}C(n,p)^{12}B$ and $^{12}C(n,np)^{11}B$ and $^{12}C(n,d)^{11}B$ reactions. The alphas from the carbon component are well resolved from the recoil deuterons down to fairly low pulse heights (e.g., $L \simeq 10$ in Fig. 5.7) and do not therefore interfere with the asymmetry measurements for neutron center-of-mass scattering angles of 80^{o} or higher. The cross-sections for the other reactions on the carbon component are relatively small and the protons and deuterons from these reactions are also confined to low pulse heights owing to the large negative Q-values ($Q<-12$ MeV) for these reactions. Therefore the proton and deuteron ridges of the LS-spectrum above $L \simeq 12$ are attributed entirely to reactions on the deuterium component of the crystal and the only effect of the carbon component is to limit the asymmetry measurements to scattering angles in the range $\theta_2^{cm} > 80^{o}$.

5.4.5 *Resolution of LS-spectra*

The fact that the L and S parameters are determined with finite resolution has two important consequences. Firstly, the angles corresponding to the angle bin boundaries defined in the LS-plane have an associated angular spread.

Secondly, within a given angle bin the $N_<$ and $N_>$ components (Fig. 5.4a) may overlap to such a degree as to affect the observed asymmetry.

Angular resolution.-- Consider initially the bin boundaries for forward recoil angles (i.e., $\theta_2^{cm} \gtrsim 130^o$) from high energy (e.g., 21.6 MeV) incident neutrons. Since these boundaries run almost normal to the L-axis the associated angular uncertainty $\Delta\theta_2^{cm}$ will be dominated by the uncertainty, ΔL, of the pulse height L and will be much less sensitive to the uncertainty of the PSD output S. The uncertainty ΔL may be converted into a deuteron energy uncertainty ΔE_d using the pulse height-energy data, L vs E_d (Bi67), and $\Delta\theta_2^{cm}$ may then be obtained by differentiating Eq. 5.2, which gives

$$\Delta\theta_2^{cm} = 2\Delta E_d \,/\, \left[E_d(0^o) \sin\theta_2^{cm} \right] \qquad \text{...Eq. 5.7}$$

where $E_d(0^o)$ is, as before, the energy of forward recoil ($\theta = 0^o$) deuterons. Angle bin boundaries for larger recoil angles (i.e., $\theta_2^{cm} \lesssim 100^o$) and lower incident neutron energies make more acute angles with the L-axis. Therefore, the uncertainty ΔS will also contribute to the uncertainty $\Delta\theta_2^{cm}$. This is taken into account by defining an associated, or effective, L uncertainty $\Delta L' = \Delta S \, (\tan\psi)$ where ψ is the angle between the bin boundary and the L-axis (see Fig. 5.9) and using the total L uncertainty ΔL_{tot} given by

$$\Delta L_{tot} = (\Delta L^2 + \Delta L'^2)^{\frac{1}{2}} \qquad \text{...Eq.5.8}$$

to determine ΔE_d.

The uncertainty $\Delta\theta_2^{cm}$ is thus determined from the intrisic uncertainties ΔL and ΔS, of the L and S measurements and these, in turn, are determined from the edge and width of the deuteron ridge as observed at the L_{max}-orientation. The results, showing $\Delta\theta_2^{cm}$ as a function of θ_2^{cm} for incident energies 7.9, 16.4, and 21.6 MeV, respectively, are given in Fig. 5.10. These values serve as a guide in choosing the bin width to be used in the asymmetry calculation.

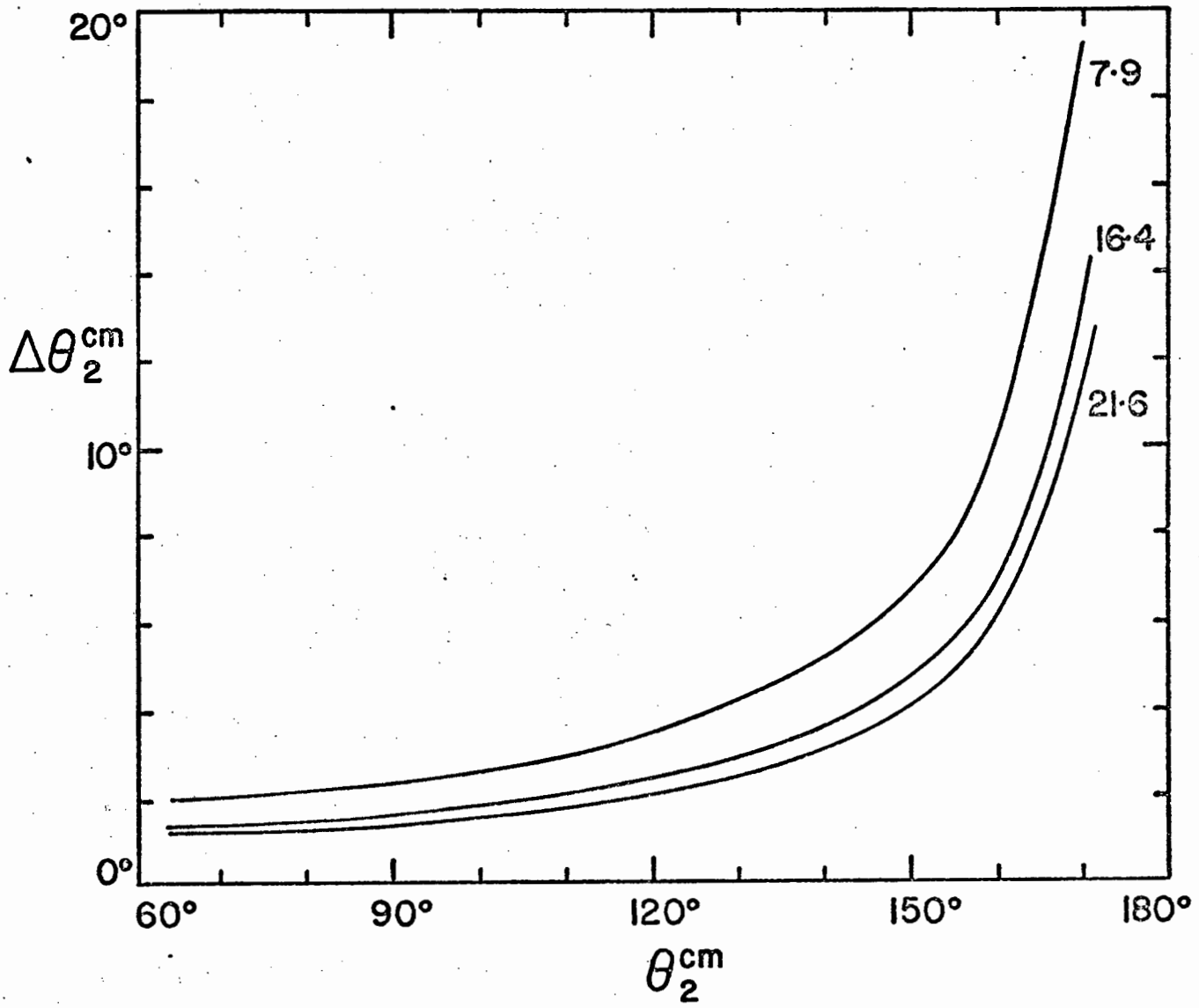

Fig. 5.10 Angular resolution of deuterated anthracene polarimeter. The uncertainty $\Delta\theta_2^{cm}$ of the neutron center-of-mass scattering angle θ_2^{cm}, as determined by the deuterated anthracene crystal polarimeter, is plotted as a function of θ_2^{cm} for the incident neutron energies 7.9, 16.4, and 21.6 MeV.

Obvious criteria for this choice are that the bin width should be $>2\,\Delta\theta_2^{cm}$ and yet be as small as possible in order to resolve the angular dependence of $P_2(\theta_2^{cm})$ as faithfully as possible. On the basis of the information in Fig. 5.10 a bin width of 10^o c.m. was chosen (e.g., $\Delta\theta_2^{cm} = 5^o$).

Resolution of the $\varepsilon(\theta)$ measurement.-- To determine the effect of LS resolution on the asymmetry measurement, consider the 'true' lower and upper components represented by the cashed curves in Fig. 5.4a and let their integrals be $M_<$ and $M_>$, respectively. Suppose that the deuteron-median S_m defines a fraction $f_<$ of $M_<$ on the low-S side and a fraction $f_>$ of $M_>$ on the high-S side. Then since $N_<$ and $N_>$ are defined as the total counts below and above S_m respectively (see Fig. 5.4b),

$$N_< = f_< M_< + (1 - f_>)M_> \qquad \text{...Eq.5.9a}$$

$$N_> = f_> M_> + (1 - f_<)M_< . \qquad 5.9b$$

The observed asymmetry defined by Eq. 5.3, that is,

$$\varepsilon_{obs} = (\pi/2)(N_< - N_>)/(N_< + N_>) \qquad \text{...Eq.5.3'}$$

is then given by

$$\varepsilon_{obs} = \left[2(f_< M_< - f_> M_>) - (M_< - M_>)\right]/(M_< - M_>). \qquad \text{...Eq.5.10}$$

If $f_< \simeq f_>$, as will be the case for small asymmetries, and if an average $f = (1/2)(f_< + f_>)$ is defined, then Eq. 5.10 reduces to

$$\varepsilon_{obs} = (2f - 1)(M_< - M_>)/(M_< + M_>). \qquad \text{...Eq.5.11}$$

Then, since the true asymmetry ε_{true} is given by

$$\varepsilon_{true} = (\pi/2)(M_< - M_>)/(M_< + M_>) \qquad \text{...Eq.5.12}$$

it follows that

$$\varepsilon_{true} = \varepsilon_{obs}/(2f - 1). \qquad \text{...Eq.5.13}$$

The asymmetry resolution correction factor f_A defined as the ratio of true to observed asymmetry is therefore

$$f_A = 1 / (2f - 1) \qquad \text{...Eq.5.14}$$

and it is determined by measuring the fraction f. In estimating f the fact that only a fraction of the events corresponding to the components $M_<$ and $M_>$ contribute to the asymmetry ε must be taken into account. The expression for $M_<$, for example, is, from (Br74b)

$$M_< = \left[k\sigma(\theta)/2\pi\right] \int_{-\pi/2}^{\pi/2} \left[1 + \varepsilon(\theta_d)\cos\phi\right] d\phi \qquad \text{...Eq. 5.15}$$

so that the asymmetry term, which contains $\cos\phi$ as a multiplicative factor, will be small for deuteron recoils at $\phi \simeq +90^\circ$ or -90°, that is, for recoils giving $S \simeq S_m$. The region of $M_<$ which is sensitive to ε is therefore that at small S and the fraction $f_<$ must be estimated for this portion. Similarly $f_>$ must be estimated for the high-S portion of $M_>$. Therefore, f is estimated (see Fig. 5.5d) for each angle bin by taking a 'standard' Gaussian and matching the point of inflection on the high-S side of this distribution to that on the high-S side of the projected spectrum (Fig. 5.5b), and determining the fraction of the 'standard' Gaussian in the region $S > S_m$. The standard Gaussian, which represents the intrinsic resolution for the asymmetry measurement is determined from the projected spectrum for the same bin, by fitting the deuteron component observed at the L_{max}-orientation (Fig. 5.5a).

The correction factor f_A is significant for measurements at forward recoil angles, that is, for neutron scattering angles θ_2^{cm} approaching 180°, because the directional difference between left and right scatterings is small at these angles, and at low recoil deuteron energies because the directional resolving power R (see Table 4.1) is smaller at low energies.

5.5 Uncertainties

The total uncertainty $\Delta P_2(\theta_2^{cm})$ of the final polarization measurement can be

regarded as the sum of three components

$$\Delta P_2(\theta_2^{cm}) = \left|P_1^{-1}\right| \left\{ \left[\Delta\varepsilon(\theta_2^{cm})\right]^2 + (\Delta\varepsilon_{sys})^2 + \left[P_2(\theta_2^{cm})\Delta P_1\right]^2 \right\}^{\frac{1}{2}} \quad \text{... Eq.5.16}$$

where P_1 is the polarization of the incident neutron beam, ΔP_1 is the uncertainty of P_1 and $\Delta\varepsilon_{sys}$ and $\Delta\varepsilon(\theta_2^{cm})$ are estimates of the systematic and statistical uncertainties of the asymmetry measurement. The statistical uncertainty is given by

$$\Delta\varepsilon(\theta_2^{cm}) = \frac{\pi}{4N(1 - f_p)} \left\{ \left|\Delta N'_A\right| + \left|\Delta N'_B\right| + \left[\frac{1}{N} + \left(\frac{\Delta f_p}{1 - f_p}\right)^2\right] \left[(\Delta N'_A)^2 + (\Delta N'_B)^2\right] \right\}^{\frac{1}{2}}$$

... Eq. 5.17

where $\Delta N'_A$ and $\Delta N'_B$ are given by

$$\Delta N'_A = \Delta N_A - f_p N_A \quad \text{...Eq. 5.18a}$$

$$\Delta N'_B = \Delta N_B - f_p N_B \quad \text{5.18b}$$

the uncertainty Δf_p of the proton fraction is given by

$$\Delta f_p = f_p \left[(1 + f_p)/N_p\right]^{\frac{1}{2}} \quad \text{...Eq. 5.19}$$

and N_p represents the number of protons in the projected spectrum (Fig. 5.5a) from which f_p is determined.

The justification for Eq.5.17 is similar to that given for the corresponding equation in (Br74b) and rests on the fact that every recoil deuteron is detected and assigned to either $N_<$ or $N_>$ component. The quantities $\Delta N'_A$ and $\Delta N'_B$ may be regarded as primary observations, since each event either increments $\Delta N'$ by $(1 - f_p)$ or decrements $\Delta N'$ by $(1 + f_p)$ and the numerator of Eq. 5.6 is insensitive to errors in f_p provided the A and B runs are normalized so that $N_A = N_B$. The uncertainty of f_p contributes to $\Delta\varepsilon(\theta_2^{cm})$ through the final terms of Eq. 5.17, which arise from the denominator of Eq. 5.6. It will be

noted that Eq. 5.17 reduces to the corresponding Eq. (12) from reference (Br74b) if $f_p = 0$.

A number of methods may be used to test the sensitivity to systematic errors and to estimate the magnitude of the systematic uncertainty $\Delta\varepsilon_{sys}$ in Eq. 5.17. The asymmetry $\varepsilon(\theta_2^{cm})$ may be measured for an unpolarized incident neutron beam (e.g., by using $\zeta = 0^o$), or 'A' and 'B' runs may be made at the 'null' orientations $\delta = 0^o$ and 180^o, or two A runs at different orientations, e.g., (ζ, δ) and ($-\zeta$,$\delta + 180^o$), may be analyzed as an AB pair. All of these tests should lead to null results and $\Delta\varepsilon_{sys}$ may be estimated from the extent to which this is in fact observed to be the case. In addition, the sensitivity of the asymmetry calculation to the choice of the deuteron median S_m may be tested in order to estimate how this may contribute to $\Delta\varepsilon_{sys}$.

CHAPTER VI

6.1 Neutron beams

6.1.1 Neutron production

The n-d polarization measurements were made by using the $T(d,n)^4He$ reaction for 21.6 and 16.4 MeV neutrons, and the $^9Be(\alpha,n)^{12}C$ reaction for 7.9 MeV neutrons. For the $T(d,n)^4He$ reaction, the neutron polarizations are well known (Wa64) (Bu67a) (Mu71) for incident deuteron energies below 20 MeV. A polarization map for this reaction given by Walter (Wa71) is shown in Fig. 6.1, where the neutron polarization is plotted as a function of the incident deuteron energy E_d and neutron reaction angle θ, both in the lab. system. For the $^9Be(\alpha,n)^{12}C$ reaction, the neutron polarization was taken from Stammbach, *et al.* (St70). The polarization map for the ground state group in this reaction is shown in Fig. 6.2, and is taken from (St70).

The values for the neutron beam polarizations, P_1 (ζ), used in this work, were taken from the reference (Wa71) for 21.6 and 16.4 MeV, and from the reference (St70) for 7.9 MeV, and are included in the tabulations of Secs. 6.2, 6.3 and 6.4.

6.1.2 Neutron time-of-flight

The times-of-flight for both the $T(d,n)^4He$ and $^9Be(\alpha,n)^{12}C$ reactions were monitored throughout this work. The flight path for the experiment was 0.5 m, and Fig. 6.3 illustrates typical time-of-flight spectra taken at this path length. Fig. 6.3a contains an ungated time-of-flight spectrum showing the prompt-γ-ray peak, the ground state neutron group, and the first-excited state group. Time-of-flight gating was used to select the ground state neutron group (7.9 Mev) as indicated in the upper curve of the figure. Fig. 6.3b contains an ungated time-of-flight spectrum taken at 21.6 MeV. The prompt-γ-ray peak is observed, as also the primary neutron peak.

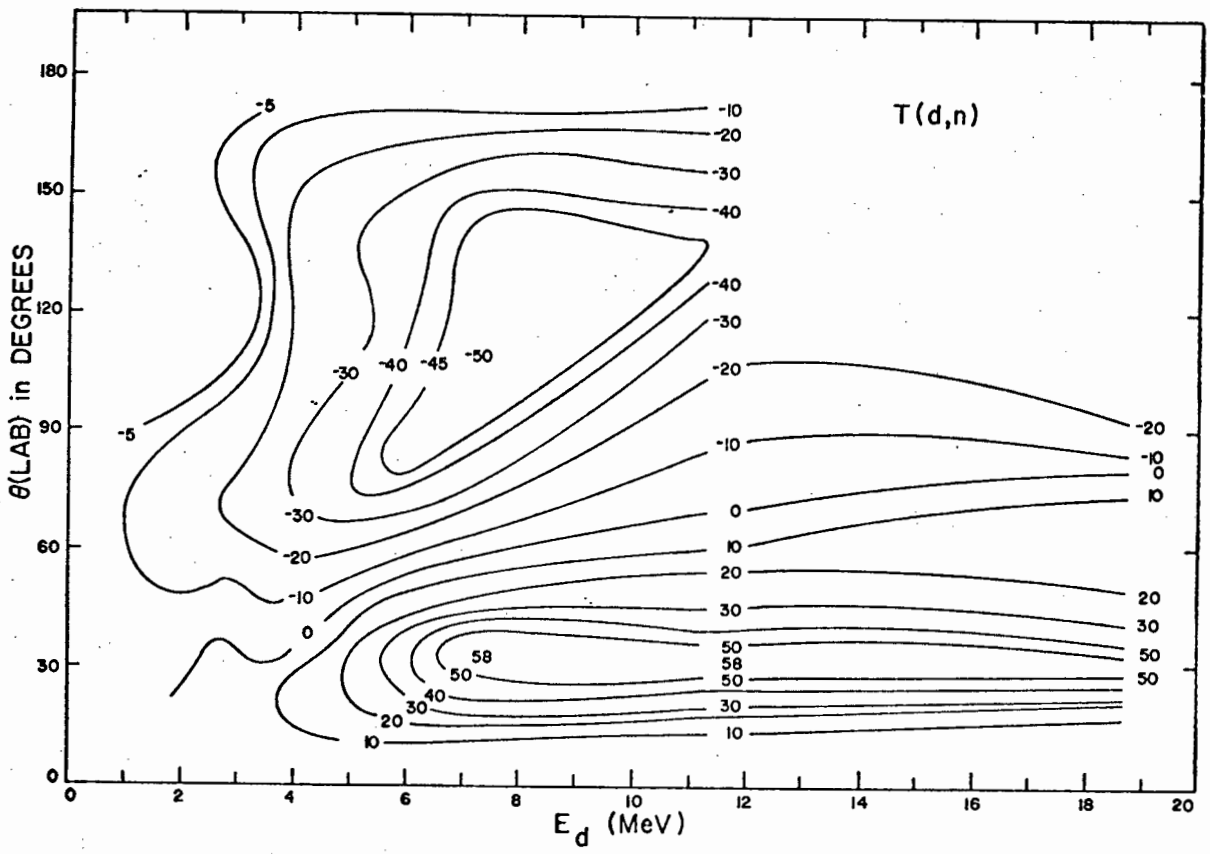

Fig. 6.1 Contour map of the polarization from the T(d,n) reaction (Wa71). The polarization of neutrons obtained from the T(d,n) reaction is plotted as a function of incident deuteron energy E_d and neutron reaction angle θ, both in the lab system. Polarizations are given in percentage.

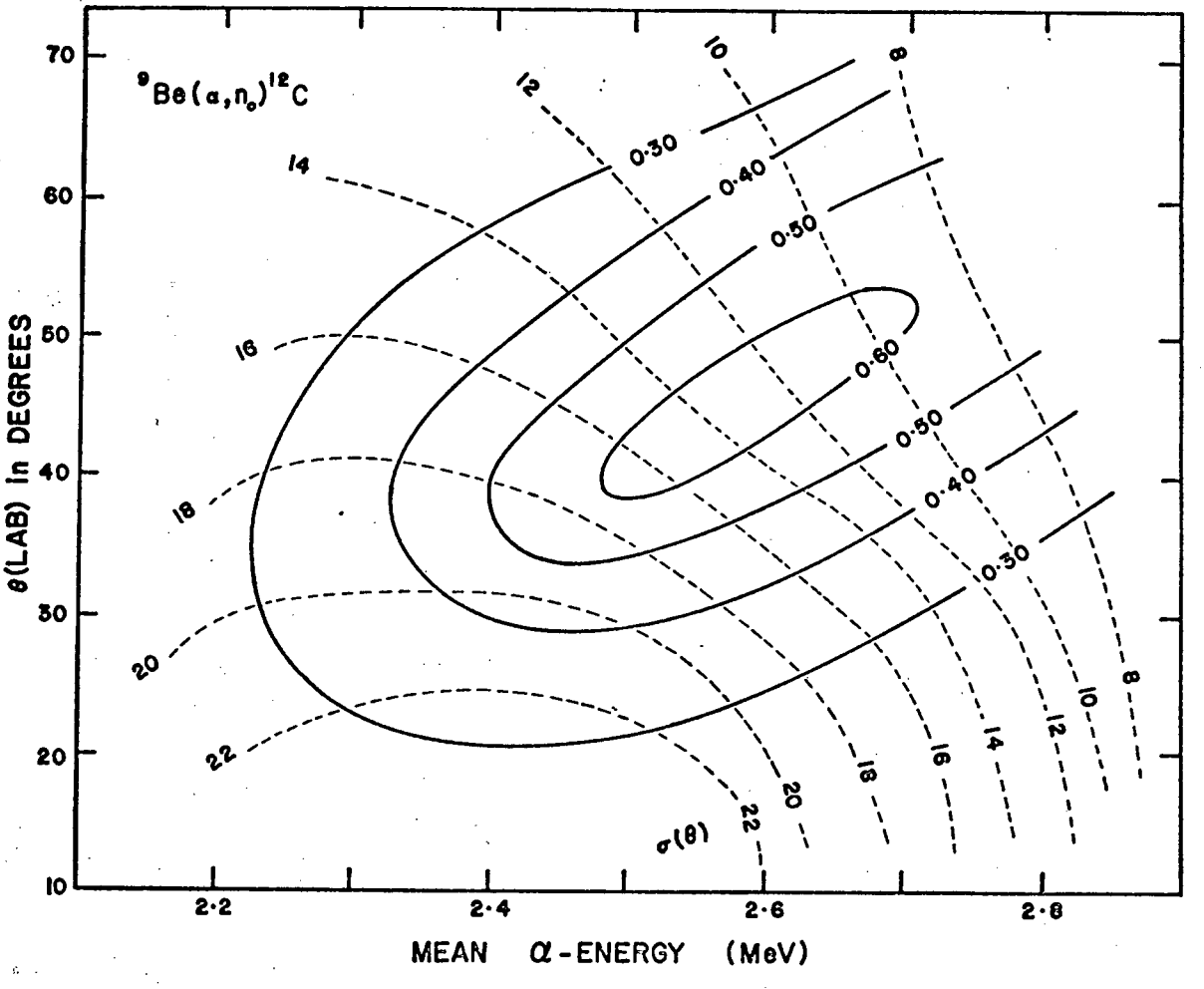

Fig. 6.2 Contour map of the polarization from the $^{9}Be(\alpha,n)$ reaction (St70). The polarization of neutrons obtained from the $^{9}Be(\alpha,n)$ reaction is plotted as a function of incident α-particle energy E_α and neutron reaction angle θ, both in the lab system. Polarizations are given in percentage.

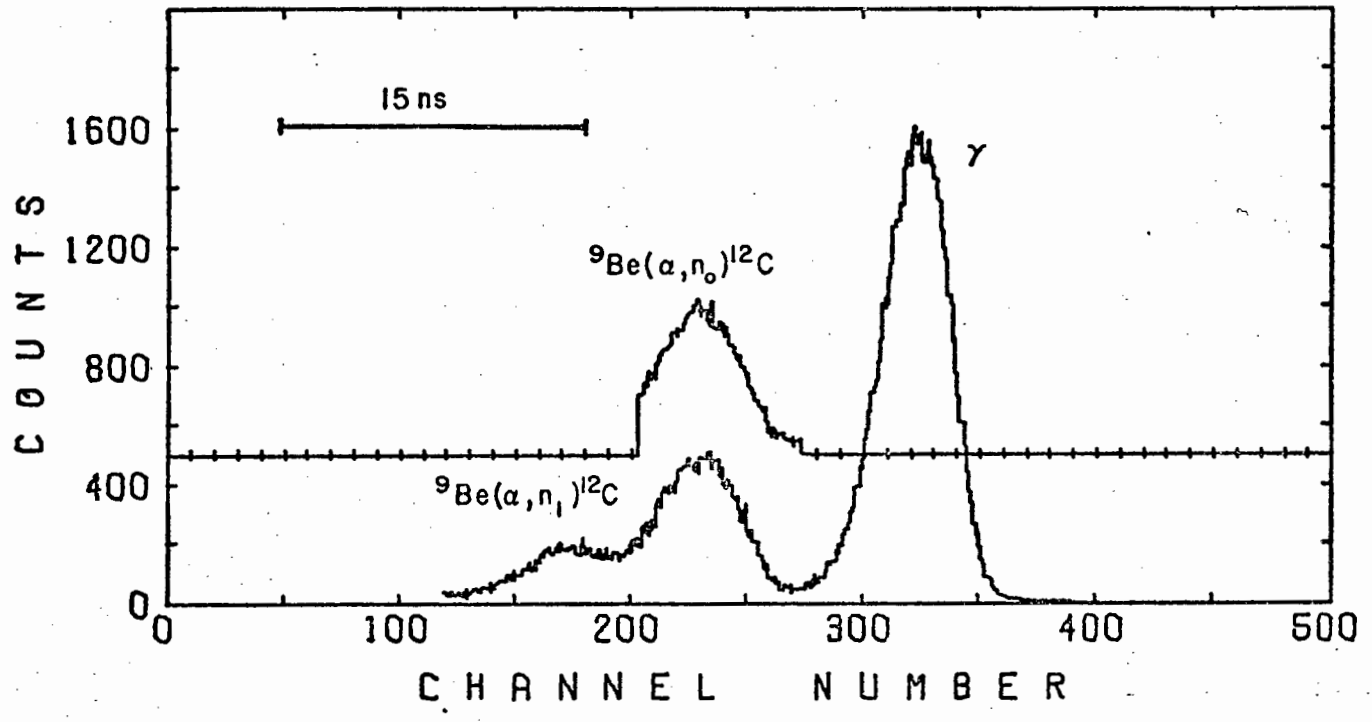

Fig. 6.3a Time-of-flight spectrum for 7.9 MeV neutrons from the $^{9}Be(\alpha,n)^{12}C$ reaction at a flight path of 0.5 m.

The lower curve is the ungated spectrum containing the prompt-γ-peak, the ground state neutron group (7.9 MeV), and the first-excited state neutron group (3.4 MeV). The upper curve is the gated spectrum selecting the ground state group only.

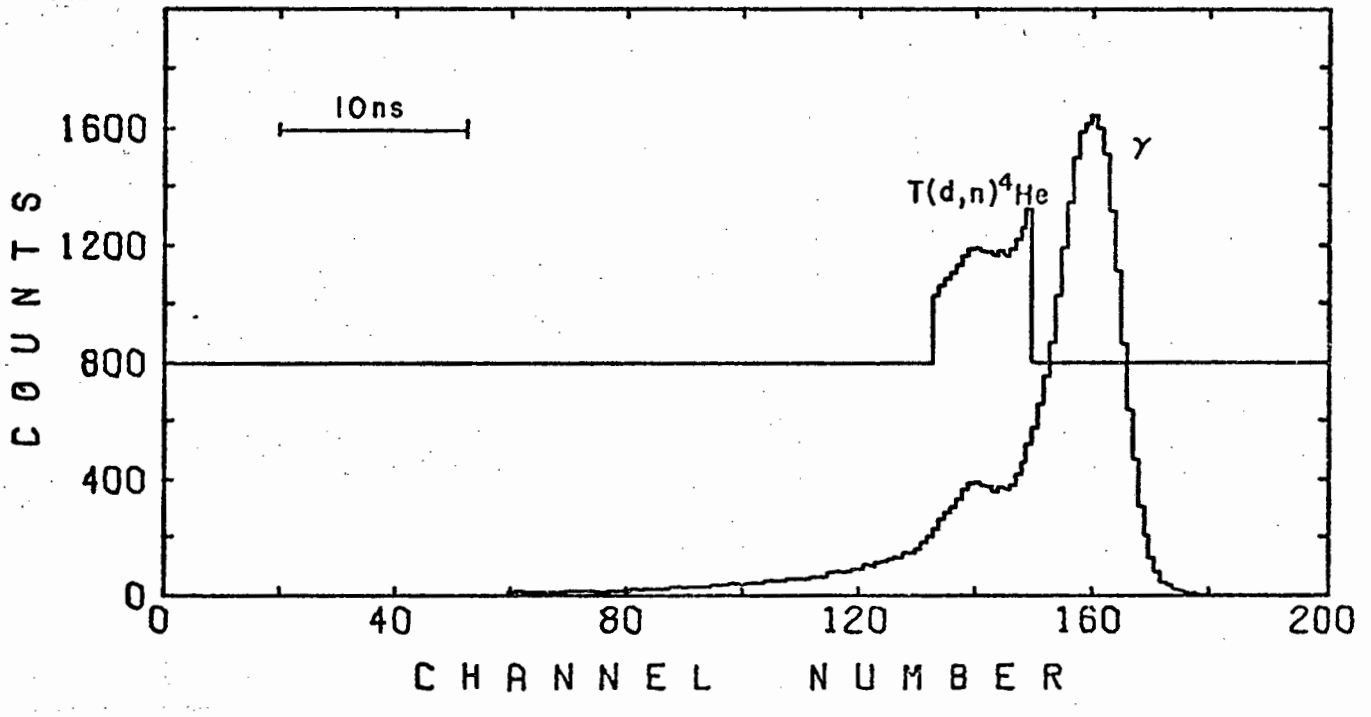

Fig. 6.3b Time-of-flight spectrum for 21.6 MeV neutrons from the $T(d,n)^{4}He$ reaction at a flight path of 0.5 m.

The lower curve is the ungated spectrum containing the prompt-γ-peak and the primary neutron group (21.6 MeV). The upper curve is the gated spectrum which selected the primary neutron group.

Again, time-of-flight gating was used to select the neutron group (21.6 MeV) and is indicated by the upper curve in the figure. The time scale is indicated in each figure.

6.2 Measurements at 21.6 MeV

6.2.1 Procedure

Before the final data were collected on which the polarization values for 21.6 MeV were based, a preliminary set of data were acquired in order to check both the crystal with light-pipe configuration, and the rotational accuracy of the goniometer used by Jones (Jo72) for the natural anthracene polarimeter. Based on these preliminary results, and due to slight modifications in experimental design, it was decided to construct a new goniometer (featured in Fig. 5.2) which gave a superior rotational accuracy for the deuterated anthracene polarimeter.

In the final experiments at 21.6 MeV, several types of runs were made, and are summarised in Table 6.1. Calibration runs were taken at the beginning and the end of the data collection. Isometric displays of the calibrations at this energy are given in Figs. 4.6a and 4.6b, and their corresponding contour plots in Figs. 4.7a and 4.7b (see Sec. 4.5 of Chapter IV). Two types of null runs (see Sec. 5.5) were performed, a zero null check (ZN), and an up-down null check (UDN) for $\delta = 0^{\circ}/180^{\circ}$. The null checks will be discussed in Sec. 6.2.2 below. Three sets of polarization runs, containing four or five A/B runs (defined in Sec. 5.1) were accumulated. The isometric display of a typical polarization run is given in Fig. 5.6, and its contour plot in Fig. 5.7 (see Chap. V). The data were acquired on an on-line PDP 15 data acquisition system and stored on magnetic tape for off-line analysis.

TABLE 6.1

SUMMARY OF RUNS AT 21.6 MeV

Run No. (Octal)	Type	ζ(deg)	δ(deg)	β(deg)	Remarks
3001	L_{max}	20	90	90	Calibrations
3002	L_{min}	20	90	0	
3025	L_{min}	-20	90	0	
3026	L_{max}	-20	90	90	
3027	$\frac{1}{2}L_{max}$	-20	90	90	
3000	T	--	--		time-of-flight
3007	ZN	0	90		Null set
3010	ZN	0	270		
3017	UDN	-20	0		
3020	UDN	-20	180		
3003	A	20	90		Polarization set
3004	B	20	270		
3005	A	-20	270		
3006	B	-20	90		
3011	B	20	270		Polarization set
3012	A	20	90		
3013	A	20	90		
3014	B	20	270		
3015	A	-20	270		Polarization set
3016	B	-20	90		
3021	A	20	90		
3022	B	20	270		
3024	B	-20	90		

During the data analysis, small L and S drifts for all spectra were neutralized upon read-in as described in Sec. 5.4.4. This was accomplished by choosing one run of each polarization set (e.g., Run 3003 of the first polarization set in Table 6.1) and shifting the other runs within the set to match up with it. Then, within each set, all A runs were summed and called 'A', and all B runs were summed and called 'B'. The (uncorrected) polarization was then calculated using the 'A' and 'B' of each polarization set, according to the method outlined in Sec. 5.2.1.

6.2.2 Results

The n-d polarization results at 21.6 MeV are tabulated in Table 6.2. The data were analyzed in angle bins of width 10° center-of-mass scattering angle (see Sec. 5.3.2) from 90° to 160°. Columns 2, 3 and 4 of Table 6.2 give the (uncorrected) polarization results for each of the three polarization sets, <P> is the average (uncorrected) polarization for all three sets, f_A is the asymmetry correction factor (see Sec. 5.4.5), and the final column which is the corrected polarization, is obtained by multiplying the average (uncorrected) polarization by the asymmetry factor. The corrected polarization at 21.6 MeV is plotted as a function of center-of-mass scattering angle in Fig. 6.4a. The results of some null asymmetry runs at 21.6 MeV are also given as a function of center-of-mass scattering angle in Fig. 6.4b. Three examples are shown: (i) the (ZN) null ($\zeta = 0^{\circ}$) showing the null asymmetry observed (runs 3007/10) using an unpolarized incident beam; (ii) the up-down null (UDN) based on runs 3017/20 in which the polarimeter was rotated 90° (about the beam) from its normal position and therefore measured the null asymmetry of recoils above and below the plane of the source reaction; and, (iii) an 'alternating' null. The 'alternating' null was formed as follows:

TABLE 6.2

n-d POLARIZATION RESULTS AT 21.6 MeV

E_n = 21.6 MeV $P_1(\delta)$ = 0.21 ±0.01 $\lvert\delta\rvert = 20^\circ$						
θ_2^{cm}	P_2(uncorrected)			<P>	f_A	P_2
	3003/04 /05/06	3011/12 /13/14	3015/16 /21/22/24			
90	.005 ±.011	.000 ±.014	-.013 ±.007	-.003 ±.005	1.01	-.003 ±.017
100	-.052 ±.009	-.063 ±.010	-.076 ±.022	-.064 ±.005	1.00	-.064 ±.017
110	-.102 ±.023	-.116 ±.025	-.133 ±.027	-.117 ±.014	1.00	-.117 ±.021
120	.027 ±.011	.019 ±.034	.024 ±.038	.023 ±.010	1.00	.023 ±.019
130	.125 ±.021	.111 ±.048	.130 ±.050	.122 ±.018	1.02	.124 ±.024
140	.181 ±.016	.145 ±.036	.152 ±.038	.159 ±.014	1.07	.170 ±.021
150	.105 ±.025	.074 ±.036	.119 ±.039	.099 ±.018	1.12	.111 ±.024
160	.046 ±.014	.054 ±.026	.062 ±.030	.054 ±.011	1.40	.076 ±.019

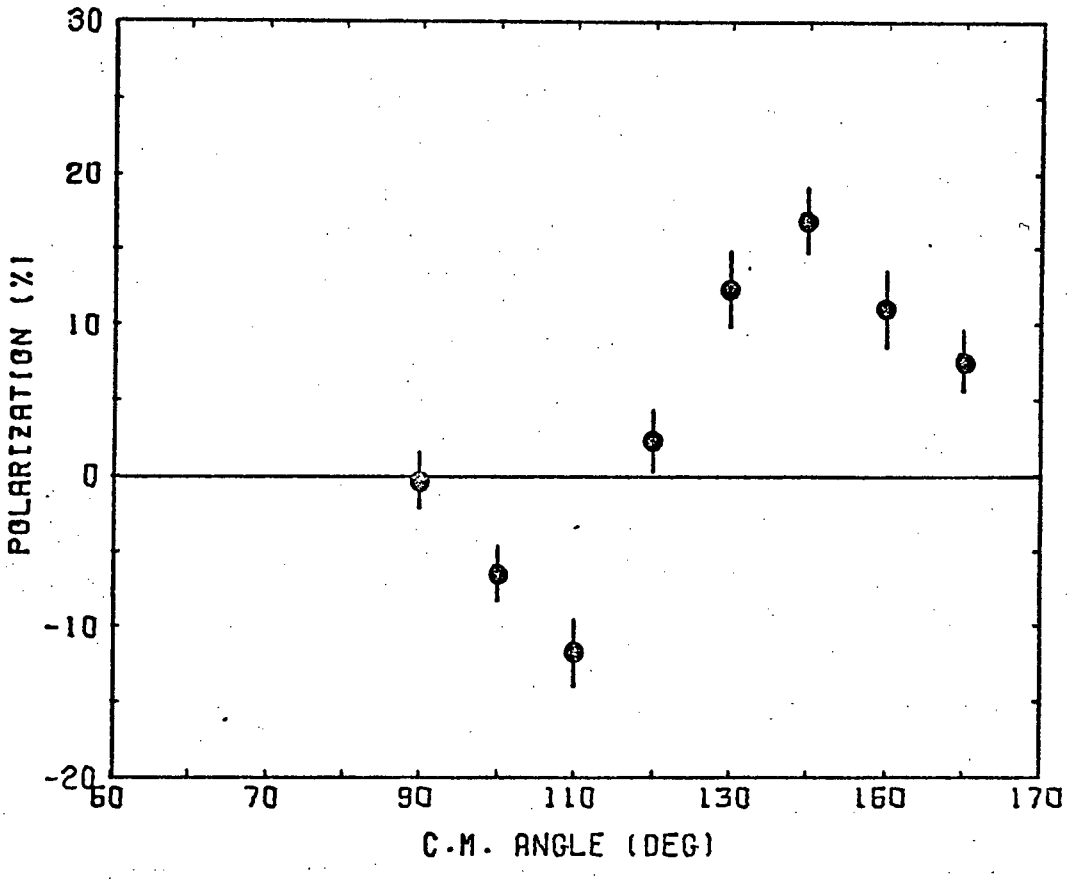

Fig. 6.4a Results of n-d polarization measurements at 21.6 MeV.

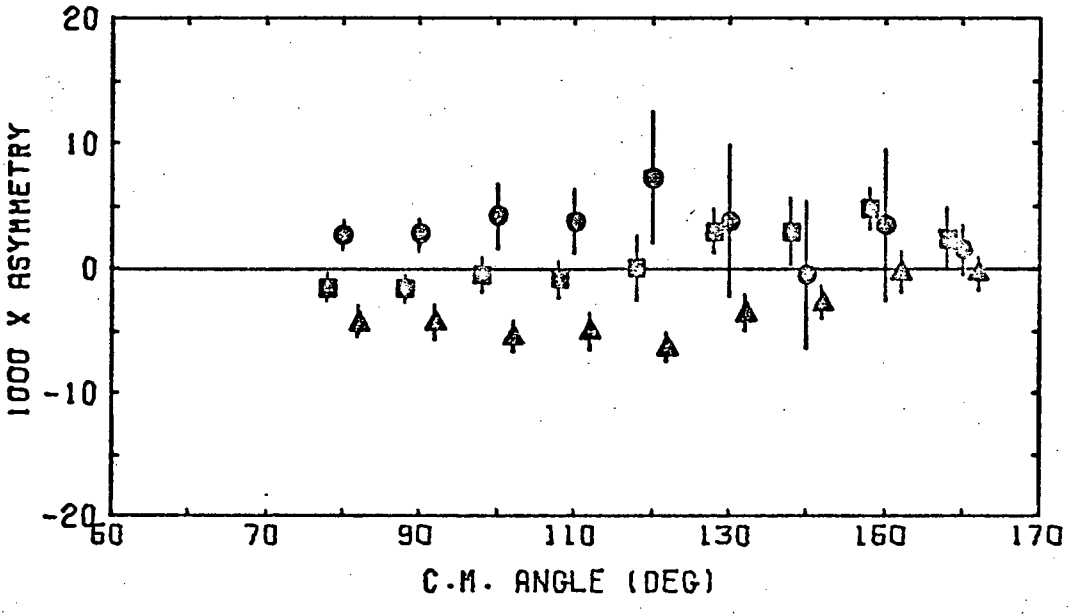

Fig. 6.4b Results of null asymmetry measurements at 21.6 MeV.

Squares show (ZN) data (runs 3007/10), circles show (UDN) data (runs 3017/20), triangles show 'alternating' null set (runs 3003/04/05/06) (see text). All data are at multiples of 10° of θ_2^{cm} but squares and triangles have been displaced $\pm 2^{\circ}$ to improve clarity of diagram.

The runs 3003, 3004, 3005 and 3006, taken at for different combinations of ζ and δ (see Table 6.1) were first normalized to the same incident neutron flux. Runs 3003 and 3004 were treated as A and B runs, respectively, as stated in the table. However, for the null check, runs 3005 and 3006 were 'alternated', that is, treated as B and A runs, respectively, instead of A and B runs. The resultant null asymmetry is therefore the average of that which would be observed for an A-A pair (3003 and 3005) and a B-B pair (3004 and 3006).

The null asymmetry values shown in Fig. 6.4b were used to determine a value for the systematic uncertainty $\Delta\varepsilon_{sys}$ (Eq. 5.16) component of the final uncertainty ΔP_2 in the final column of Table 6.2. A value of $\Delta\varepsilon_{sys} = 0.0035$ calculated as the root mean square of all the measurements shown in Fig. 6.4b was used.

6.3 Measurements at 16.4 MeV

6.3.1 Procedure

As in the case for 21.6 MeV, there were preliminary data taken for 16.4 MeV. The accuracy of the goniometer was assured, and the experimental alignment was verified for the more backward (lab) angle of 80° at which the 16.4 MeV data were accumulated.

For the final experiments at 16.4 MeV, the types of runs made are summarized in Table 6.3. The calibration runs were taken at the beginning and the end of the experiment, and also periodically during the running. Isometric displays of the calibrations at 16.4 MeV are shown in Figs. 6.5a and 6.5b. Fig. 6.5a is the LS-spectrum for 16.4 MeV neutrons directed parallel to the c'-axis, and therefore the L_{max}-orientation, and Fig. 6.5b is the LS-spectrum for 16.4 MeV neutrons directed parallel to the b-axis of the crystal, and therefore the L_{min}-orientation. The symbols on the figures have the same meaning as in Fig. 4.6, Sec. 4.5. Throughout this series a digital offset was used on the ADC processing the S-parameter. The offset was adjusted to exclude the Compton electron ridge from the region of interest of the LS-spectrum, thereby reducing the count rate processed by the analyzing system. This explains why no Compton ridge is seen in Figs. 6.5a and 6.5b.

The null checks performed at this energy were up-down nulls similar to those of type (ii) described in Sec. 6.2.2 above. Three sets of polarization runs containing an A and a B run were acquired. A fourth set of polarization runs was rejected, since the drifts of the spectra fell outside the narrow tolerance applied to all polarization sets (see Sec. 5.5).

TABLE 6.3

SUMMARY OF RUNS AT 16.4 MeV

Run no.	Type	δ (deg)	δ (deg)	β (deg)	Remarks
1645	L_{min}	80	270	0	Calibrations
1646	L_{max}	80	270	90	
1651	L_{min}	80	270	0	
1652	L_{max}	80	270	90	
1657	L_{min}	80	270	0	
1658	L_{max}	80	270	90	
1667	L_{min}	80	270	0	
1668	L_{max}	80	270	90	
1669	$\frac{1}{2}L_{max}$	80	270	90	
1600	T	--	--		Time-of-flight
1649	UDN	80	180		Null set
1650	UDN	80	0		
1655	UDN	-80	0		
1656	UDN	-80	180		
1661	UDN	-80	0		Null set
1662	UDN	-80	180		
1663	UDN	80	180		
1664	UDN	80	0		
1647	B	80	270		Polarization set
1648	A	80	90		
1653	A	-80	270		Polarization set
1654	B	-80	90		
1659	A	-80	270		Polarization set
1660	B	-80	90		
1661	A	80	90		Rejects
1662	B	80	270		

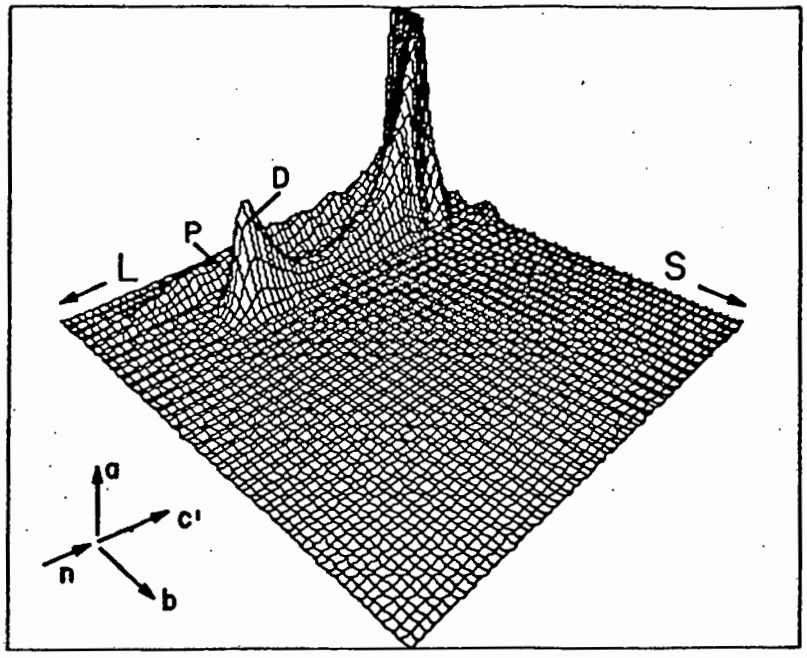

Fig. 6.5a LS-spectrum for 16.4 MeV neutrons directed parallel to the c'-axis of the deuterated anthracene crystal (maximum-L orientation). The ridges are due to breakup protons (P) and recoil deuterons (D). The vertical scale is arbitrarily cut off at 500 counts.

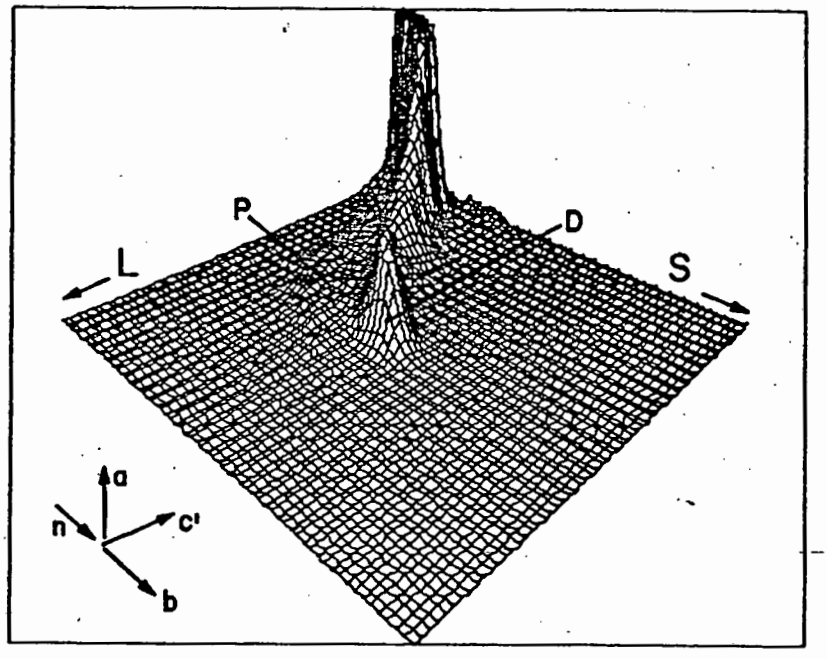

Fig. 6.5b LS-spectrum for 16.4 MeV neutrons directed parallel to the b-axis of the deuterated anthracene crystal (minimum-L orientation). The ridges are due to breakup protons (dispersed) (P) and recoil deuterons (D). The vertical scale is arbitrarily cut off at 500 counts.

The isometric display of a 16.4 MeV polarization run is illustrated in Fig. 6.6. This figure demonstrates the versatility of the PDP 15 data acquisition system. The data were accumulated in buffer mode at the same dispersion as shown for the calibration runs in Fig. 6.5. The dispersion was doubled when the buffer tape was scanned, so that the region corresponding to the lower half of the S-scale in Fig. 6.5 was spread over the full S-scale in Fig. 6.6.

During the analysis, the small L and S drifts in the runs were neutralized as for the 21.6 MeV data, and (uncorrected) polarization values were calculated from the A and B runs of each set.

6.3.2 Results

The n-d polarization results at 16.4 MeV are tabulated in Table 6.4. The symbols in the table have the same meaning as in Table 6.2 described in Sec. 6.2.2. The corrected polarization at 16.4 MeV, listed in the final column, is plotted as a function of center-of-mass scattering angle in Fig. 6.7a. The results of the null asymmetry runs at 16.4 MeV are plotted as a function of the center-of-mass scattering angle for two sets of data in Fig. 6.7b. A value of $\Delta\varepsilon_{sys} = 0.0021$ for the 16.4 MeV data was obtained from these measurements using the same methods as for the 21.6 MeV results.

6.4 Measurements at 7.9 MeV

6.4.1 Procedure

Several short, preliminary experiments were performed at 7.9 MeV since this incident energy is convenient in the respect that the spectra are uncomplicated by the breakup protons present in the 21.6 and 16.4 MeV data. This early work played a major rôle in determining the optimum light-pipe design described in Chap. IV.

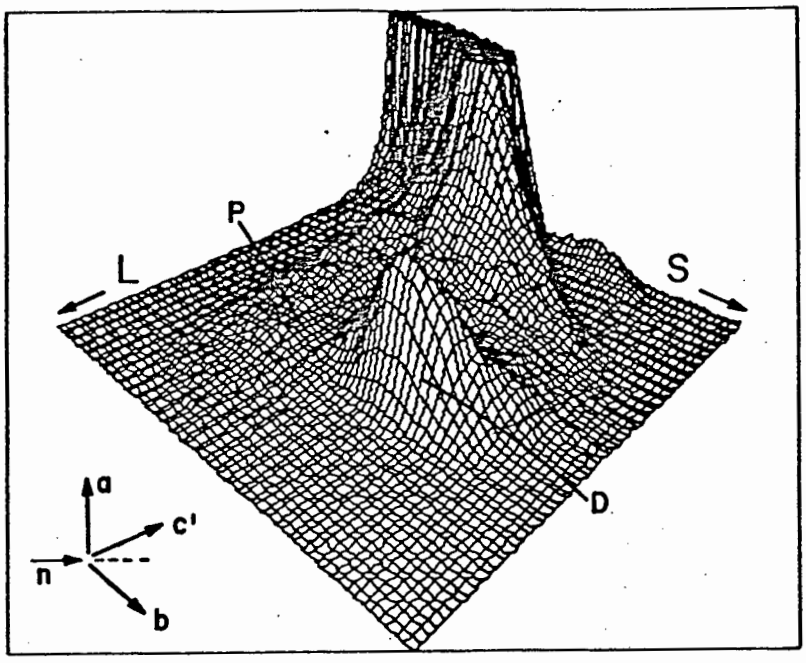

Fig. 6.6 LS-spectrum for 16.4 MeV neutrons in the direction $(\theta,\phi) = (90^{\circ},40^{\circ})$ in the bc'-plane (polarization orientation).

The ridges are due to breakup protons (P) and recoil deuterons (D). The S-dispersion is doubled so that the region corresponding to the lower half of the S-scale in Fig. 6.5 is spread over the full S-scale in this figure. The counts (vertical) scale in this plot is arbitrarily truncated at 500 counts.

TABLE 6.4

n-d POLARIZATION RESULTS AT 16.4 MeV

E_n = 16.4 MeV $P_1(\delta)$ = 0.46 ±0.02 $\lvert\delta\rvert = 80^\circ$						
θ_2^{cm}	P_2(uncorrected)			<P>	f_A	P_2
	1647/48	1653/54	1659/60			
90	.020 ±.008	.057 ±.007	.027 ±.007	.035 ±.011	1.02	.035 ±.012
100	.002 ±.009	.024 ±.008	-.023 ±.011	.000 ±.013	1.02	.000 ±.014
110	.048 ±.013	.058 ±.018	.006 ±.014	.037 ±.011	1.03	.038 ±.018
120	.100 ±.029	.112 ±.027	.061 ±.017	.091 ±.015	1.04	.095 ±.017
130	.174 ±.026	.131 ±.029	.161 ±.016	.155 ±.014	1.10	.171 ±.017
140	.139 ±.024	.155 ±.024	.161 ±.023	.152 ±.014	1.15	.174 ±.017
150	.106 ±.013	.097 ±.012	.081 ±.012	.095 ±.007	1.21	.114 ±.009
160	.057 ±.024	.057 ±.023	.029 ±.019	.048 ±.013	1.43	.068 ±.014

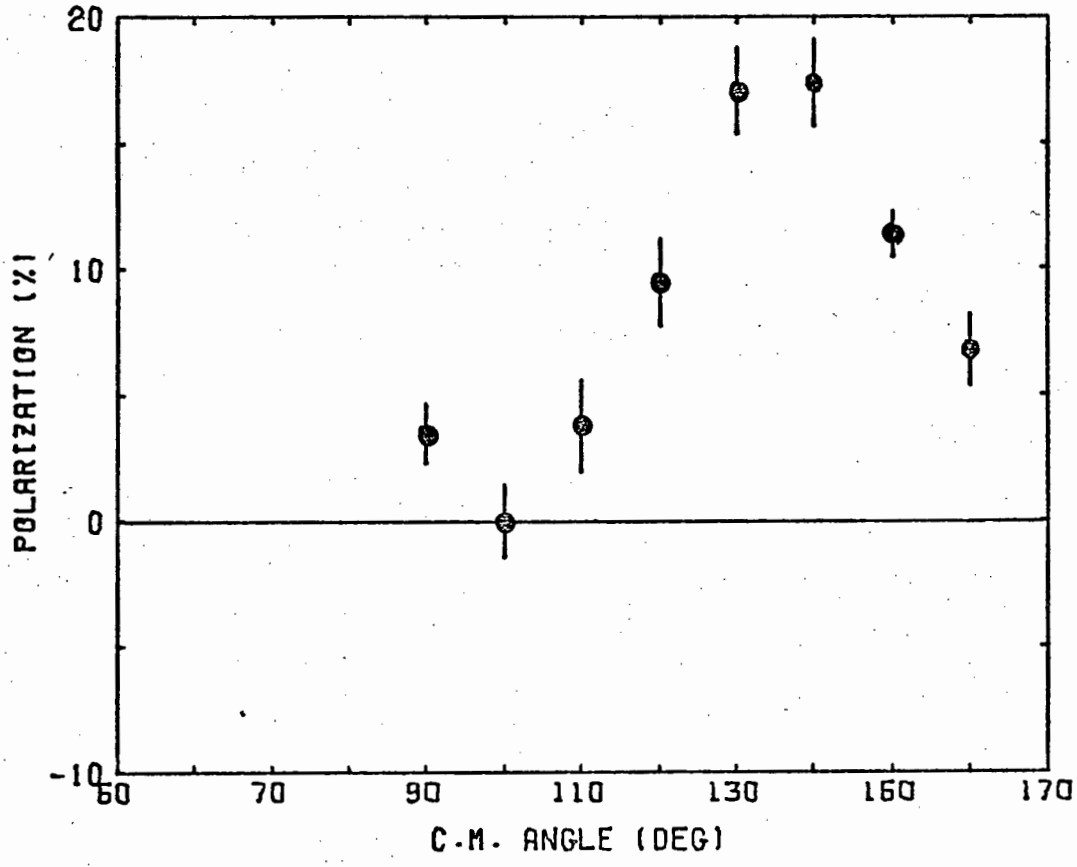

Fig. 6.7a Results of n-d polarization measurements at 16.4 MeV.

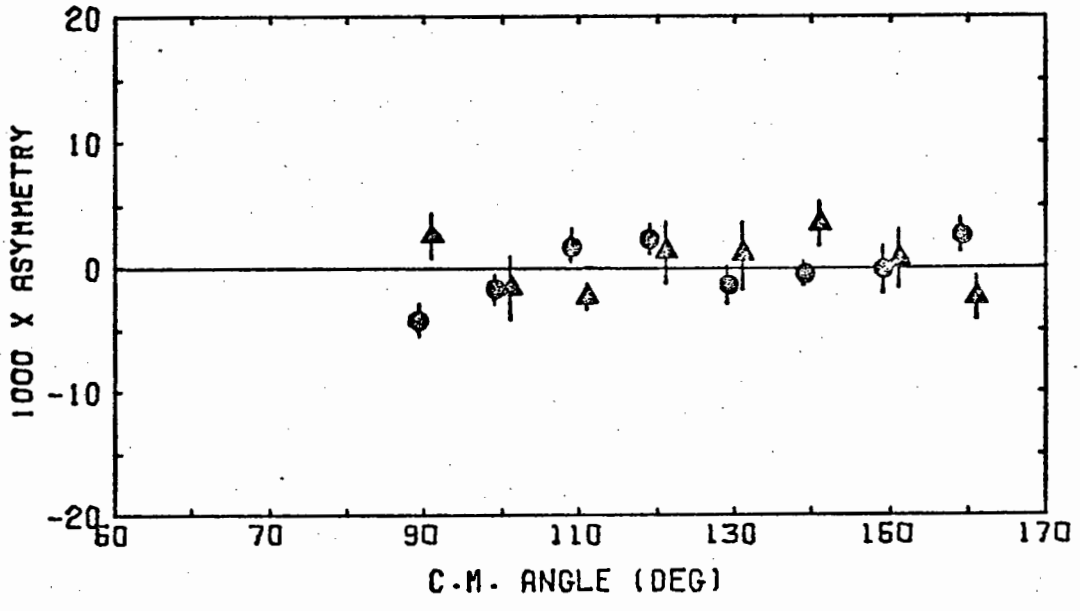

Fig. 6.7b Results of the two sets of null asymmetry measurements listed in Table 6.3.

Circles are set 1 (runs 1649/50/55/56). Triangles are set 2 (runs 1661/62/63/64).

For the final experiments at 7.9 MeV, the types of runs made are summarized in Table 6.5. Calibration runs were taken at the beginning and the end of the experiment, and periodically throughout. In addition, a digital offset was used to exclude the Compton electon ridge as was done at 16.4 MeV. Figs. 6.8a and 6.8b are isometric displays of runs made at the L_{max}-orientation, and L_{min}-orientation, respectively (see Sec. 6.3.1), for 7.9 MeV neutrons. The various types of time-of-flight calibrations are indicated in the table. The null runs are of the up-down type (see Sec. 6.2.2) similar to those used for both the 21.6 and 16.4 MeV experiments. Four polarization sets including an A run and a B run were accumulated at 7.9 MeV.

Fig. 6.9 is the isometric display of a typical polarization run for 7.9 MeV neutrons. In these isometric figures for 7.9 MeV, it is observed that there is no complication due to breakup protons.

Again, the small drifts in L and S were neutralized upon read-in for each polarization set. The (uncorrected) polarization was calculated using the A and B run for each set.

6.4.2 *Results*

The n-d polarization results at 7.9 MeV are tabulated in Table 6.6. The symbols are defined in Sec. 6.2.2. The corrected polarization at 7.9 MeV given in the last column of the table, is plotted as a function of center-of-mass scattering angle in Fig. 6.10a. The results from the up-down null asymmetry runs at 7.9 MeV are plotted as a function of the center-of-mass scattering angle for two sets of up-down null runs in Fig. 6.10b. A value of $\Delta\epsilon_{sys} = 0.0022$ for the 7.9 MeV data was obtained from these measurements using the same methods as for the 21.6 and 16.4 MeV data.

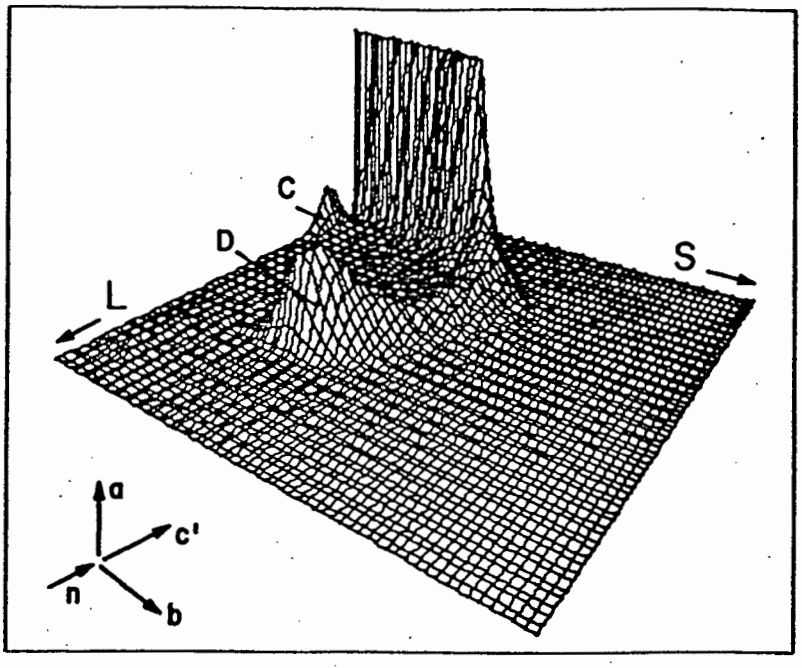

Fig. 6.8a LS-spectrum for 7.9 MeV neutrons directed parallel to the c'-axis of the deuterated anthracene crystal (maximum-L orientation). The ridges are due to Compton electrons (C) and recoil deuterons (D). The vertical scale is truncated at 500 counts.

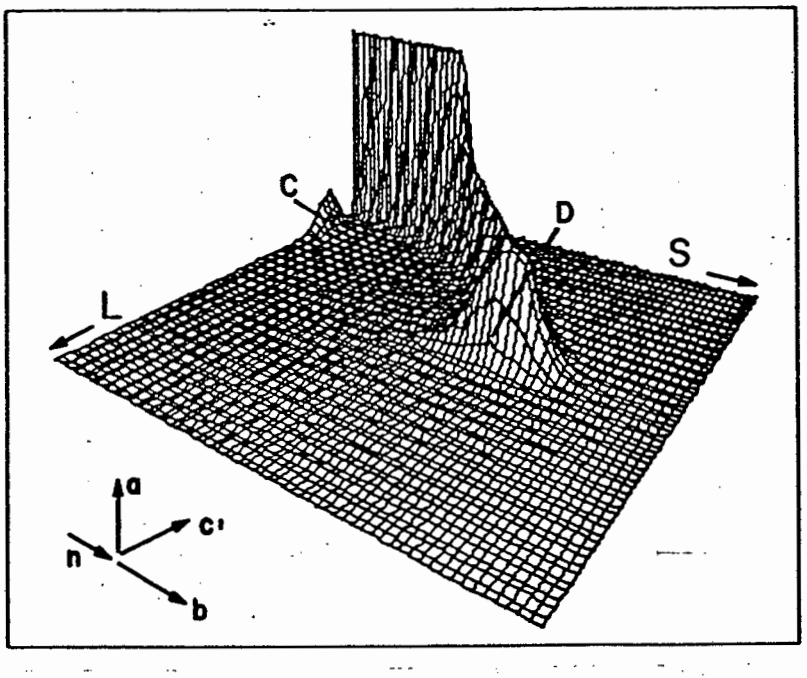

Fig. 6.8b LS-spectrum for 7.9 MeV neutrons directed parallel to the b-axis of the deuterated anthracene crystal (minimum-L orientation). The ridges are due to Compton electrons (C) and recoil deuterons (D). The vertical scale is truncated at 500 counts.

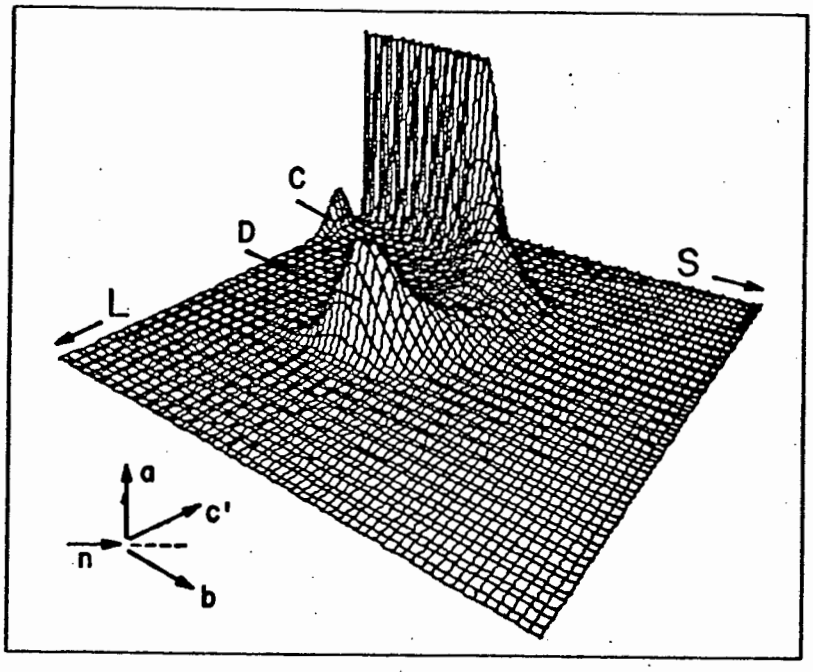

Fig. 6.9 LS-spectrum for 7.9 MeV neutrons in the direction $(\theta,\phi) = (90^{o},40^{o})$ in the bc'-plane (polarization orientation).

The ridges are due to Compton electrons (C) and recoil deuterons (D). The deuteron ridge is seen to be broadened relative to that in Fig. 6.8a. The vertical scale is truncated at 500 counts.

TABLE 6.5

SUMMARY OF RUNS AT 7.9 MeV

Run no.	Type	δ (deg)	δ (deg)	β (deg)	Remarks
1804	L_{max}	40	90	90	Calibrations
1805	L_{min}	40	90	0	
1810	L_{min}	40	270	0	
1811	L_{max}	40	270	90	
1812	L_{min}	-40	270	0	
1813	L_{max}	-40	270	0	
1822	L_{min}	40	270	0	
1823	L_{max}	40	270	90	
1824	$\frac{1}{2}L_{max}$	40	270	90	
1800	T	--	--		Time-of-flight
1801	T	--	--		Time-of-flight, at $\frac{1}{2}L_{max}$
1802	T	--	--		Time-of-flight, bitten
1803	T	--	--		Time-of-flight, 20ns out
1829	T	--	--		Time-of-flight,
1830	T	--	--		Time-of-flight, 20ns out
1831	T	--	--		Time-of-flight, at $\frac{1}{2}L_{max}$
1808	UDN	40	0		Null set
1809	UDN	40	180		
1816	UDN	-40	0		
1817	UDN	-40	180		
1818	UDN	-40	180		Null set
1819	UDN	-40	0		
1827	UDN	40	0		
1828	UDN	40	180		
1806	A	40	90		Polarization set
1807	B	40	270		
1814	A	-40	270		Polarization set
1815	B	-40	90		
1820	B	-40	90		Polarization set
1821	A	-40	270		
1825	B	40	270		Polarization set
1826	A	40	90		

TABLE 6.6

n-d POLARIZATION RESULTS AT 7.9 MeV

E_n = 7.9 MeV			$P_1(\delta)$ = 0.60 ±0.02			$\lvert\delta\rvert = 40^o$	
θ_2^{cm}	P_2(uncorrected)				<P>	f_A	P_2
	1806/07	1814/15	1820/21	1825/26			
100	.029 ±.007	-.002 ±.005	-.006 ±.005	.031 ±.007	.013 ±.010	6.10	.079 ±.063
110	.038 ±.008	.023 ±.006	.014 ±.005	.040 ±.003	.029 ±.006	3.14	.091 ±.026
120	.047 ±.010	.045 ±.007	.037 ±.007	.053 ±.005	.046 ±.003	2.51	.115 ±.025
130	.050 ±.006	.049 ±.004	.049 ±.004	.058 ±.008	.052 ±.002	1.85	.096 ±.020
140	.031 ±.010	.032 ±.006	.029 ±.006	.035 ±.006	.032 ±.004	1.92	.061 ±.014
150	.013 ±.009	.014 ±.005	.011 ±.006	.016 ±.006	.014 ±.005	2.24	.031 ±.010
160	.007 ±.014	.003 ±.009	.002 ±.011	.004 ±.011	.004 ±.006	3.47	.014 ±.018

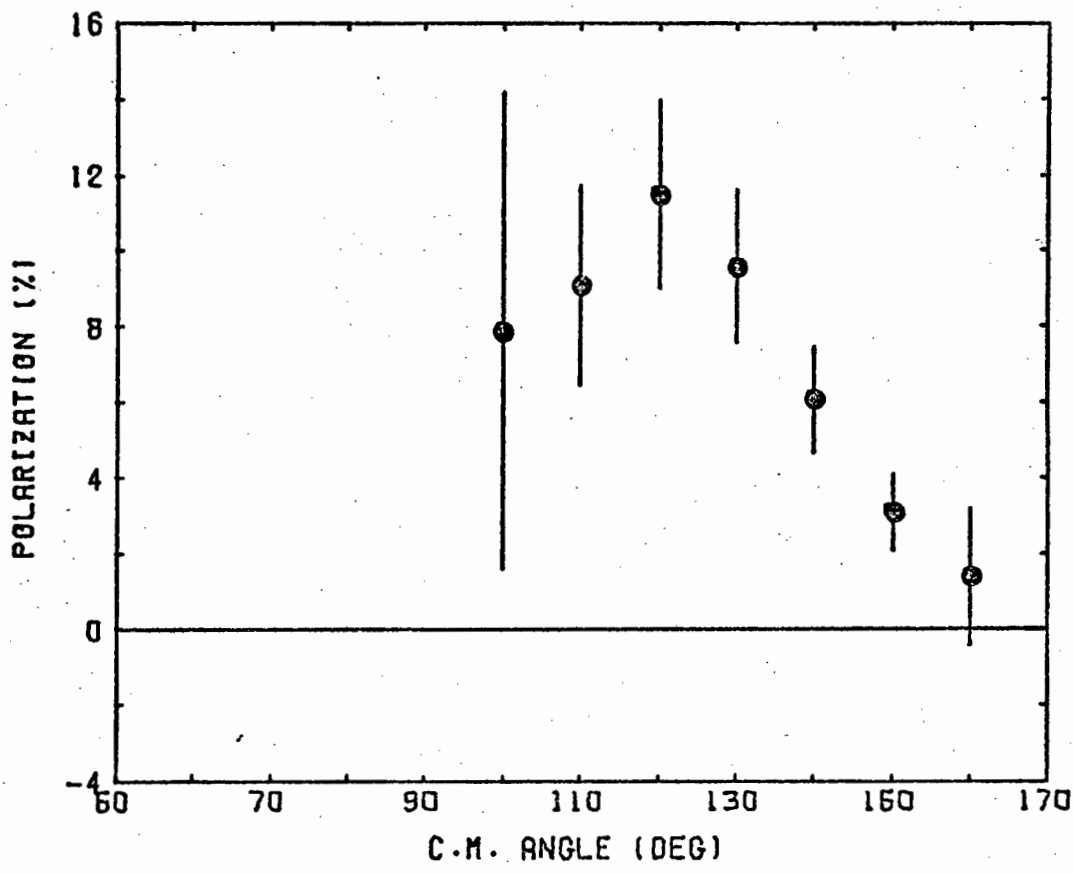

Fig. 6.10a Results of n-d polarization measurements at 7.9 MeV.

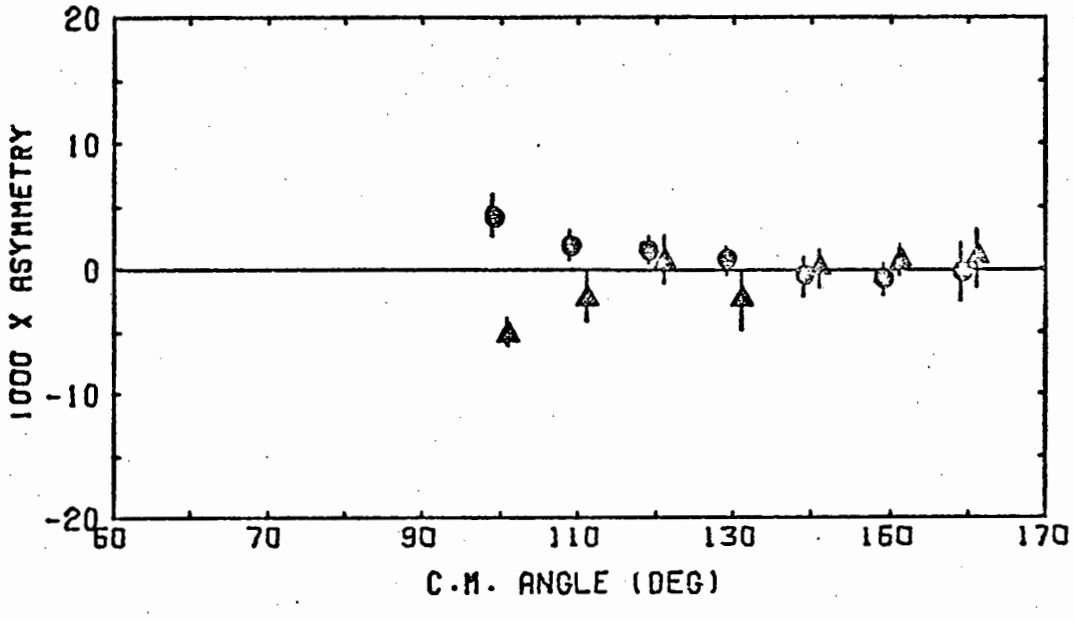

Fig. 6.10b Results of the two sets of null asymmetry measurements listed in Table 6.5.

Circles are set 1 (runs 1808/09/16/17). Triangles are set 2 (runs 1818/19/27/28).

A notable feature of the 7.9 MeV data is the fact that the asymmetry correction factors f_A (see Table 6.6) are much larger than the corresponding factors for the 21.6 and 16.4 MeV data (see Tables 6.2 and 6.4). This is a consequence of the fact that the directional resolving power R (see Table 4.1 and discussion in Chap. IV) drops off with recoil deuteron energy. It is this factor which sets the lower angle limit of $\theta_2^{cm} = 100^o$ for the measurements at 7.9 MeV. For lower values of θ_2^{cm} the recoil deuteron energy is too low (less than 4 MeV) to resolve left and right recoils ($R \lesssim 1$) at the polarization orientation of the crystal.

CHAPTER VII

RESULTS AND CONCLUSIONS

7.1 Polarization data

The results from the polarization measurements for neutron-deuteron scattering at 21.6, 16.4 and 7.9 MeV (Chap. VI) are reproduced and compared to the previously available n-d data at or near these energies, and also with p-d data, in Figs. 7.1, 7.2 and 7.3, respectively. Also shown in these figures are theoretical values (solid curves) based on the work of Pieper (Pi72b). Pieper gave theoretically calculated curves at 2.0, 5.5, 10.0, 14.1, 22.7, 40.0 and 70.0 MeV. The solid curves shown in Figs. 7.1, 7.2, and 7.3 are computer interpolations of Pieper's curves and were made using a spline-interpolation procedure.

The present data at 21.6 MeV (see Fig. 7.1) are consistent with the recent measurements of Morris, *et al.* (Mo74) at 21.1 MeV, and also confirm that the negative dip observed between $\theta = 80^{\circ} - 120^{\circ}$ is shallower than indicated by the earlier n-d measurements of Malanify, *et al.* (Ma66) and Walter and Kelsey (Wa63). The data also show the characteristic positive peak in the polarization at backward angles ($\theta_2^{cm} \simeq 135^{\circ}$). However, the present data are systematically lower than the recent n-d measurement of Morris, *et al.* (Mo74) at 130° (see Fig. 7.1) and than the trend of the p-d data of Faivre, *et al.* (Fa69) at 20.1 and 22.7 MeV, as shown by the dashed curve in Fig. 7.1. This feature might perhaps be related to the limited angular resolution of the present technique at large values of θ_2^{cm} (see Fig. 4.8) coupled with the fact that $P_2(\theta_2^{cm})$ appears to vary rapidly at $\theta_2^{cm} \simeq 135^{\circ}$. These factors would tend to lower the observed values of $P_2(\theta_2^{cm})$.

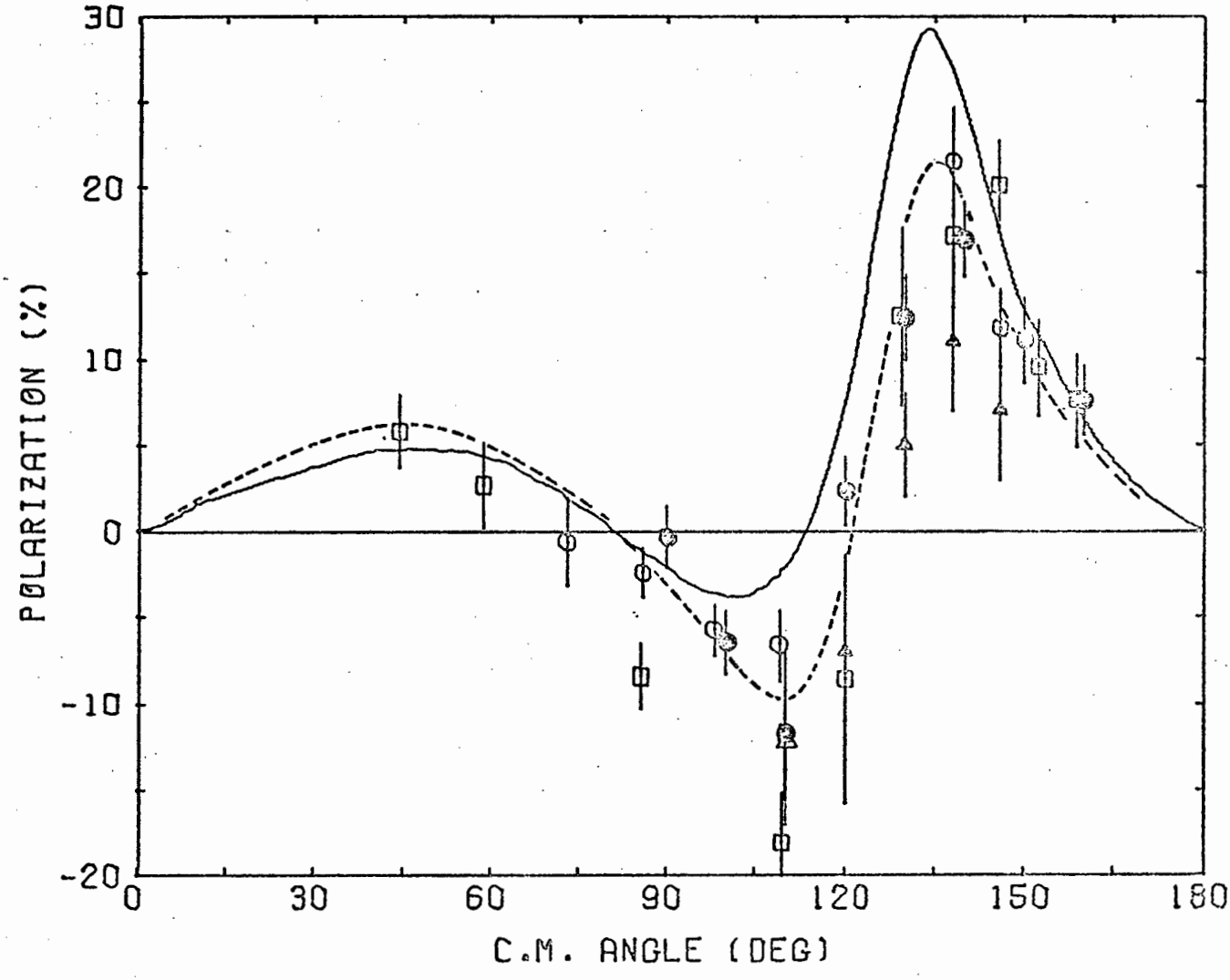

Fig. 7.1 Polarization in N-d scattering near 21.6 MeV.

n-d; □ - 22.7 MeV (Ma66), ○ - 21.1 MeV (Mo74), △ - 23.7 MeV (Wa63), ● - this work;

p-d; dashed curve shows the trend at 20.1 and 22.7 MeV (Fa69).

The interpolated (solid) curve in Fig. 7.1, based on the theoretical calculation of Pieper, fits the experimental data (p-d and n-d) reasonably well at $\theta_2^{cm} \lesssim 90^o$ and at $\theta_2^{cm} \gtrsim 150^o$, but is systematically higher than the observed values at intermediate angles. The consistency of the different sets of experimental data in this region suggests that the theoretical calculation will need to be modified to remedy this discrepancy.

The data obtained at 16.4 MeV and shown in Fig. 7.2 are consistent with the other data (p-d and n-d) shown in this figure. The present datum at $\theta_2^{cm} = 130^o$ is lower than the value of Morris, *et al.* (Mo74) at this angle and incident energy and lower than the value expected for the p-d polarization based on the measurements of Faivre, *et al.* (Fa69) at an incident energy of 17.5 MeV. As at 21.6 MeV, the angular resolution of the present technique, together with the rapid variation of polarization with angle could be partially responsible for this discrepancy.

The interpolated theoretical curve for incident energy 16.4 MeV is in better agreement with the experimental data (Fig. 7.2) than that for incident energy 21.6 MeV.

The data obtained at 7.9 MeV are also consistent with other measurements (p-d and n-d) at or near this energy as shown in Fig. 7.3. The interpolated theoretical curve for this energy fits the experimental data reasonably well although it is systematically lower than experiment at $\theta_2^{cm} \lesssim 90^o$, and systematically higher than experiment in the region $120^o \lesssim \theta_2^{cm} \lesssim 150^o$.

The general conclusions indicated by the n-d and p-d polarization data at incident energies near 7.9, 16.4 and 21.6 MeV are therefore:

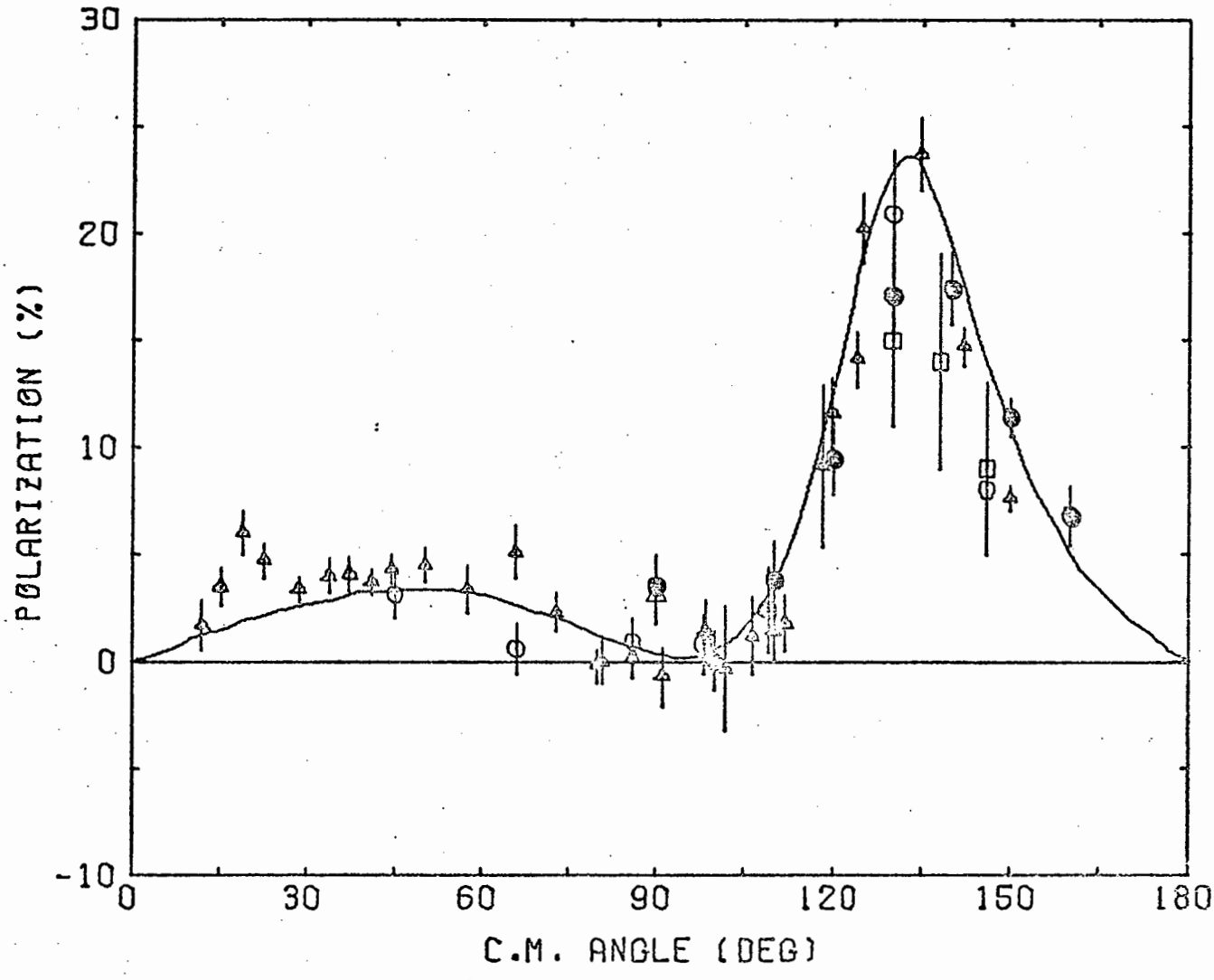

Fig. 7.2 Polarization in N-d scattering near 16.4 MeV.

n-d; □ - 16.4 MeV (Wa63), ○ - 16.8 MeV (Mo74), ◍ - 16.4 MeV, this work;

p-d; △ - 17.5 MeV (Fa69).

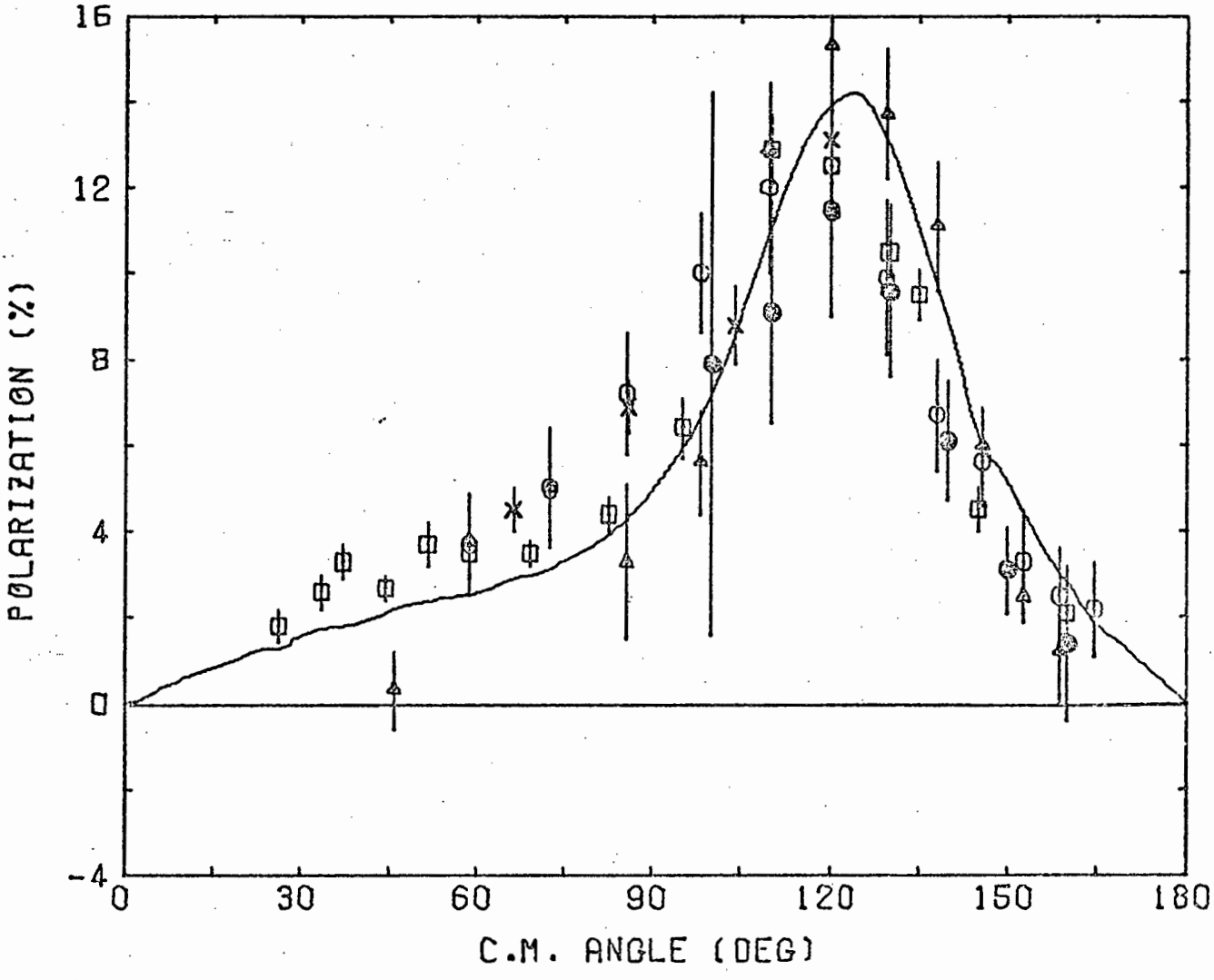

Fig. 7.3 Polarization in N-d scattering near 8 MeV.

n-d; O - 7.8 MeV (Ta70), Δ - 7.9 MeV (Br71a), ⊗ - 7.9 MeV, this work;

p-d; □ - 8.0 MeV (Cl67) - 8.0 MeV (Gr66).

(i) that there is no discrepancy between the n-d and p-d polarization at these energies; and

(ii) that the theoretical calculations of Pieper, *et al.* (Pi72b) reproduce the experimental polarization values reasonably well at incident energies in the range 7-16 MeV but predict higher polarization values than experiment at backward angles ($\theta_2^{cm} \gtrsim 90^\circ$) for higher incident energies, e.g., in the neighborhood of 21.6 MeV.

Conclusion (i) stands in contradiction to the n-d data of Malanify, *et al.* (Ma69) at 21.6 MeV, and rests on the recent measurements of Morris, *et al.* (Mo74) and on the present measurements at this energy. This conclusion also implies that the comparison of p-d and n-d polarization values at these energies provides no evidence of the breaking of charge symmetry of nuclear forces. In view of this conclusion it would be all the more interesting to obtain further polarization in n-d scattering at still higher energies, for example, at 35 MeV where the measurements of Zamudio-Cristi, *et al.* (Za73) have indicated significant discrepancies between the n-d and p-d polarization.

7.2 Improvements to the experiment

It is clear from the data shown in Figs. 7.1, 7.2 and 7.3 that a really searching test of charge symmetry of the type considered here will require considerably more accurate polarization measurements and especially will require improved techniques for the measurement of the n-d polarization. In the present technique and in many polarization measurements the main limitations of accuracy arise from systematic uncertainties rather than statistical uncertainties. Spin precession solenoids are now widely used

to avoid systematic errors arising from mechanical rotations or the interchange of left and right detectors. This method is particularly applicable to the more standard double scattering experiments in which such an interchange of detectors is required. In the present method, however, the advantages of a solenoid would probably be marginal since the mechanical rotation of the small crystal detector is minimal and can be carried out with high precision.

The deuterated anthracene polarimeter on the other hand is very sensitive to electronic stability. Even though electronic drifts can be neutralized to a large degree in the data analysis, these effects probably constitute the main source of systematic uncertainty in the present work. An obvious way to attack this problem would be to introduce digital stabilization in the L and S channels of the electronic system. In principle this could be done by stabilizing the edge of the deuteron bump electronically 'on-line' in the same way as is now done "off-line", during the data analysis.

7.3 Further applications.

7.3.1 Polarization work.

It is within the means available locally to continue this work at different incident energy, using other source reactions. Preliminary work has been done using the $^{14}N(d,n_o)^{15}O$ reaction, which has been described by Busse, *et al.* (Bu70). The incident deuteron energy was 5.5 MeV, and the energy and polarization of the primary neutron group were 10 MeV, and 0.30, at $\delta = 30^{\circ}$ (lab). Fig. 7.4 is an example of the 10 MeV data. Figs. 7.4a is an LS- spectrum of the data taken with the deuterated crystal at the maximum L-orientation, that is, the neutron beam is parallel to the c'-axis. Fig. 7.4b is the LS-spectrum of the 10 MeV data taken with the crystal at the polarization

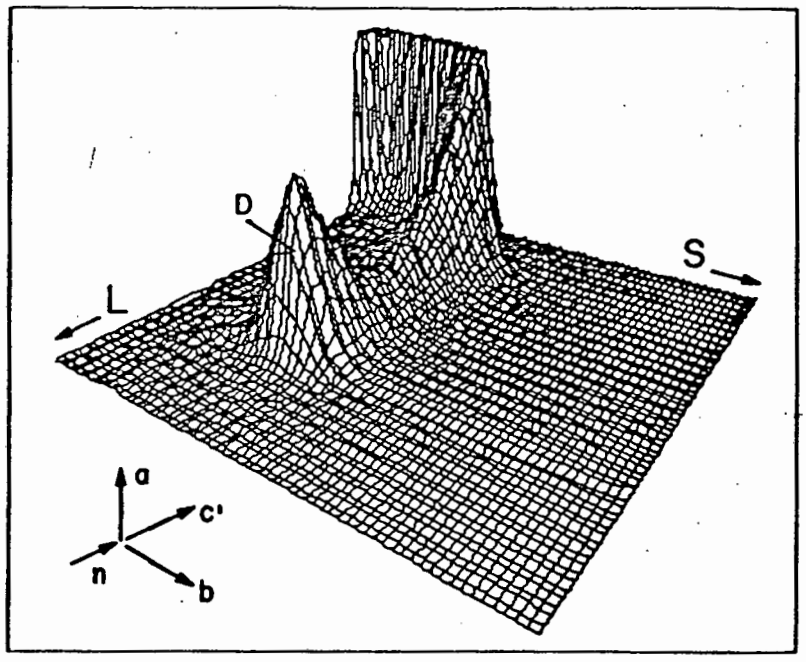

Fig. 7.4a An LS-spectrum for 10 MeV neutrons directed parallel to the c'-axis of the deuterated anthracene crystal (maximum-L orientation).
The ridge is due to recoil deuterons (D). The vertical scale is arbitrarily cut off at 500 counts.

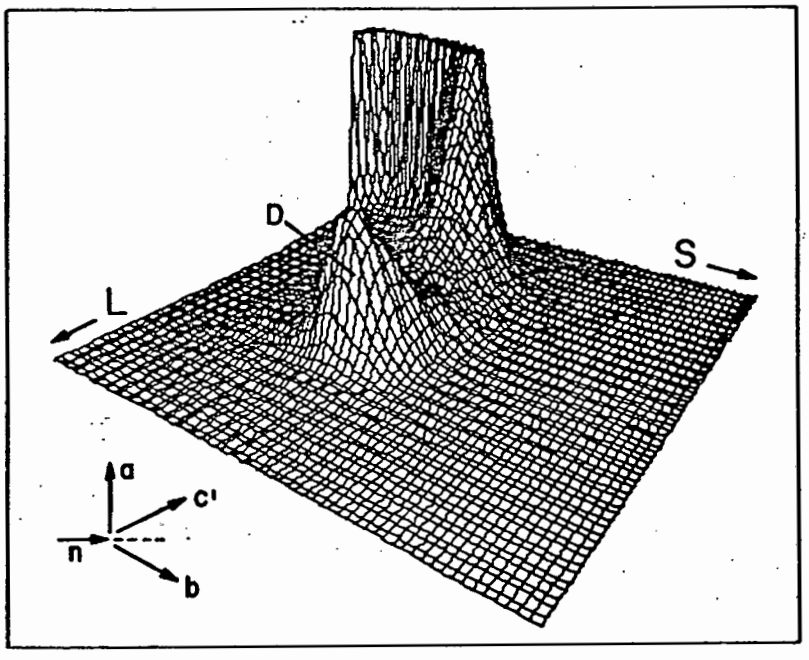

Fig. 7.4b An LS-spectrum for 10 MeV neutrons on the deuterated anthracene crystal at 'polarization orientation'.
The beam is directed between the b- and c'- axes at
$(\alpha,\beta) = (\theta,\phi)_{\text{crystal}} = (90^{\circ},40^{\circ})$.
The ridge is due to recoil deuterons (D).
The vertical scale is arbitrarily cut off at 500 counts.

orientation of $(\alpha,\beta) = (90^{\circ}, 40^{\circ})$, at which the characteristic broadening of the deuteron ridge is observed. Results at this energy could be compared to those of Walter and Kelsey (Wa63) for n-d scattering, and those of Faivre, *et al.* (Fa69) for p-d scattering at the near-by energy of 11.0 MeV.

Another reaction of interest is the $^{15}N(d,n_o)^{16}O$ reaction, the polarization and angular distribution of which have been measured at incident deuteron energies of 4.35 and 5.50 MeV (Bu67b) which produce a polarized neutron beam of 14.1 and 15.1 MeV, respectively. For both these energies the cross section is greatest at 30° (lab), and the polarizations have their greatest absolute value, 0.3 and 0.6, respectively, at this angle (Wa71). If extreme backward angles can be used, the 5.50 MeV incident beam will further produce a polarized neutron beam, $P_1 = 0.4$, of 12.5 MeV at 160° (lab). Furthermore, an incident deuteron beam of 2.6 MeV can produce a polarized beam, $P_1 = 0.48$, of 12.1 MeV energy at 45° (lab) (Wa71). The major difficulty with the $^{15}N(d,n_o)^{16}O$ reaction is that the figure of merit is down (Wa71) relative to the other reactions mentioned above. One must therefore pay the price of longer running times; however, good polarization data at these additional energies might be well worth the price.

7.3.2 Other applications for the deuterated crystal.

In addition to the polarization experiments, the deuterated anthracene crystal may be used for other types of experiments. Currently an investigation is in progress for measuring the sum of the cross sections for the (n,α) and $(n,n')3\alpha$ reactions on carbon, as a function of incident neutron energy in the range 16 to 22 MeV (St75). In this work, pulse shape discrimination is employed to identify the α-particles from these reactions, and the recoil deuteron from D(n,n) elastic scattering. Thus the cross section for α-production can be determined relative to the elastic scattering cross section. There may also be applications of the deuterated crystal in the study of deuteron photo-disintegration, particularly if the angular distribution of the photoprotons is of interest.

BIBLIOGRAPHY

(Aa64) R. Aaron, R.D. Amado and Y.Y. Yam, Phys. Rev., 136 (1964) B650

(Aa65) R. Aaron, R.D. Amado and Y.Y. Yam, Phys. Rev., 140 (1965) B1291

(Aa66) R. Aaron and R.D. Amado, Phys. Rev., 150 (1966) 857

(Aa72a) J.C. Aarons and I.H. Sloan, Phys. Rev., 5 (1972) 582

(Aa72b) J.C. Aarons and I.H. Sloan, Nucl. Phys., A182 (1972) 369

(Aj60) F. Ajzenberg-Selove and P.H. Stelson, Phys. Rev., 120 (1960) 500

(Al67) E.O. Alt, P. Grassberger and W. Sandhas, Nucl. Phys., B2 (1967) 167

(Am63) R.D. Amado, Phys. Rev., 132 (1963) 485

(Am66) R. Amado, Phys. Rev., 141 (1966) 902

(Am69) R.D. Amado, 'The Three-Nucleon Problem', Annual Rev. Nucl. Science, 19 (1969) 61

(Am72) R.D. Amado, Proc. Conf. on Few Particle Problems in the Nucl. Interaction, ed. I. Slaus, Amsterdam: North Holland Publishing Co., (1972) 254

(Ar67) J. Arvieux, Nucl. Phys., A102 (1967) 513

(Ba61) Basel Convention, Proc. Int. Symp. on Polarization Phenomena of Nucleons, Basel, 1960, (Helv. Phys. Acta, Suppl. VI, Birkhauser Verlag, 1961) 436

(Ba66) H.H. Barschall, Proc. Second Int. Symp. on Polarization Phenomena (Birkhauser, Basel, 1966) 393

(Be63a) A.F. Behof, G.P. Lietz, S.F. Trevino and S.E. Darden, Nucl. Phys., 45 (1963) 253

(Be63b) L.E. Beghian, K. Sugimoto, M.H. Wächter and J. Weber, Nucl. Phys., 42 (1963) 1

(Be63c) G. Bellettini, C. Bemporad, C. Cerri and L. Foa, Nucl. Instr. and Meth., 21 (1963) 106

(Be64) G. Bellettini, C. Bemporad and C. Cerri, Nucl. Instr. and Meth. 27 (1964) 38

(Be72) Gy. Bencze, Nucl. Phys., A196 (1972) 135

(Bh72) S.C. Bhatt, J.S. Levinger and E. Harms, Phys. Letts., 40B (1972) 23

(Bi67) J.B. Birks, The Theory and Practice of Scintillation Counting. (Pergamon Press, Ltd., London, 1967)

(Bl52) J.M. Blatt and V.F. Weisskopf, Theoretical Nuclear Physics, (John Wiley and Sons, New York, 1952)

(Bl65) E. Blignaut and J.J. Kritzinger, Nucl. Instr. and Meth., 36 (1965) 176

(Bo61) L.M. Bollinger and G.E. Thomas, Rev. Sci. Instr., 32 (1961) 1044

(Br58) F.D. Brooks, 'Scintillation Counters with Pulse Shape Selection to Distinguish Neutrons from Gamma-rays', Liquid Scintillation Counting, (pergamon Press, London, 1958) 268

(Br59) F.D. Brooks, Nucl. Instr. and Meth., 4 (1959) 151

(Br60) J.E. Brolley, Jr., and J.L. Fowler, 'Fast Neutron Physics, Part I' (Interscience Publishers, New York, 1960) 73

(Br67) G. Breit, Rev. Mod. Phys., 39 (1967) 560

(Br69) G.E. Brown and A.M. Green, Nucl. Phys., 137 (1969) 1

(Br71a) R. Brüning, B. Zeitnitz and R. Arvieux, Proc. 3td Int. Symp. on Polarization Phenonmena in Nuclear Reactions, (eds. H.H. Barschall and W. Haeberli; Univ. of Wisconsin Press, Madison, 1971) 445

(Br71b) F.D. Brooks and D.T.L. Jones, Proc. 3rd. Int. Symp. on Polarization Phenomena in Nuclear Reactions, (eds. H.H. Barschall and W. Haeberli; Univ. of Wisconsin Press, Madison, 1971) 430

(Br72) T.J. Brady and I.H. Sloan, Phys. Letts., 40B (1972) 55

(Br74a) F.D. Brooks and D.T.L. Jones, Nucl. Instr. and Meth., 121 (1974) 69

(Br74b) F.D. Brooks and D.T.L. Jones, Nucl. Instr. and Meth., 121 (1974) 77

(Br74c) J. Bruinsma, W. Ebenhöh, J.H. Stuivenberg and R. van Wagenigen, Nucl. Phys., A228 (1974) 52

(Bu52) R.A. Buckingham, S.J. Hubbard and H.S.W. Massey, Proc. R. Soc., A211 (1952) 183

(Bu59) W.P. Bucher, W.B. Beverly, G.C. Cobb and F.L. Hereford, Nucl. Phys., 13 (1959) 164

(Bu67a) W. Busse, J. Christianson, D. Hilscher, U. Morfeld, J.A. Scheer and W.U. Schröder, Nucl. Phys., A100 (1967) 490

(Bu67b) W. Busse, B. Efken, D. Hilscher, J.A. Scheer and W.U. Schröder, Z. Phys. 206 (1967) 404

(Bu68) S.N. Bunker, J.M. Cameron, R.F. Carlson, J.R. Richardson, P. Tomas, W.T.H. van Oers and J.W. Verba, Nucl. Phys., A113 (1968) 461

(Bu70) W. Busse, B. Efken, D. Hilscher, J.A. Scheer and W. Wenning, Nucl. Phys., A152 (1970) 354

(Ca59) L. Castillejo and L.S. Singh, Nuovo Cimento, 11 (1959) 131

(Ca72) R.T. Cahill, Nucl. Phys., A194 (1972) 599

(Ce64) M. Cerineo, K. Ilakovac, I. Slaus, P. Tomas and V. Valkovic, Phys. Rev., 133 (1964) B948

(Ch53) R.S. Christian and J.L. Gammel, Phys. Rev., 91 (1953) 100

(Cl60) T.B. Clegg and W. Haeberli, Nucl. Phys., A95 (1967) 608

(Co60) J.G. Coon, (unpublished) quoted by C.D. Swartz and G.E. Owen, 'Fast Neutron Physics, Part I', eds. J.B. Marion and J.L. Fowler, (Interscience Publishers, Inc., 1960) 211

(Co64a) H.E. Conzett, G. Igo and W.J. Knox, Phys. Rev. Letts., 12 (1964) 222

(Co64b) H.E. Conzett, H.S. Goldberg, E. Shield, R.J. Slobodrian and S. Yanabe, Phys. Letts., 11 (1964) 68

(Cr59) L. Crangerg, Phys. Rev., 114 (1959) 174

(Cr71) D.S. Cramer and L. Cranberg, Nucl. Instr. and Meth., 93 (9171) 405

(Da60) S.E. Darden, C.A. Kelsey and T.R. Donoghue, Nucl. Phys., 16 (1960) 351

(Da65) J.M. Daniels, 'Oriented Nuclei',(Academic Press, New York, 1965) 165

(De59) L.M. Delves and D. Brown, Nucl. Phys., 11 (1959) 432

(De62) L.M. Delves, Nucl. Phys., 33 (1962) 482

(De69) L.M. Delves and A.C. Phillips, Rev. Mod. Phys., 41 (1969) 497

(De71) L.M. Delves and M.A. Hennel, Nucl. Phys., A168 (1971) 347

(Do72a) P. Doleschall, Phys. Letts., 38B (1972) 298

(Do72b) P. Doleschall, Phys. Letts., 40B (1972) 443

(Do72c) P. Doleschall, J.C. Aarons and I.H. Sloan, Phys. Letts., 40B (1972) 605

(Do73) P. Doleschall, Nucl. Phys., A201 (1973) 264

(Do74) P. Doleschall, Nucl. Phys., A220 (1974) 491

(Du68) I. Duck, 'Three-Particle Scattering - A review of Recent Work on the Nonrelativistic Theory, Advances in Nucl. Phys., eds. Baranger and Vogt, New York: Plenum Press (1968) 343

(Ek56) H. Ekstein, Phys. Rev., 101 (1956) 880

(El62) A.J. Elwyn, R.O. Lane and A. Langsdorf, Jr., Phys. Riv., 128 (1962) 799

(Fa61a) L.D. Faddeev, Soviet Physics JETP, 12 (1961) 1014

(Fa61b) L.D. Faddeev, Soviet Physics-Dokl., 6 (1961) 384

(Fa63) L.D. Faddeev, Soviet Physics-Dokl., 7 (1963) 600

(Fa65) L.D. Faddeev, 'Mathematical Aspects of the Three-Body Problem in the Quantum Scattering Theory', (Israel Program for Scientific Translations, Jerusalem, 1965)

(Fa69) J.C. Faivre, D. Garreta, J. Jungerman, A. Papineau, J. Sura, and A. Tarrats, Nucl. Phys., A127 (1969) 169

(Fe35) E. Feenberg and J.K. Knipp, Phys. Rev., (1935) 906

(Fe59) E.M. Ferreira, Phys. Rev., 115 (1959) 1727

(Fe62) A.T.G. Ferguson and R.E. White, Nucl. Phys., 33 (1962) 477

(Fi73) A. Fiori, J. Arvieux, Nguyon Van Sen, G. Perrin, F. Merchez, J.C. Gondrand and R. Darvrs-Blanc, Phys. Rev., C8 (1973) 2019

(Fl57) N.N. Flerov and E.A. Tamanov, Sov. Jour. Atomic Energy, 3 (1957) 776

(Ga57a) J.L. Gammel and R.M. Thaler, Phys. Rev., (1957) 291

(Ga57b) J.L. Gammel and R.M. Thaler, Phys. Rev., (1957) 1337

(Ga68) D. Garreta, A. Papineau, J. Sura and A. Tarrats, Phys. Rev. Letts., 21 (1968) 1393

(Ge58) E. Gerjuoy, Annals of Phys., 5 (1958) 58

(Gi60) J.H. Gibbons and H.W. Newson, 'Fast Neutron Physics, Part I', eds. J.B. Marion and J.L. Fowler, (Interscience Publishers, Inc., New York, 1960) 133

(Gi66) W.R. Gibson, A.R. Johnson, E.A. McClatchie, J.H.P.C. Megaw and R.J. Griffiths, Proc. Int. Nucl. Phys. Conf., Gatlinburg, Tennessee, 1966 (Academic Press, New York, 1968) 1026

(G59) R.J. Glauber, 'High Energy Collision Theory' Lectures in Theoretical Physics, eds. W.E. Brittin and L.G. Dunham, New York: Interscience Publishers, Inc., (1959) 315

(Go63) M.D. Goldberg, 'Progress in Fast Neutron Physics' eds. G.C. Phillips, J.B. Marion and J.R. Risser (Univ. of Chic. Press, Chicago, 1963) 3

(Gr66) W. Grüebler, W. Haeberli and P. Extermann, Nucl. Phys., 77 (1966)394

(Ha47) A.O. Hanson and J.L. McKibben, Phys. Rev., 72 (1947) 673

(Ha65) S.J. Hall, A.R. Johnston and R.J. Griffiths, Phys. Letts., 14(1965) 212

(Ha67) W. Haeberli, Ann. Rev. Nucl. Sci., 17 (1967) 373

(Ha70) W. Haeberli, 'Polarization in Nucleon-Deuteron Scattering', Three-Body Problem in Nuclear and Particle Physics eds. J.S.C. McKee and P.M. Rolph, Amsterdam: North Holland Publishing Co., (1970) 188

(He59) P.H. Heckmann, Z. Phys., 157 (1959) 139

(He61a) P.H. Heckmann, H. Hansen, and A. Flammersfeld, Z. Phys., 162 (1961)84

(He61b) P.H. Heckmann, W. Sander, and A. Flammersfeld, Z. Phys., 165 (1961)12

(He72) M.A. Hennel and L.M. Delves, Phys. Letts., 40B (1972) 20

(Hü65) J. Hüfner and A. de-Shalit, Phys. Letts., 15 (1965) 52

(Hu71) C. -Y Hu, Phys. Rev., C3 (1971) 2151

(Hy64) L.G. Hyman, R.M. Schwarz and R.A. Schluter, Rev. Sci. Instr., 35 (1964) 393

(I163) K. Ilakovac, L.G. Kuo, M. Petrivac, I. Slaus and P. Tomas, Nucl. Phys., 43 (1963) 254

(Ja71a) A.D. Jackson, A. Lande and P.U. Sauer, Phys. Letts., 35B (1971) 365

(Ja71b) S. Jaccard, J. Piffaretti, R. Viennet and J. Weber, Proc. 3rd Int. Symp. on Polarization Phenomena in Nuclear Reactions, (eds. H.H. Barschall and W. Haeberli: Univ. of Wisconsin Press, Madison, 1971) 448

(Ja72) S. Jaccard and R. Viennet, Nucl. Phys., A182 (1972) 541

(Jo65) A.R. Johnson, W.R. Givson and J.H.P.C. Megaw, Phys. Letts., 19 (1965) 289

(Jo66) A.R. Johnston, W.R. Gibson, E.A. McClatchie, J.H.P.C. Megaw and R.J. Griffiths, Phys. Letts., 21 (1966) 309

(Jo68) A.R. Johnston, J.H.P.C. Megaw, W.R. Gibson and F.G. Kinston, Nucl. Phys., A122 (1968) 689

(Jo72) D.T.L. Jones, 'Polarization in Neutron-Proton Scattering at 16 and 22 MeV', Ph.D. thesis,1972 (unpublished)

(Jo74) D.T.L. Jones and F.D. Brooks, Nucl. Phys. A222 (1974) 79

(Ki61) W.F. Kienzle and A. Flammersfeld, Z. Phys., 165 (1961) 1

(Ki62) Kineo Tsukada and Shiroh Kikuchi, Nucl. Instr. and Meth., 17 (1962) 286

(Ki67) J. Kirkbride, E.C. Yates and D.G. Crandall, Nucl. Instr. and Meth., 52 (1967) 293

(Kl71) W.M. Kloet and J.A. Tjon, Phys. Letts., 37B (1971) 460

(Ko73) K.L. Kowalski and D. Feldmen, Phys. Rev., 130 (1963) 276

(Ko64) D.R. Koehler and R.A. Mann, Phys. Rev. 135 (1964) B91

(Ko72) K.L. Kowalski and S.C. Pieper, Phys. Rev., C5 (1972) 324

(Kr70a) J. Kraus and K.L. Kowalski, Phys. Letts., 31B (1970) 263

(Kr70b) J. Kraus and K.L. Kowalski, Phys. Rev., C2 (1970) 1319

(Kr72) J.J. Kritzinger, G.F. Ackermann, W. Amoraal, H. Schmitt, T. Swart, and R. Verbruggen, SUNI Annual Research Report, SUNI-23(1972) 1

(Kr73) J.J. Kritzinger, G.F. Ackermann, W. Amoraal, H. Schmitt, T. Swart and R. Verbruggen, SUNI Annual Research Report, SUNI-28 (1973) 1

(Lo64) C. Lovelace, Phys. Rev., 135 (1964) B1225

(Ma60) J.B. Marion, '1960 Nuclear Data Tables, Part 3', USAEC, 1960.

(Ma63) J.B. Marion, 'Progress in Fast Neutron Physics' eds. G.C. Phillips, J.B. Marion and J.R. Risser (Univ. of Chic. Press, Chicago, 1963) 23

(Ma66) J.J. Malanify, J.E. Simmons, R.B. Perkins and R.L. Walter, Phys. Rev., 146 (1966) 632

(Ma68) J.B. Marion and F.C. Young, 'Nuclear Reaction Analysis' (North Holland Publishing Co., Amsterdam, 1968)

(Ma70a) P. Marmier and E. Sheldon, 'Physics of Nuclei and Particles, vol. II, (Academic Press, New York, 1970)

(Ma70b) R.A. Malfiet and J.A. Tjon, Ann. of Phys., 61 (1970) 425

(Mc68) I.E. McCarthy, 'Introduction to Nuclear Theory' (John Wiley and Sons, Inc., New York, 1968).

(McK67) J.S.C. McKee, D.J. Clark, R.J. Slobodrian and W.F. Tivol, Phys. Letts., 24B (1967) 240

(McK70) J.S.C. McKee, 'The Three-Body Problem in Nuclear Physics', Rep. Prog. Phys., 33 (1970) 691

(Me68) J.H.P.C. Megaw, A.R. Johnson, W.R. Gibson and F.G. Kingston, Nucl. Phys., A122 (1968) 689

(Mi62) A. Mitra, Nucl. Phys., 32 (1962) 529

(Mi63) A. Mitra and V. Bhashin, Phys. Rev., 131 (1963) 1265

(Mi69) A.N. Mitra, 'The Nuclear Three-Body Problem', Adv. in Nuclear Physics, eds. M. Baranger and E. Vogt, New York: Plenum Press, (1969) 1

(Mo71) C.L. Morris and S.T. Thornton, Nucl. Instr. and Meth., 96(1971) 281

(Mo74) C.L. Morris, R. Rotter, W. Dean and S.T. Thornton, Phys. Rev., C9 (1974) 1687

(Mu71) G.S. Mutchler, W.B. Broste and J.E. Simmons, Phys. Rev., C3 (1971) 1031

(No63) H.P. Noyes, Phys. Rev. 130 (1963) 2025

(No67) H.P. Noyes, SLAC - PUB - 256, (Jan. 1967)

(No68) H.P. Noyes and H. Fieldeldey, SLAC - PUB - 409 (April 1968) (Invited paper presented at the Conf. on Three-Particle Scattering in Quantum Cechanics, Texas A and M, April, 1968)

(Ok71) K. Okamoto and C. Pask, Ann. of Phys., 68 (1971) 18

(Ol68) D.B. Olivier and G.F. Knoll, IEEE Trans. on Nucl. Sci., NS-15 (1968) 122

(Pa73) G. Pauletta, 'The Neutron-Deuteron Breakup Cross Section between 8 and 22 MeV', Ph.D. thesis, 1973 (unpublished)

(Ph66) A.C. Phillips, Phys. Rev., 142 (1966) 984

(Ph68) A.C. Phillips, Nucl. Phys., A107 (1968) 209

(PHI70) 'The Philips Application Book for Photomultipliers' by J.M. Schonkeren, eds. H. Koter and L.J. Thompson, (supplied by South African Philips (Pty) Ltd., 1970)

(Pi72a) S.C. Pieper and K.L. Kowalski, Phys. Rev., C5 (1972) 306

(Pi72b) S.C. Pieper, Nucl. Phys., A193 (1972) 529

(Pi72c) S.C. Pieper, Phys. Rev., C6 (1972) 1157

(Po70) L.E. Porter, L.C. McIntyre and W. Haeberli, Nucl. Instr. and Meth., 89 (1970) 237

(Pu68) R.D. Purrington and J.L. Gammel, Phys. Res., 168 (1968) 1174

(RCA70) 'The RCA Photomultiplier Manual'
(supplied by the RCA Corp., 1970)

(Sa58) L. Sartori and S.I. Rubinow, Phys. Rev., 112 (1958) 214

(Sc65) E. Schwarz, Helv. Phys. Act., 38 (1965) 877

(Se57) J.D. Seagrave and L. Cranberg, Phys. Rev., 105 (1957) 1816

(Se69) R.G. Seyler, Nucl. Phys. A124 (1969) 253

(Se70) J.D. Seagrave, 'The Elastic Channel in Nucleon-Deuteron Scattering'
Three-Body Problem in Nuclear and Particle Physics,
eds. J.S.C. McKee and P.M. Rolph, Amsterdam:
North Holland Publishing Co., (1970) 41

(Si63) A.G. Sitenko and V.F. Karchenko, Nucl. Phys. 49 (1963) 1265

(Si69a) M. Simonius,'Theory of Polarization Measurements I:
Formalism and Determination of the Scattering Amplitudes from
Measurements', Report, February 1969.

(Si69b) M. Simonius, 'Theory of Polarization Measurements II:
Mathematical Tools Bilinear Equations' Report February 1969

(Sla72) I. Slaus, 'Some Aspects of the Three Nucleon Problem'
Few Particle Problems in the Nuclear Reaction
eds. Slaus, Moszkowski, Haddock and van Oers, Amsterdam:
North Holland Publishing Co., (1972) 272

(Slo67) I.H. Sloan, Phys. Letts., 25B (1967) 84

(Slo68) I.H. Sloan, Phys. Rev., 165 (1968) 1587

(Slo69a) I.H. Sloan, Nucl. Phys., A139 (1969) 337

(Slo69b) I.H. Sloan, Phys. Rev., 185 (1969) 1361

(Slo71) I.H. Sloan, Nucl. Phys., A168 (1971) 211

(Slo72a) I.H. Sloan, Nucl. Phys., A182 (1972) 549

(Slo72b) I.H. Sloan, Nucl. Phys., A188 (1972) 193

(Slo72c) I.H. Sloan and J.C. Aarons, Nucl. Phys., A198 (1972) 321

(Sm70) D.L. Smith and T.G. Miller, Nucl. Phys., A147 (1970) 509

(St70) Th. Stammbach, G. Spalik, J. Taylor and R.L. Walter,
Nucl. Instr. and Meth., 80 (1970) 304

(St75) A.P. Stevens, F.D. Brooks and I.J. van Heerden,
South African Institute of Physics, 20th Ann. Conf.,Durban,
1975, item 2.2

(Ta51) M. Taketani, S. Nakamura and M. Sasaki, Prog. Theoret. Phys.
(Kyoto), 6 (1951) 581

(Ta70) J. Taylor, G. Spalek, Th. Stammbach, R.A. Hardekopf and R.L. Walter,
Phys. Rev., C1 (1970) 803

(Tj70) J.A. Tjon, B.F. Gibson and J.S. O'Connell, Phys. Rev. Letts., 25
(1970) 540

(Ts62) K. Tsukada and S. Kikuchi, Nucl. Instr. and Meth., 17 (1962) 280

(Ts65) K. Tsukada, S. Kikuchi and Y. Miyagawa, Nucl. Instr. and Meth., 37
(1965) 69

(Va67a) W.T.H. van Oers, and R.W. Brockman, Jr., Nucl. Phys., A92 (1967) 561

(Va67b) W.T.H. van Oers and J. D. Seagrave, Phys. Letts., B24 (1967) 562

(Va67c) W.T.H. van Oers and I. Slaus, Phys. Rev., 160 (1967) 853

(Ve57) M. Verde, 'Handbuch der Physik' vol. 39, ed. S. Flügge, Berlin: Springer-Verlag (1957) 144

(Wa63) R.L. Walter and C.A. Kelsey, Nucl. Phys., 46 (1963) 66

(Wa64) R.L. Walter, W. Benenson, T.H. May and C.A. Kelsey, Nucl. Phys., 59 (1964) 235

(Wa69) R.K. Walter, J.C. Hopkins, E.R. Kerr, J.T. Martin, A. Niiler, J.D. Seagrave, R.H. Sherman and D.R. Dixon, Abstract, Boulder Colorado Meeting of Am. Phys. Soc. (Oct 30, 1969)

(Wa71) R.L. Walter, Proc. 3rd Int. Symp. on Polarization Phenomena in Nuclear Reactions (eds. H.H. Barschall and W. Haeberli: Univ. of Wisconsin Press, Madison, 1971) 317

(Wh73) J.A. Wheeler, Phys. Rev., (1937) 1107

(Wh58a) R.E. White, A. Chisholm and D. Brown, Nucl. Phys., 7 (1958) 233

(Wh58b) W. Whaling 'Handbuch der Physik', vol. 34, ed. S. Flügge, Berlin: Springer-Verlag, (1958) 193

(Wi66) D.H. Wilkinson, 'The Isobaric Mass Formula and Coulomb Energies in the 1p-shell', Isobaric Spin in Nuclear Physics, eds. J.D. Fox and D. Robson, (Proc. Conf. Isobaric Spin Nucl. Phys., Tallahassee, Fla., March 1966)

(Wo56) L. Wolfenstein, Phys. Rev., 92 (1953) 123

(Wu48) T.Y. Wu and J. Ashkin, Phys. Rev., 73 (1948) 986

(Ya54) Y. Yamaguchi, Phys. Rev., 95 (1954) 1628, 1635

(Yu35) H. Yukawa, Proc. Math. Soc., Japan, 17 (1935) 48

(Za72) J. Zamudio, B.E. Bonner, F.P. Brady, J.A. Jungerman and J. Wang, 'Proc. Conf. on Nuclear Structure Study with Neutrons, Budapest, Hungary, 1972' (Central Research Institute for Physics, Budapest, Hungary, 1972)

(Za73) J. Zamudio-Cristi, B.E. Bonner, F.P. Brady, J.A. Jungerman and J. Wang, Phys. Rev. Letts., 31 (1973) 1009

(Ze74) B. Zeitnitz, R. Maschuw, P. Suhr, W. Ebenhöh, J. Bruinsma and J.H. Stuivenberg, Nucl. Phys., A231 (1974) 13.